Westinghouse Non-Proprietary Class 3

AP600 Passive Residual Heat Removal Heat Exchanger Test Final Report

Westinghouse Energy Systems

Westinghouse Non-Proprietary Class 3

WCAP-13573
Revision 3

AP600 Passive Residual Heat Removal Heat Exchanger Test Final Report

Westinghouse Energy Systems

WCAP-13573
Revision 3

AP600
PASSIVE RESIDUAL HEAT REMOVAL
HEAT EXCHANGER TEST
FINAL REPORT

April 1997

by
L. E. Hochreiter
F. E. Peters
D. L. Paulsen

WESTINGHOUSE ELECTRIC CORPORATION
Energy Systems Business Unit
Nuclear Services Division
P.O. Box 355
Pittsburgh, Pennsylvania 15230-0355

TABLE OF CONTENTS

TABLE OF CONTENTS (Cont.)

LIST OF TABLES

LIST OF TABLES (Cont.)

LIST OF FIGURES

LIST OF FIGURES (Cont.)

LIST OF FIGURES (Cont.)

1.0 ABSTRACT

Two series of tests were performed in the AP600 Passive Residual Heat Removal (PRHR) Test Facility to broaden the existing database and to examine different design configurations for the PRHR heat exchanger (HX). The purpose of the tests was to provide design information and data on the heat transfer behavior from a long vertical HX, submerged in a large tank of water at ambient pressure.

The tests covered the entire range of forced and natural circulation conditions considered in the AP600 accident analysis. Tests were also performed to examine boildown of the in-containment refueling water storage tank (IRWST) and its impact on PRHR performance. The data from these tests support the AP600 PRHR design and are used to assess the PRHR performance.

2.0 INTRODUCTION

The AP600 reactor is a pressurized water reactor (PWR) designed to use a natural circulation heat exchanger (HX) as the safety-related means of removing core decay heat and sensible heat following certain design basis events. The passive residual heat removal (PRHR) HX removes core decay heat to mitigate loss of heat sink events and is actuated on either a low steam generator (SG) secondary-side water level followed by the failure of the nonsafety-related startup feedwater system to operate; a low wide-range SG water level; or on a safety injection, "S," signal. In the AP600, the PRHR HX replaces the safety-related auxiliary feedwater system used in current operating plants.

The PRHR HX transfers heat from the reactor coolant system (RCS) to the containment by heating and boiling the water in the in-containment refueling water storage tank (IRWST). The steam produced transfers heat to the inside of the containment shell by condensation, which is assisted by the passive containment cooling system (PCS). The condensate is collected by gutters on the containment shell and returned to the IRWST. Therefore, the PRHR HX, in conjunction with the PCS, provides a heat sink for an indefinite amount of time.

As shown in Figure 2-1, the PRHR HX receives hot reactor coolant from the RCS hot leg and discharges the cooled fluid to a steam generator channel head. Natural circulation PRHR flow is developed from the density difference of the cold water in the PRHR tubes above the reactor core and the hot water in the inlet line to the HX. However, if the PRHR is actuated with the reactor coolant pumps (RCPs) operating, the PRHR flow will be greater. When the RCPs are operating, the flow rate through the PRHR HX is expected to be approximately five to seven times higher than the flow rate expected during natural circulation flow.

The tube spacing for the PRHR is larger than that used in most commercial kettle reboilers [Reference 1]. The tube-to-tube spacing for the horizontal section is a 1.5-inch square pitch, and the vertical section is a 1.5-inch by 3-inch rectangular pitch. Larger pitch-to-diameter ratios reduce the possible tube-to-tube interaction when boiling is initiated. The structure supporting the HX (see Figure 2-2) is open to provide minimum resistance to the natural circulating flow from the IRWST.

The PRHR HX is used during many design basis events and is especially important in mitigating loss of heat sink events such as loss of normal feedwater and feedwater line break. To properly model the PRHR HX performance in the computer code analysis of these events, it was determined that boiling heat transfer testing would be necessary. In particular, the testing was intended to provide information regarding boiling heat transfer on the long tubes and the effect of mixing and voiding in the pool during HX operation over the range of conditions that could occur during design basis events.

Separate effects tests were performed to characterize the heat transfer performance of the PRHR HX and the effects of the mixing characteristics of the IRWST during the AP600 phase I Program. The results of the phase I tests presented in Reference 2 cover a limited range of expected PRHR operating conditions and parameters. A second series of tests [Reference 3] (phase II) were performed to

broaden the range of conditions investigated. Both series of tests examined an earlier PRHR design. The previous PRHR design consisted of 6 single rows of 75 tubes, each distributed throughout the IRWST. The tubes were 18 feet long and were placed 4 feet below the IRWST water level with no horizontal sections.

The final design for the PRHR HX incorporates C-tube configuration with a top and bottom horizontal section connected by a long vertical section of tubes. Figure 2-1 shows the AP600 C-tube PRHR design. The top and bottom portions of the HX contain 42 percent of the total surface area while the vertical portion contains 58 percent. Analysis and evaluations were performed to verify that the results of these tests are applicable to the current C-tube PRHR HX configuration [Reference 4].

This report describes the test performed on the original PRHR design (no horizontal sections) and the applicability of this data for the final C-tube PRHR configuration.

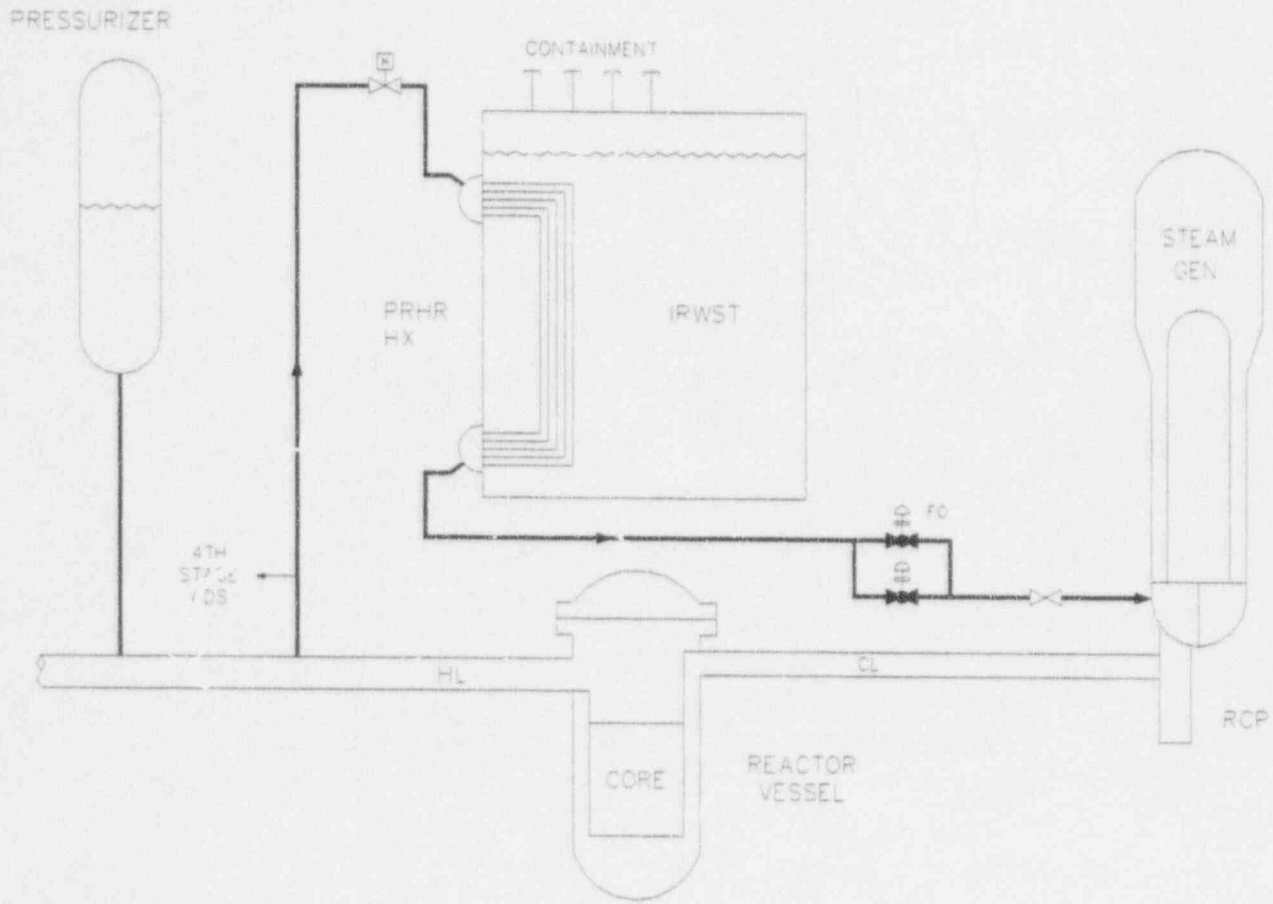

Figure 2-1 AP600 Passive Residual Heat Removal Heat Exchanger

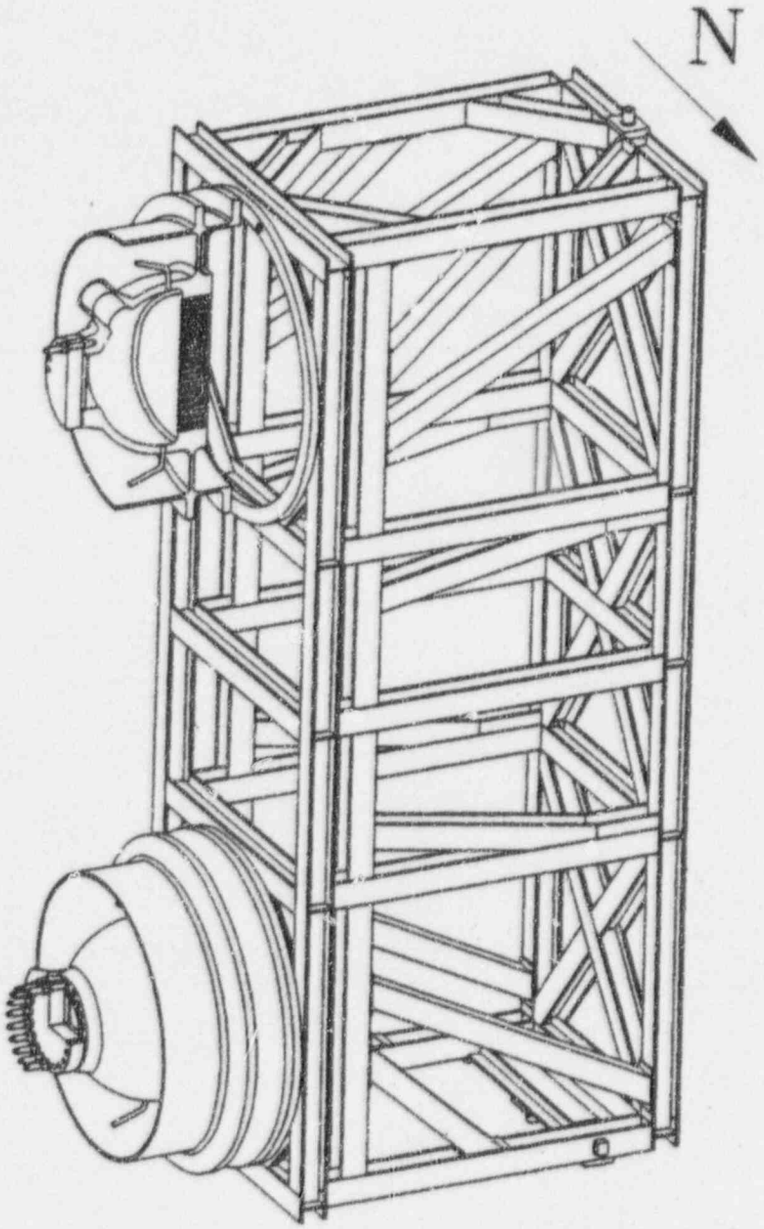

DIMETRIC VIEW

SUPPORTS AND TUBE BUNDLE
NOT SHOWN FOR CLARITY

SCALE 1:32

Figure 2-2 Passive Residual Heat Removal Support Structure

3.0 TEST OBJECTIVES

The primary objective of the passive residual heat removal heat exchanger (PRHR HX) test was to verify the thermal performance of the PRHR HX. This objective was achieved by testing HX tubes over the range of prototypic plant conditions and flow rates. A range of tube flow rates that correspond to the expected range of PRHR flow rates were tested. Inlet temperatures were varied from the maximum expected PRHR inlet temperature down to the minimum reactor coolant system (RCS) temperature that the PRHR would be required to operate. From the test data, a design heat transfer correlation was developed for the computer codes that are used to analyze the performance of the PRHR HX.

Secondary objectives of the test were to:

- Determine the applicability of different heat transfer correlations for the PRHR design
- Determine the mixing characteristics of the IRWST
- Determine the minimum time required for significant steam release from the IRWST to containment
- Determine what effect the water level above the tubes has on steam release from the IRWST to containment

The PRHR HX consists of rows of vertical tubes that are connected to horizontal tube sections to the inlet and exit plenums of the PRHR. The configuration basis of the test was to model a segment of tubes in the middle of a long row of tubes. This test configuration models tubes that experience a restricted flow of pool water because of the effects of being located in the middle of a long row of tubes. By modeling the most restricted HX tubes, the test conservatively predicts is the overall heat transfer performance of the PRHR HX.

The horizontal portion of the PRHR was not modeled in the tests; therefore, additional analyses and evaluations were performed to justify the applicability of the vertical data to the horizontal sections.

4.0 FACILITY DESCRIPTION

4.1 Scaling Basis for the Passive Residual Heat Removal Tests

There was no formal scaling study performed for the passive residual heat removal (PRHR) tests; however, there was an engineering scaling analysis performed on the key phenomena of interest. The test facility accurately represents at full height and full pressure, the tube flows from a pumped flow condition to a natural circulation condition typical of the PRHR. The primary system fluid Prandtl and Reynolds numbers were preserved on a one-to-one basis with AP600 plant values for different flow conditions by maintaining full AP600 temperature and pressure conditions. Therefore, the driving temperatures for heat transfer between the primary and the secondary side (in-containment refueling water storage tank [IRWST] simulation) were preserved and varied over the expected range for the AP600. The three heat exchanger (HX) tubes were of similar tube material, wall thickness, inside diameter, and pitch relative to the planned PRHR HX. The test used stainless steel tubes, whereas the AP600 PRHR will use Inconel. There is a 10 percent difference in the tube material thermal conductivity. Therefore, the temperature differences and the thermal resistances between the primary fluid temperature and the secondary IRWST temperature were similar in the test as to the AP600 plant.

The effects of adjacent rows of tubes were examined by two different methods. Temperature traverses were made in the secondary fluid in the IRWST simulation adjacent to the HX tubes. The temperature traverses indicated the region of influence of one tube in the flow. The results indicated that the larger pitch to-diameter ratio used in the PRHR design (P/D = 2 for adjacent tubes, and P/D = 4 for parallel rows of tubes) would provide thermally independent behavior. More typical P/D ratios are 1.3 to 1.5 for heat exchangers. A second series of tests examined the effects of placing baffles in front of the tubes as well as behind the tubes to simulate adjacent rows of tubes. It was observed that the heat fluxes for these different cases were almost the same as the cases with no baffle plates. In some cases, the heat fluxes were slightly enhanced due to the increased convection in the region around the tubes as the smaller volume of water was heated and accelerated upward as a result of the buoyant effects in the flow.

4.2 Summary Description of the Test Facility

The test section replicates at full scale and prototypic flow, pressure, and temperature conditions, with three HX tubes from PRHR HX, which transfer AP600 primary system core decay heat to an IRWST. The IRWST coolant flow generated by buoyant forces is most restricted in the central part of the long array of tubes. These tubes are expected to have less thermal conductance to the pool than tubes on the outside of the tube array. The central position of the tubes is simulated by providing parallel, vertical baffle walls between the large pool that exists in the IRWST and the location of the three vertical HX tubes. The walls impose a two-dimensional flow symmetry around each tube.

The IRWST is modeled by a tall, circular tank filled with water at atmospheric pressure, which is nominally filled to a level 2 feet above the top of the HX tubes. The IRWST has an outside diameter of 4 feet and a height of 32 feet. The tank can be filled to 24 feet above the bottom. The IRWST is equipped with an internal cylindrical baffle 4.5 inches from the tank wall. Three HX tubes are positioned on a radial plane with 1.5 inches between the tubes and the baffle and the IRWST wall (see Figure 4-1).

A separate test was conducted before designing the test section to provide insight into thermal and flow behavior. An electrical heating rod similar to an HX, but shorter, was placed between transparent baffles in a transparent tank of water that measured 4-foot by 2-foot and was 1.5 feet deep. Thermal stratification with nearly uniform temperatures on horizontal planes was observed during transient heating. The testing showed how the convection pattern develops initially around the heater rod, and only after the tank bulk temperature approaches a boiling temperature, does the vigorous boiling around the heater rod produce strong buoyant currents in the tank, which are able to reduce the stratification by mixing. Other observations were:

- Significant steaming from the free surface takes place only after the bulk temperature has approached the boiling point
- The length of baffle plates did not have an impact on the flow pattern
- The distance between the heater rod and the back wall of the tank did have an effect on the "pumping action" of the heater rod

Because of this latter observation, a provision was made for different locations of the back wall in the PRHR test. The guides for a removable wall are shown in Figure 4-1. The back wall simulates the IRWST wall, and the tubes are placed at distance of the PRHR HX from the IRWST wall.

The test section tubes are supplied with pressurized water to a maximum of 2500 psig and 650°F to test PRHR HX performance at all prototypic conditions. The primary high-pressure water circulation system is equipped with a canned motor pump and an electrical, temperature-controlled water heater. An accumulator pressurized with high-pressure nitrogen maintains the system pressure. Flow in each HX tube is regulated by a manual valve at the outlet, while primary system flow is maintained by throttled recirculation to the pump inlet to provide satisfactory pump and heater flow. Figure 4-2 shows the test system piping and its components to scale. The secondary-side water is maintained at prototype conditions during transient heat-up and for saturated boiling at steady-state for all the primary flow and temperature conditions.

Heat transfer is measured by recording water temperatures at various distances from the inlet inside two tubes, on the tube walls, and outside in the tank water throughout the baffled space as well as the larger tank volume. Pressures, primary flows and secondary steaming flow rates, and water levels are also measured.

4.3 Heat Exchanger Characteristics, Operating Parameters, and Instrumentation Summary

The three HX tubes have the following characteristics:

Material:	Type 304 stainless steel, ref. heat no. 477009
Dimensions:	Nominal – 0.75-inch OD, 0.065-inch wall thickness (see specifications ASTM-A-269/213)
	Measured – 0.748-inch OD, 0.0665-inch wall thickness
	Nominal Length – 18 feet
	Tube Spacing – 1.5 inch (centerline-to-centerline pitch)
Thermal conductivity:	Increasing from 9.8 Btu/hr-°F-ft. at 271°F to 11.5 Btu/hr-°F-ft. at 646°F
Volume of water in the tank:	2182 gallons (727.3 gallons per tube) with water level 24 feet above bottom of the tank

The test operating parameters are:

- Primary water temperature – 250°F to 650°F
- Primary water pressure – 50 to 2300 psig (above saturation pressure)
- Single HX tube flow – 0.3 to 10 gallons/min.
- Number of operating HX tubes – one, two, or three
- Tank water level above top of tubes – 1 to 7 feet
- Initial tank water level – 24 feet above bottom
- Tank temperature – ambient or less than 120°F to boiling at 212°F
- Baffles – back wall baffle may be behind tubes, partial baffle may be in front of tubes

The instrumentation includes:

- 14 thermocouples (TCs) inside each of 2 HX tubes (28 TCs) measuring primary water temperatures at the center of the tubes along their length.

- 12 TCs at the outer surface of each of 2 HX tubes (24 TCs) measuring temperatures along the length of the tubes.

- 7 TCs measuring primary water temperatures, 1 each at outlet of water heater, at inlet manifold to HX, before each of three flowmeters in outlet lines from three tubes, one in return line from HX near the pump, and one at the bottom of the accumulator.

- 120 TCs at various elevations and locations in the model IRWST.
- 3 TCs on rotating traverses near the outer HX tube at three elevations inside the tank wall.
- 1 TC at the top of the tank steam vent pipe.
- 3 primary water flow orifice meters and differential pressure transducers (DP cells) in outlet line from each HX tube.
- 1 primary system pressure transducer before the inlet to the HX tubes.
- 1 primary system pump differential pressure transducer between inlet and outlet.
- 1 accumulator level differential pressure transducer.
- 1 tank level differential pressure transducer.
- 1 tank steam vent flow vortex flowmeter.

4.4 Detailed Description of Test Facility

4.4.1 Test Heat Exchanger

The test HX consists of three HX tubes (0.75-inch OD by 0.065-inch wall thickness), 18.16 feet long that are mounted vertically in the baffled section of the model IRWST. The HX tubes, the IRWST, and the baffle and internal supports are fabricated from type 304 stainless steel. The HX tubes are manifolded from a 1.5-inch Schedule 80 pipe at the top of the supply tank to the 0.75-inch stainless steel tubes prior to entering the supply tank. The tubes pass through an 8-inch stainless steel blind flange into the tank 20 feet from the bottom of the tank. As shown in Figure 4-2, the center tube is at 20 feet, but the inlet tube to the HX tube nearest the tank wall is 2 inches below that and the inlet tube to the HX tube nearest the baffle is 2 inches above. All three supply lines are connected to the HX tubes below that, 8 inches below the middle tube's elbow. Tees are provided in the middle and outside tubes to allow tubes for thermocouple pass through. Figure 4-3 shows the inlet configuration of the tubes and the location of the thermocouples.

The three tubes are held by four stainless steel spacers, located 5 feet apart, which also slide on a 3/8-inch diameter thermocouple support tube. Except for the second support from the top, the spacers are tack-welded to the middle HX tube. The second one is welded to the support tube. Differential thermal expansion is accommodated by the supports. The supports are 0.062 inches thick and 1.5 inches high to minimize flow resistance. The small support tube for thermocouple leads is located at the tank wall, 2.5 inches above the line of tubes on the inlet side of the baffled tank water space.

The two outer HX tubes are fastened to tees 20 inches from the bottom of the tank with 3/4-inch pipe threads holding thermocouple connectors. At the bottom of the tank, all three HX tubes are connected to 0.75-inch diameter outlet tubes that pass through bellows fastened to an oval 10-inch by 13.50-inch by 0.50-inch thick blind flange. The middle outlet tube is bent to offset it 2.625 inches to provide room for the 1.50-inch diameter, 5-inch long bellows. The bellows can accommodate 2 inches of thermal expansion.

The tank is constructed from 48-inch OD by 0.75-inch thick stainless steel pipe. The tank is 32 feet high. Figure 4-4 is a typical cross section view of the tank, HX tubes, baffle location, and construction and position of thermocouples in the tank water at numerous elevations. The baffle is 30 feet high and extends to within 2 feet of the top. The baffle is formed from four sections of 0.25-inch thick stainless steel, 89.875 inches high formed to an outside diameter of 38.5 inches over a 240-degree sector and having a 3-inch wide flange at each edge. The sections are held by bolting through 1-inch OD tubes, 4.5 inches long, eight or ten per section, and the tank wall, as shown in Figure 4-4. The "back wall" at the end of the baffle is gasketed and bolted to the baffle and, with a clamp, to the tank wall. A 2-inch angle is used at the ends of the baffle for additional support and to hold the baffle round. All bolts are seal-welded to the tank after assembly.

Pairs of 0.50-inch square bars, 0.25 inches apart, are welded to the tank wall and the baffle opposite. One set is 11.85 inches behind the HX tubes, and another is 17.77 inches behind, while the back wall is 23.69 inches behind at the average radius. The sets of bars serve as guides for inserting 0.05-inch thick stainless steel strips, 30 feet high, to block flow at various distances from the tubes to simulate various stand off distances of the HX from the IRWST walls. Additional guides are located 11.85 inches and 23.69 inches in front of the tubes. These guides hold similar strips 8 inches from the bottom of the tank and 22 feet from the bottom (2 feet below the nominal tank water level). The stripes permit investigation of the impact baffles (simulating) on HX performance, flow, and mixing in the tank.

The tank contains four viewing ports (see Figure 4-2), three to observe boiling on the HX tubes and one to observe the water line behavior. The view ports (Pyrex and Sodaline glass) provide a 6-inch diameter portal for viewing on the 6-inch, 150-lb. flanges. The flanges are rated at 150 psig at the tank operating conditions. An additional flange is located near the edge on the tank cover plate above the row of HX tubes. A moisture separator (see Figure 4-2), formed of three plates, is located in front of the 4-inch diameter steam vent pipe at the top of the tank. The vent pipe is reduced to 3 inches before a vortex type steam flowmeter.

The tank is drained through several 2-inch, Schedule 40 stainless steel pipe drain lines and is filled through 1.5-inch, Schedule 40 pipes (see Figure 4-2). Heated makeup water (approximately 130°F) is supplied from the laboratory into the top of the tank at the top of the HX through valve IV-5. Makeup water is required when tank temperatures increase to above 200°F. The makeup water tends to sink to the bottom of the tank prior to mixing.

The test IRWST is shown in Figure 4-5. It is covered with 2 inches of thermal insulation over the sides, bottom, and cover except at the viewing and thermocouple ports and vertical channels for thermocouple leads. The channels are formed by 3.50-inch wide stainless sheet metal tack welded to the outside of the tank. The channels are located in front of thermocouple sets at "E," "H," "J," and "K," and one 6-inch wide channel is located in front of sets "F" and "G" (see Figure 4-4). Figure 4-5 also shows the work platforms provided at elevations of 10, 20, and 30 feet above the foundation (7, 17, and 27 feet above bottom of 32-foot tall tank). The first two platforms are 41 inches wide and cover two 60-degree segments of a hexagonal plan around the tank. The top has a full hexagonal platform 36 inches wide. Ladders, alternately placed and safety-caged above 10 feet, connect the platforms. Checkered plate flooring is used some places, and rectangular bar grating in others. The platforms are supported from stainless steel bars, 6 inches wide by 5/16 inches thick and 6 feet long welded vertically on edges to the tank. The four support legs for the tank are 8-in.^{2} H beams, each 9 feet tall and welded to the tank wall.

4.4.2 High-Pressure Primary System

The principal components of the primary system are a high-pressure circulating pump, an electrical heater, a high-pressure accumulator, circuit fill, drain and control valves, and protection for the fired high-pressure system.

4.4.2.1 Circulation Pump

The pump is a two-stage, high-pressure, 50-gallon-per-minute (design) canned motor, and 3450-rpm unit manufactured by the Chempump Division of the Crane Company in Warrington, Pennsylvania (model GHDT-20K). The characteristic of its 8.375-inch diameter impeller is 588 feet of head at zero flow, declining linearly to 556 feet at 50 gpm, and nonlinearly to 531 feet at 80 gpm. The net positive suction head (NPSH) varies from approximately 4 to 14 feet in this range. The pump is rated at 20 horsepower, 2500 psig, and 650°F. The motor is cooled by auxiliary cooling water. Internal winding sensors trip the pump off when excessive temperatures are reached. High primary water temperatures and high flows (and pump power) cause trips occasionally during operation. The pump is shown on the left in Figure 4-6. The pump's net efficiency is near 25 percent. Inlet piping is 2.5 inches, and outlet piping is 1.5 inches. Thermal distortion during operation, particularly start-up and shutdown, leads to small leakage from the high-pressure system. An orifice and filter or strainer are used in the pump discharge piping. The orifice (0.688-inch bore) provides flow resistance to increase the system pressure drop so that the pump operates in a desirable head and flow regime (see Figure 4-2).

4.4.2.2 Electrical Heater

The primary water heater is a specially designed and manufactured unit rated at 350 kW, three-phase, 480 volts, a design pressure of 2500 psig, and a peak service water temperature of 650°F. The heater was fabricated by Watlow Industries using 2 8-inch Schedule 120 pipes (SA-335P11 special carbon

steel) and caps, 8-inch 1500 lb. flanges (SA-182F11 steel) holding 15 Incoloy sheathed heating elements in each section. Each heater element is 96 inches long with a 0.475-inch diameter and produces 48 watts per square inch of surface. The two sections are joined at the flanged ends by a cross over pipe. The inlet (bottom) and outlet (top) flanges are 4-inch, 1500 lb., and couple with 2.50-inch Schedule 80 system inlet and outlet pipes. The unit is shown in Figure 4-7. All parts are well insulated.

Two type K (chromel-alumel) thermocouples are installed in each heating section. They are used with a temperature controller (Watlow Series 8[illegible]) to regulate power from a 450-ampere silicon controlled rectifier power controller. The maximum power is 321 kW at the supplied line voltage of 460 volts. The power control is in the cabinet in the foreground of Figure 4-7, and the supply circuit breaker is on the building wall (upper right).

4.4.2.3 Accumulator

The accumulator is a 14-foot, 10-inch vessel fabricated from 12-inch, Schedule 120 pipe (A 106 C steel). The bottom of the accumulator is connected to the primary circulation system after the heater outlet by a 2.50-inch, Schedule 80 pipe. A threaded pipe connection on the side at the top is connected to a regulated supply of nitrogen from a high-pressure cylinder (5000 psig). The regulator can bleed gas from the accumulator if pressure rises above the set pressure, but not at a high rate. At the top of the accumulator, a 1.50-inch, 1500-lb. flange connects to a relief valve, which is set to vent automatically if pressure rises to above 2500 psig. A ruptured disk provides additional safety relief at a pressure above 3000 psig. Since the blowdown can be rapid for hot steam flashing from the primary system, the two safety devices vent into a 55-gallon drum filled with water.

4.4.2.4 Piping and Valves

Primary system piping from control valve CV-4 to the HX inlet tubes and from the individual tube control valves CV-1, CV-2, and CV-3 is 1.50-inch, Schedule 80 steel pipe. The recirculation line, whose flow is controlled by valve CV-5, is the same up to the HX return line where it becomes a 2.50-inch pipe. The primary system may be filled by opening isolation valve IV-4 to vent air. Deionized water is used to fill the primary system through valves IV-1 and IV-2. The level in the accumulator is adjusted during filling by venting through valve CV-6. This valve can also be used to lower system pressure during warming and expansion of the system water. The system may be drained through valves IV-1 and IV-3 and other valves on the pump and accumulator.

4.5 Instrumentation

Instrumentation for the PRHR HX testing (see Figure 4-8) includes thermocouples to register temperature in and on the HX tubes, in the secondary-side tank water, and in primary heating and circulating system; pressure transducers for primary system pressure and flow through standard orifices

and water levels in the accumulator and tank; a flowmeter for steam flow from the tank; and a watt meter to register heater input power. The specific instruments are presented in Table 4-1.

4.5.1 Thermocouples

Two types of thermocouples are used:

- Chromel-alumel double-precision (type KK) ungrounded junction in 304 stainless steel sheaths with double-precision extension wires for high fluid temperatures in the primary system and HX tubes

- Copper-constant double-precision (type TT) ungrounded junction in 304 stainless steel sheaths with double-precision extension wires for low fluid temperatures in the secondary water tank

The outer and middle HX tubes are instrumented with 0.032-inch sheath diameter thermocouples. There are 14 thermocouples inside each tube, 12 of which are mounted on a 3/32-inch diameter support rod, and 2 are installed at each end of the tube, measuring the inlet and outlet fluid temperatures. The thermocouples measuring the test tube fluid temperature are spaced 1.5 feet apart and are tied to the inside support rod, which is centered within the tube with 1/16-inch stainless steel strips 1/2-inch wide and 5/8-inch long that are tack-welded to the 3/32-inch rod at 1.5-foot intervals. The rod protrudes through and is welded to the 90-degree elbow at the top of the tube.

The vertical locations of these thermocouples are tabulated in Table 4-2. Seven thermocouples are led to the top of each tube, and seven are led to the bottom. At each end, they pass through special high-pressure seals that are semi-elastic disks, with holes for the thermocouples, compressed between pressure plates having similar holes and keyed to the body of a fitting whose screw cap provides the compression. Each fitting is threaded into tees at the ends of the HX tubes where the thermocouples are routed to and through the tank wall via swage-type tube connectors, into which they are soldered. The tube connectors are threaded into circular plates that are part of blind flanges mounted in 8-inch diameter flanges on the tank. The connectors are installed to be flush with the inside radius of the tank. The thermocouple penetrations are located 14 inches from the bottom of the tank and 19 feet from the bottom of the tank.

Thermocouples are also mounted near the outside surface of the tubes in machined grooves. The transverse grooves are 0.40 inches long and 0.025 inches deep and are spaced 1.5 feet apart. To assure that the tube integrity is not jeopardized at the test conditions, samples of the tube, with machined grooves, were pressurized and ruptured. In addition, a finite element analysis of the grooved tube was performed to determine whether the grooves would limit the primary fluid operating pressure. No effect of the groove on the tube strength was noticed. The tip of an 0.020-inch sheathed thermocouple is inserted into the 0.025-inch x 0.025-inch groove and brazed over with silver solder (melting temperature near 1000°C), thus restoring the tube surface to its original configuration and avoiding the impact of the boiling regime on the tube surface. The sheathed thermocouples are

mounted closer to the outside tube surface rather than to the bottom of the groove. There are 12 thermocouples on each tube, spaced 1.5 feet apart, at the elevations tabulated in Table 4-2. The thermocouple leads are routed to a 3/8-inch diameter support tube, 2.50 inches in front of the line of tubes at the tank wall. Half the thermocouple leads are routed to the top and half to the bottom of the HX where they pass through the tank wall in pressure-sealed fittings mounted in blind flanges on the tank wall.

The tank water temperatures are measured with 120 copper-constantine, 0.032-inch diameter stainless steel sheath thermocouples. The thermocouple elevations are shown in Table 4-3, and the lettered locations are illustrated in Figure 4-4. The thermocouples at locations "C" and "D" in the central part of the tank are fastened to two 1/4-inch stainless steel rods, 30 feet long, hooked onto U bolts welded to the bottom of the tank and fastened to a 2-inch angle spanning the uppermost baffle flange at the top. The thermocouples, 11 at each location, penetrate the tank wall soldered into 1/4-inch tubes held by swage-type tube connectors screwed into 1/4-inch pipe half couplings welded into the vessel 23 inches below the top. All the other thermocouples at locations "E," "F," "G," "H," "J," and "K" are held in place 2.25 inches inside the tank wall by 1/8-inch tube stubs. The thermocouples are soldered into tubes that penetrate the vessel wall with a swage-type tube connector in a 1/8-inch pipe half coupling welded at a total of 98 locations.

All thermocouple wires are led down or up thermocouple lead channels to a cable tray just below the first work platform and from there into the laboratory building.

Three additional 1/16-inch sheathed thermocouples are used to traverse tank water temperatures near the outer HX tube at three elevations, just below the lower two viewing ports and just above the third one. Figure 4-9 shows the installation of these rotating traverse thermocouples and the indicator for manually traversing. Data channels are listed in Table 4-3.

4.5.2 Flowmeters

Flow is measured at the outlet of each of the HX tubes by measurement of the differential pressure across precision orifices. The orifices are mounted in 0.75-inch, Schedule 80 pipe welded ring type orifice flanges equipped with flange taps (see Figure 4-10) having a minimum of 12 inches of straight length upstream and 10 inches downstream of the orifice surfaces. Three sets of orifices are used to accommodate the full range of flows required during the test program (see Table 6-2 in Section 6.0 of this document). The pressure drops across the orifices are measured with Foxboro and Honeywell differential pressure transducers (channels 182, 187, and 188) calibrated to 0 to 107 inches of water for the two larger orifices and 0 to 30 inches for the small orifices. The Honeywell differential pressure transducer (channel 188) was replaced for the small orifice tests. The pressure transducers are specified to have an accuracy of ±0.25 percent of full scale. The calibration correlations and data reduction are presented in Section 6.0.

The vapor flow exiting from the tank is monitored with a 3-inch Foxboro vortex flowmeter. The total mass flow rate out of the vessel is only an indication, since the exit temperature and pressure are not recorded at the meter and the sensor calibration was in terms of mass flow rate under saturated conditions at 2 psig.

4.5.3 Pressure and Level Gauge

The primary system pressure is measured (channel 180) at the inlet of the HX tubing by a Rosemont pressure transducer with a range of 0 to 2500 psig.

Differential pressure transducers are used to monitor the water level in the accumulator (chan... and the tank (channel 184). The transducers are calibrated to ranges of 0 to 207 inches and 0 to 415 inches of water, respectively. An additional differential pressure transducer (Foxboro) measures the pressure drop across the primary system pump (channel 185) and is calibrated over the range of 0 to 250 psi.

The pressure transducers indicated above are specified to have an accuracy of ±0.25 percent of full scale.

4.5.4 Wattmeter

The heater power is controlled by two silicon controlled rectifier (SCR) controllers. A combination wattmeter and watt-hour meter measures combined power to the two sections of the 350 kW high-pressure water heater. The meter is rated for three-phase, three wire circuits (delta) having 0 to 480 volts and 0 to 500 amperes. The watt meter range is 0-500 kW for an output signal of 0-10 volts that is recorded on channel 200. The watt-hour meter range is 0-500 kWh and above that it resets to zero. The watt-hour meter (channel 201) has a 0 to 10 volt output signal registered on channel 201. The meter is located inside the laboratory building. Voltage leads are connected to the power input wires in the heater control cabinet at the side of the test HX. Current transducers are on two of the input power leads in the heater control cabinet.

4.5.5 Data Acquisition and Recording

All instrumentation is connected to a model 2240 John Fluke Mfg. Co. Data Logger, using a low level scanner with 3 pole low thermal-emf reed relays and a high performance A/D converter using dual slope integration over 5 line cycles (slow speed, 3 readings per second) or 1 line cycle (fast speed, 15 readings per second). Accuracy is 0.01 percent of reading plus 0.008 percent of range. Resolution for either type K or T thermocouples is 0.1°F in the 32°F to 750°F range. Isothermal blocks are used and provide a maximum 0.1°F gradient between any terminals and 0.01°F reference junction stability. Digital data are transmitted for storage and retrieval to a personal computer with hard disk and for eventual recording on diskettes. The recorded information includes data and time of scan, channel number and temperatures (°F or °C), and voltages, as programmed in the Data Logger. The data

acquisition system is shown in Figure 4-11. The Data Logger is rack-mounted with its channel increasing expander chassis. A video display terminal is used to observe data during testing.

4.6 Testing Procedures

Prior to testing the following steps are followed:

Initial filling of the tank - Close isolation valves IV-5, 6, 7, and 9; open IV-8 to fill; monitor tank level, channel 184, until test level is achieved; close IV-8.

Filling and pressurizing the primary system - Open high point vent valve, IV-4; close accumulator vent valve, CV-6; verify that CV-1, 2, 3, 4, and 5 are not closed; when water comes out at IV-4, close IV-4; monitor water level in the accumulator, channel 183, and fill to 50 inches; close fill valves IV-1 and 2; bleed air from all pressure transducers and the pump; set nitrogen pressure regulator, CV-7 to 200 psig +/-15 psig; turn on pump for 2 minutes, then stop pump; recheck accumulator level and open high point vent valve IV-4 to vent air from system; assure that at least 45 +/-5 inches of water is in accumulator; reset nitrogen pressure regulator to 500 +/-15 psig.

Primary system heat-up - Turn on pump and verify it is running properly; verify proper accumulator pressure and water level; set water temperature controller to 460°F; turn on water heater; monitor primary system temperature and pressure as it heats, channel 179 for heater outlet temperature and channel 180 for system pressure; start taking data at appropriate conditions; if test requires higher temperature, reset controller and raise accumulator pressure accordingly to prevent boiling using information from steam tables.

Before beginning a test, prerequisites are to be performed. These include the following:

1. Record test parameters including test ID number, number of flowing HX tubes, tube flow rate and inlet temperature.

2. Check and verify the current revision of the test procedure, that instruments to be used are calibrated, that all instrumentation is functioning, accumulator water level is 45 +/-5 inches and accumulator pressure is at least 500 +/-15 psig, and that secondary tank water level is as required.

3. Ve[illegible] pump is on and set control valves for active tubes.

4. Adjust CV-4 and CV-5 to produce required flow in primary circuits.

5. Balance tube flows to +/-0.3 gpm.

6. Name the data acquisition record output file with the test ID number.

During a test, the following instructions are followed for four types of tests:

A. Transient Tests

1. Set conditions required for the test identified. Close CV-4 and preheat primary water to the required temperature.

2. Assure that tank level is set to 24 feet + 0.5 feet and that all tank thermocouples read < 120°F.

3. Open valve CV-4 and start Data Logger at 1-minute intervals.

4. At 20 minutes into test, set Data Logger at 5-minute intervals.

5. Monitor system parameters until tank has reached bulk boiling. This is defined as when all thermocouples except Nos. 75, 94, 113, and 132 are 212°F +/- 5°F.

B. Steady-State Tests

1. Set conditions required for the test identified.

2. Once steady-state bulk boiling is attained, assure tank level is 24 feet + 0.5 feet. Take 10 continuous sets of data. Steady state is defined as when all thermocouples except Nos. 75, 94, 113, and 132 are at 212°F +/- 5°F. (Record the maximum primary inlet temperature for this test).

3. Reduce primary inlet temperature to the next multiple of 50°F. Once the tube outlet temperature remains constant (+1°F over 1-minute interval), take 10 continuous sets of data. Repeat until all inlet temperatures have been tested.

4. Record all inlet temperatures that have been used in the test.

C. Uncovery Tests

1. Set required tank level conditions for the specified test.

2. Set inlet temperature to 600°F. Heat tank up to bulk boiling. Once the desired tube inlet temperature has been attained and the tube outlet temperatures remain constant (+1°F over 1-minute interval), take 10 continuous scans.

3. Set inlet temperature to 500°F. Once the desired tube inlet temperature has been attained and the tube outlet temperatures remain constant (+1°F over 1-minute interval), take 10 continuous scans.

4. Set inlet temperature to 400°F. Once the desired tube inlet temperature has been attained and the tube outlet temperatures remain constant (+1°F over 1-minute interval), take 10 continuous scans.

D. Plume Tests

1. Set required conditions for this test. Heat tank up to bulk boiling.

2. Rotate each of three traverse thermocouples until maximum temperature is observed by the tank thermocouple being rotated.

3. Record temperature and thermocouple position where maximum tank temperature was observed for all three traverses.

After each test has been completed, the following procedures are performed to properly collect and store the data:

1. Computer files are examined to ensure that the data have been written to the correctly named file.

2. Data file was copied to a floppy diskette (to backup the data on the hard disk).

3. The floppy diskette is examined to ensure that the file has been written to the floppy diskette.

TABLE 4-1
LIST OF INSTRUMENTS

Location Transducer I.D.	Type of Transducer	Make/Model	Range	Manufacturer's Specified Accuracy	Standard Deviation of Calibration Correlation
Fluke DAS		Model 2240 SN 2385069	80 to 400 mV	±(0.02% reading + 0.015% range + 7 μV)	±0.02 mV
			0 - 40 volt	±(0.02% reading + 0.015% range + 7 μV)	±0.006 volts
			Thermocouple	±0.8°F (0.5°C)	±0.6°F (±0.5°C)
Thermocouples					
Channel 1 to 52 Channel 173 to 179 Channel 190 to 193	Thermocouple (Type KK)	Marlin double precision	N/A	±2°F (±1.1°C)	
Channel 53 to 172	Thermocouple (Type TT)	Marlin double precision	N/A	±2°F (±1.1°C)	
Pressure Transducers					
Channel 180	Pressure (Piezoresistive)	Rosemont 1GP9E22M1 SN 403727	0 - 2500 psig	±0.25% of full scale	2.2 psig
182[1]	Pressure (Piezoresistive)	Foxboro 843D SN 23530	0 - 107 in. H_2O	±0.25% of full scale	0.01 in H_2O
183	Pressure (Piezoresistive)	Foxboro SN 23528	0 - 207 in. H_2O	±0.25% of full scale	in. H_2O
184	Pressure (Piezoresistive)	Foxboro SN 23527	0 - 415 in. H_2O	±0.25% of full scale	0.14 in H_2O
185	Pressure (Piezoresistive)	Foxboro SN 23529	0 - 250 psig	±0.25% of full scale	0.16 psi
187[1]	Pressure (Piezoresistive)	Foxboro SN 20934	0 - 107 in. H_2O	±0.25% of full scale	1.04 in. H_2O
188	Pressure (Piezoresistive)	Honeywell SN 23561	0 - 107 in. H_2O	±0.25% of full scale	0.03 in H_2O

TABLE 4-1 (Continued)
LIST OF INSTRUMENTS

Location Transducer I.D.	Type of Transducer	Make/Model	Range	Manufacturer's Specified Accuracy	Standard Deviation of Calibration Correlation
188 (after 10/20/90)	Pressure (Piezoresistive)	Honeywell SN 23807	0 - 30 in. H_2O	±0.25% of full scale	0.19 in H_2O
Flow Meters					
189	Vortex flowmeter	Foxboro SN 5422879	180 - 3170 lb/hr	±0.5% of full scale	
Watt Meters					
200	Watt-hour meter	S/N 2570	0 - 500 kw	±0.5% of full scale	
201	Watt-hour meter	S/N 2570	0 - 500 kwh	±0.5% of full scale	

Notes:

(1) Sensor range adjusted to 0-30 inches of water after October 20, 1990.

TABLE 4-2
THERMOCOUPLE LOCATIONS IN CENTER AND ON SURFACE OF PRHR HEAT EXCHANGER TUBES

	Thermocouple No. & Channel			
Elevation from Bottom of Tank (inches)	Outer Tube Fluid	Middle Tube Fluid	Outer Tube Surface	Middle Tube Surface
236	14	28		
230	13	27		
221			40	52
212	12	26		
203			39	51
194	11	25		
185			38	50
176	10	24		
167			37	49
158	9	23		
149			36	48
140	8	22		
131			35	47
122	7	21		
113			34	46
104	6	20		
95			33	45
86	5	19		
77			32	44
68	4	18		
59			31	43
50	3	17		
41			30	42
32	2	16		
23			29	41
12	1	15		

TABLE 4-3
THERMOCOUPLE LOCATIONS IN SECONDARY SIDE TANK OF PRHR HEAT EXCHANGER

Position	Azimuthal Location
C	90°, 4 in. outside baffle in line with tubes
D	Center of tank
E	74°, inside baffle, 5.0 in. behind tubes
F	98°, inside baffle, 3.0 in. in front of tubes
G	106°,inside baffle, 6.0 in. in front of tubes
H	123°, inside baffle, 12.4 in. in front of tubes
J	205°, inside baffle, 43.2 in. in front of tubes
K	325°, inside tank, 2.25 in. from wall, 20.6 in. from baffle

TABLE 4-3 (Continued) THERMOCOUPLE LOCATIONS IN SECONDARY SIDE TANK OF PRHR HEAT EXCHANGER								
	Thermocouple No. & Channel							
Elevation from Bottom of Tank (inches)	C	D	E	F	G	H	J	K
336	63	74	93	112	131	150	161	172
312	62	73	92	111	130	149	160	171
287	61	72	91	110	129	148	159	170
275	60	71	90	109	128	147	158	169
257			89	108	127	146		
239	59	70	88	107	126	145	157	168
221			87	106	125	144		
203	58	69	86	105	124	143	156	167
185			85	104	123	142		
167	57	68	84	103	122	141	155	166
149			83	102	121	140		
131	56	67	82	101	120	139	154	165
113			81	100	119	138		
95	55	66	80	99	118	137	153	164
77			79	98	117	136		
59	54	65	78	97	116	135	152	163
41			77	96	115	134		
23	53	64	76	95	114	133	151	162
5			75	94	113	132		

TABLE 4-4 ADDITIONAL INSTRUMENTATION OF PRHR HEAT EXCHANGER TEST	
Data Channel	**Thermocouples**
173	Water in outer HX tube outlet
174	Water in middle HX tube outlet
175	Water in inner HX tube outlet
176	Water at bottom of accumulator
177	Water at inlet to HX inlet manifold
178	Steam venting from tank in vent pipe
179	Water at heater outlet
Level and Flowmeter Transducers (80 - 400 mV. range)	
181	Primary system pressure
182	Outer HX tube orifice flowmeter pressure difference, FM-1
183	Accumulator level, differential pressure
184	Tank level, differential pressure
185	Pump pressure rise, differential pressure
187	Middle HX tube orifice flowmeter pressure difference, FM-2
188	Inner HX tube orifice flowmeter pressure difference, FM-3
189	Tank steam vent vortex flowmeter output
Thermocouples	
190	Lower traverse in tank water
191	Middle traverse in tank water
192	Upper traverse in tank water
193	Primary return flow from HX near pump
Wattmeter (0-10 Volts)	
200	Heater supply power (kW)
201	Heater supply energy (kWh)

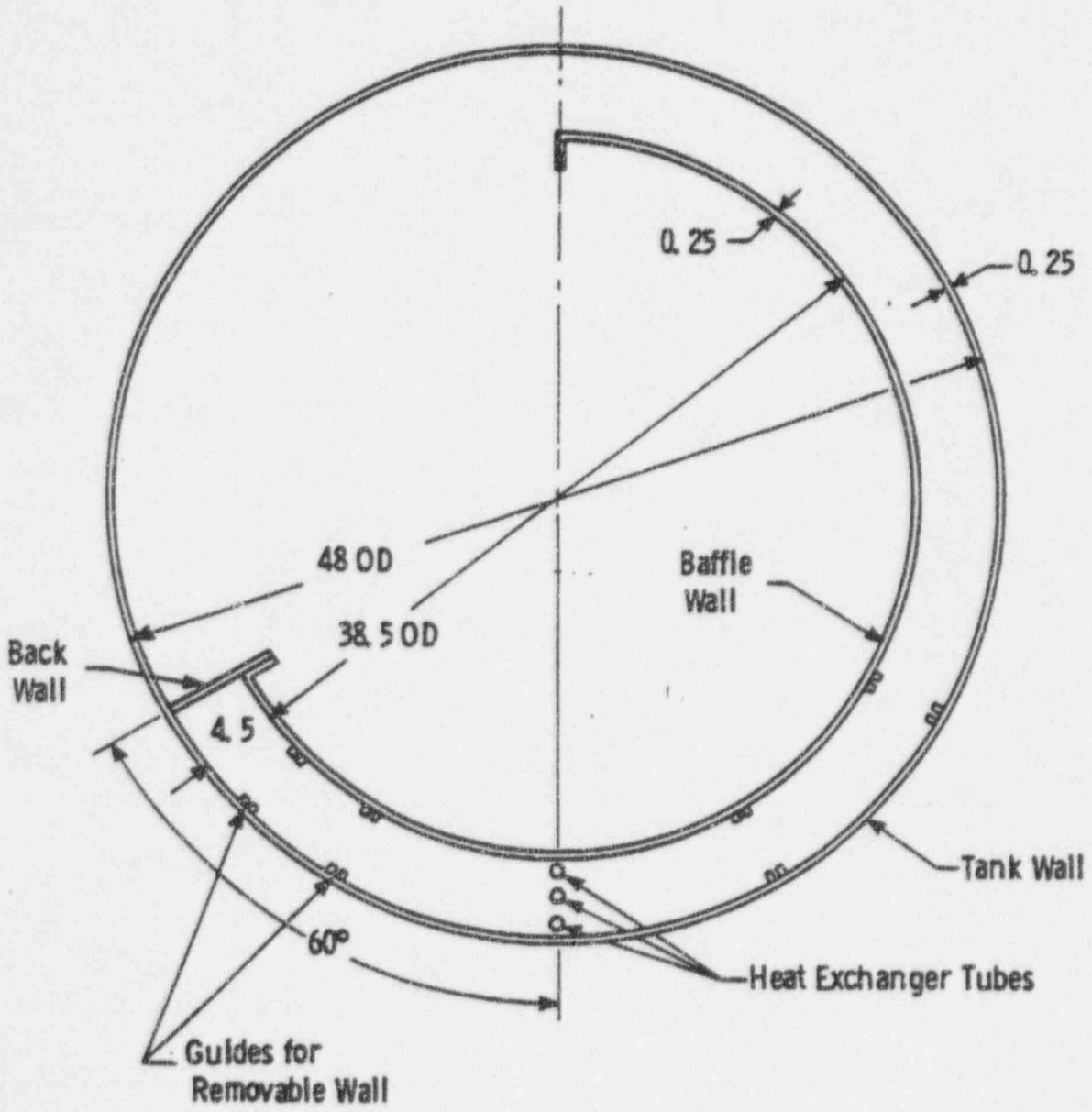

Figure 4-1 Plan View of the Passive Residual Heat Removal Heat Exchanger Test Section

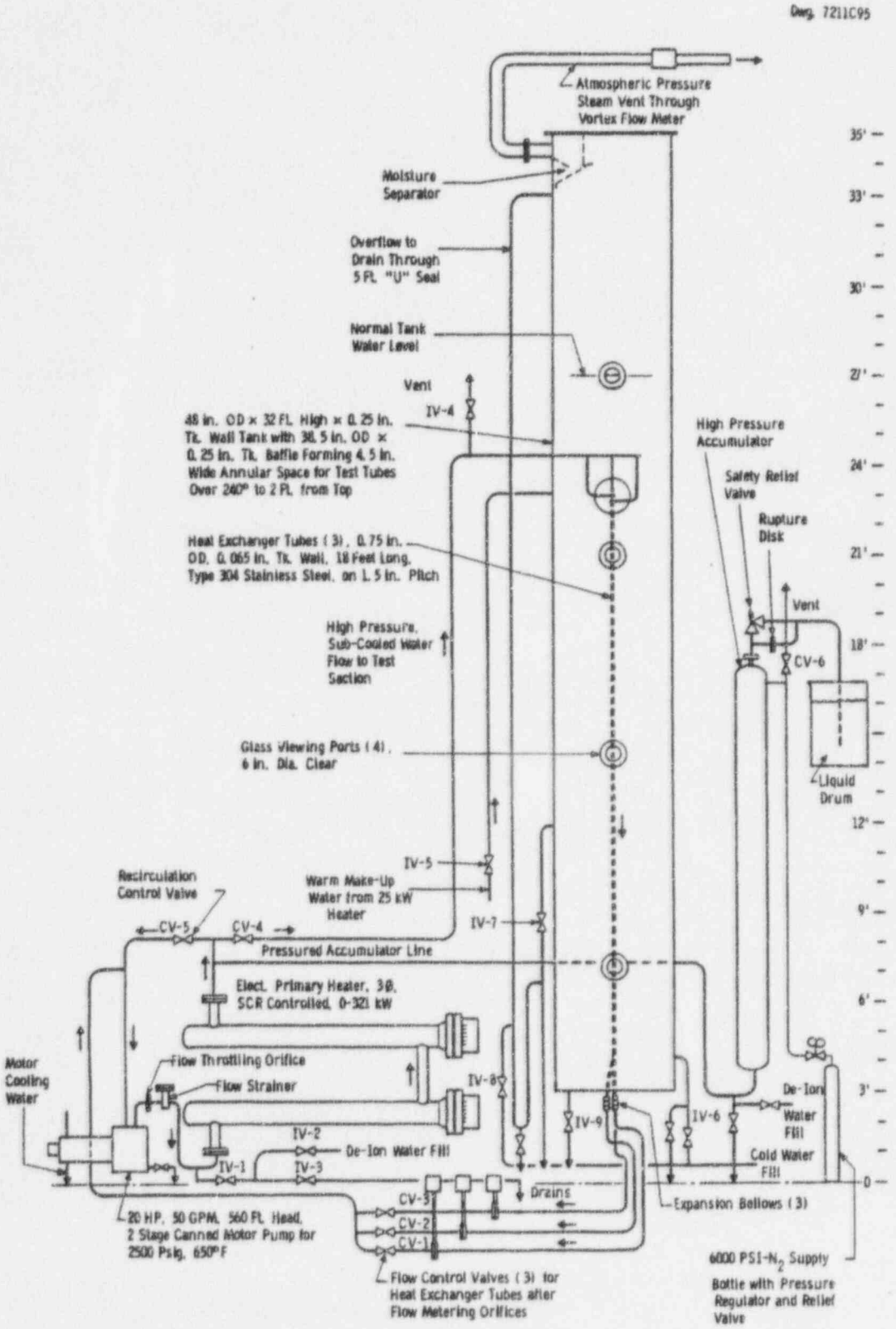

Figure 4-2 Passive Residual Heat Removal Heat Exchanger Test Facility

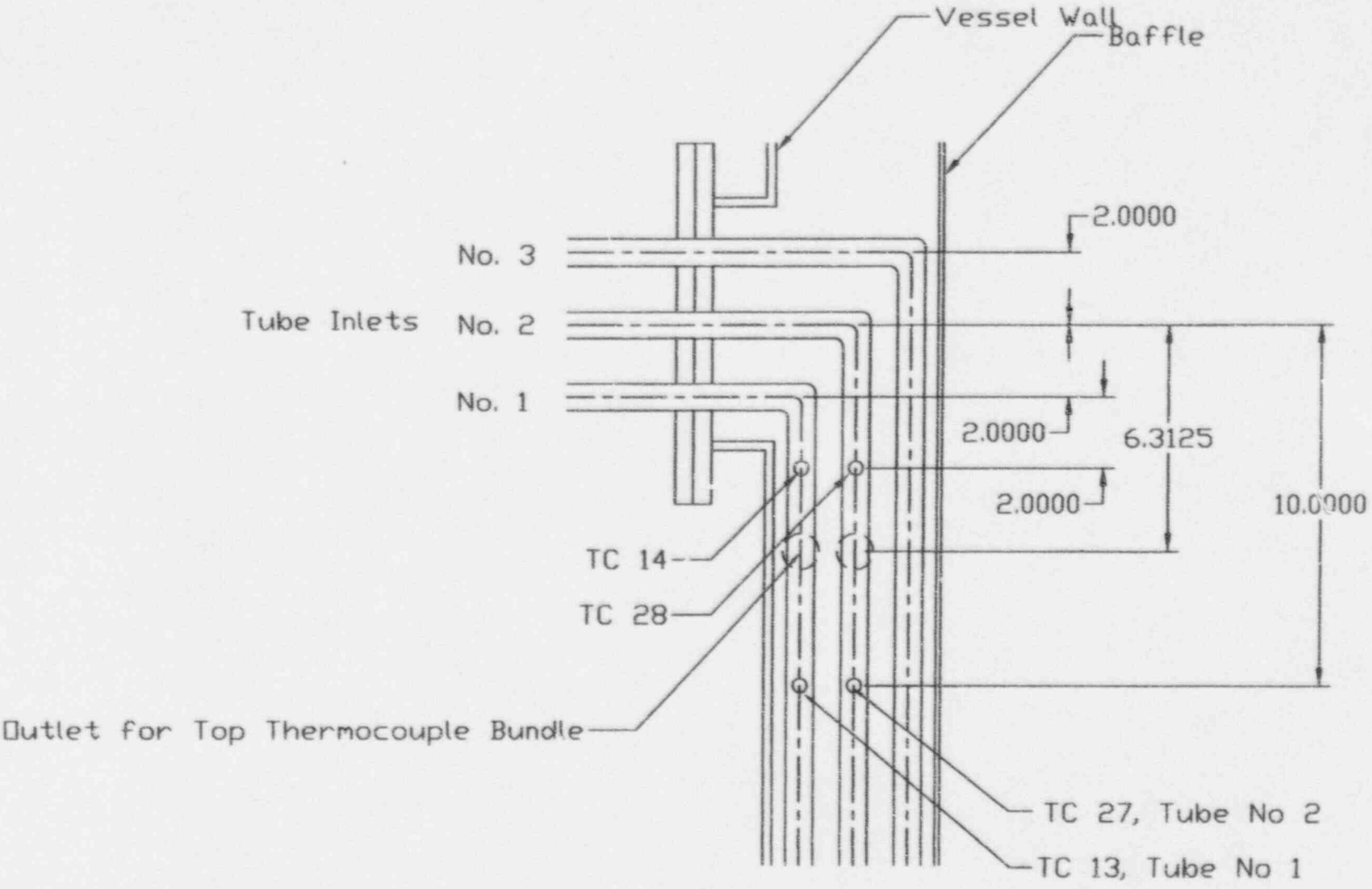

Figure 4-3 PRHR Inlet Configuration and Thermocouple Location

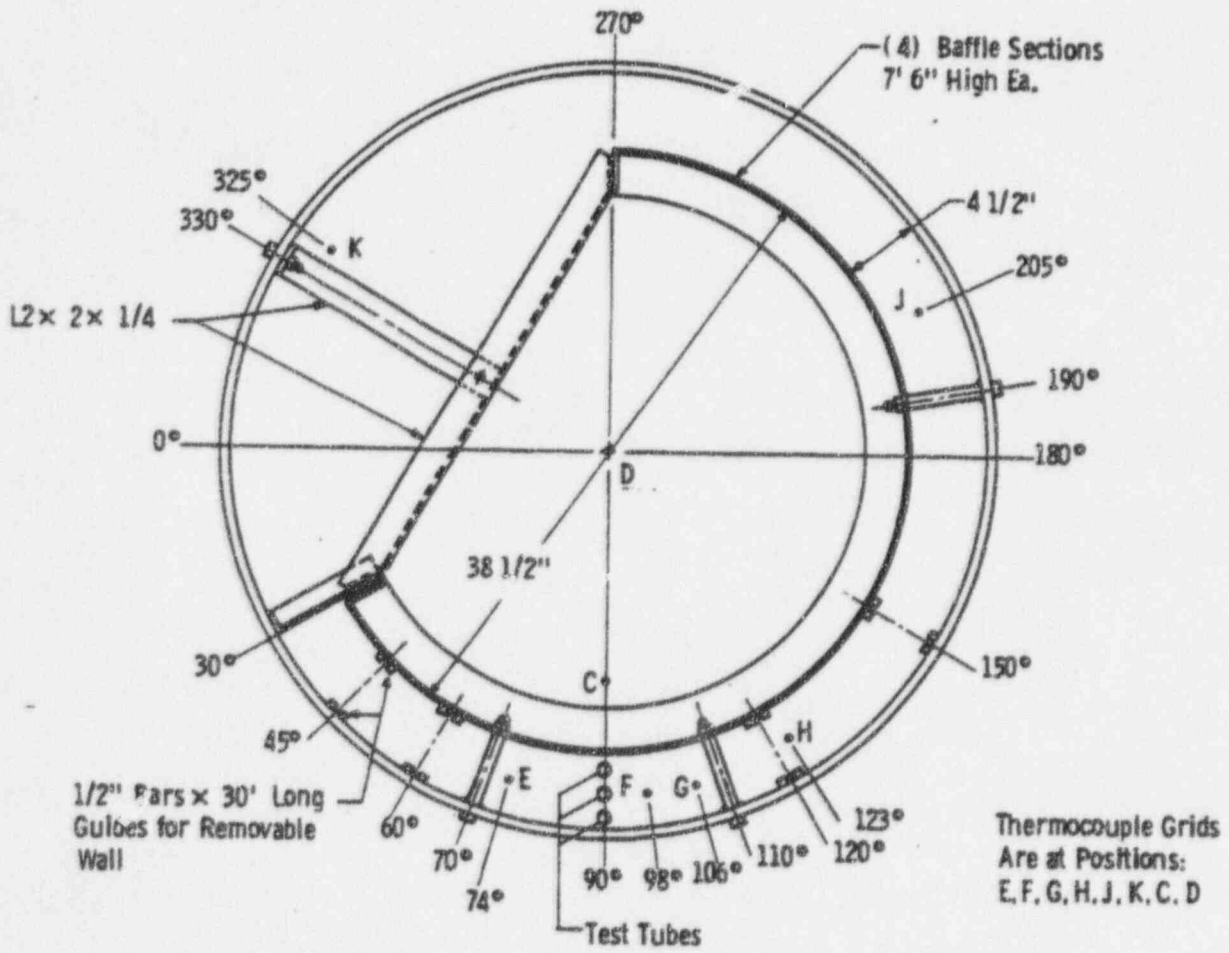

Figure 4-4 Detailed Cross-Section View of Test Heat Exchanger

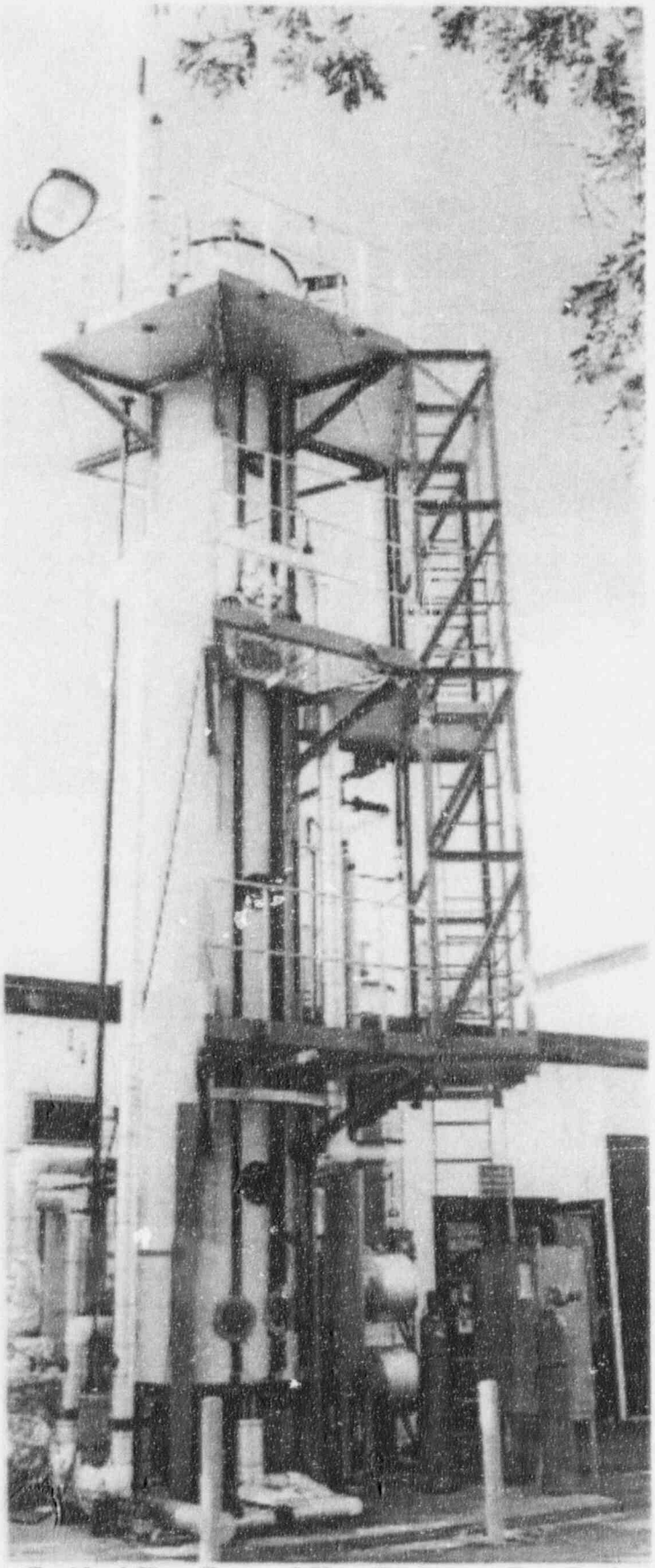

Figure 4-5 Passive Residual Heat Removal Heat Exchanger Test Tank and Work Platforms

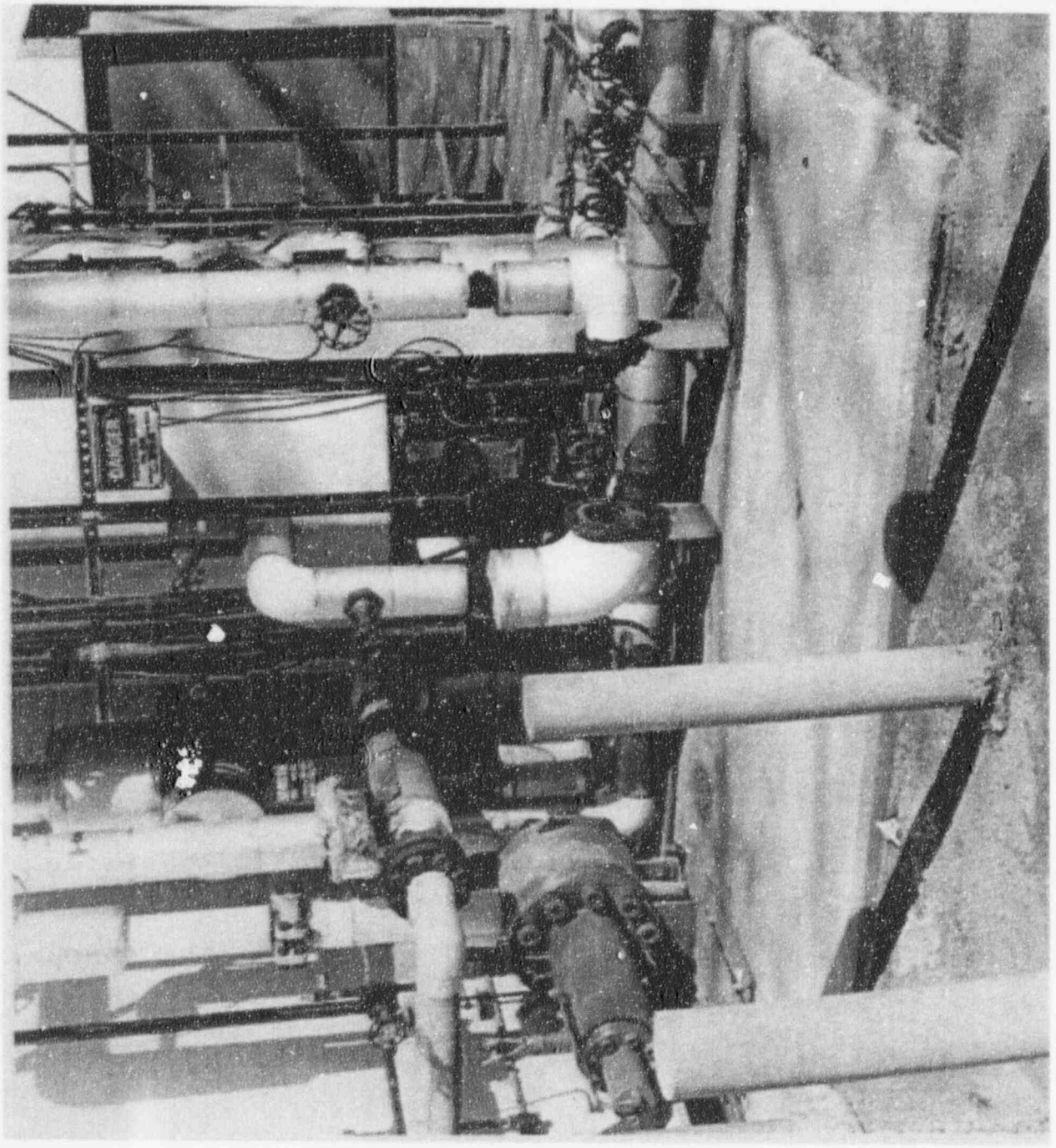

Figure 4-6 Passive Residual Heat Removal Heat Exchanger Primary Circuit Pump Shown on Left, Tank in Middle, Exchanger Tube Return Lines on Right on Top of Foundation

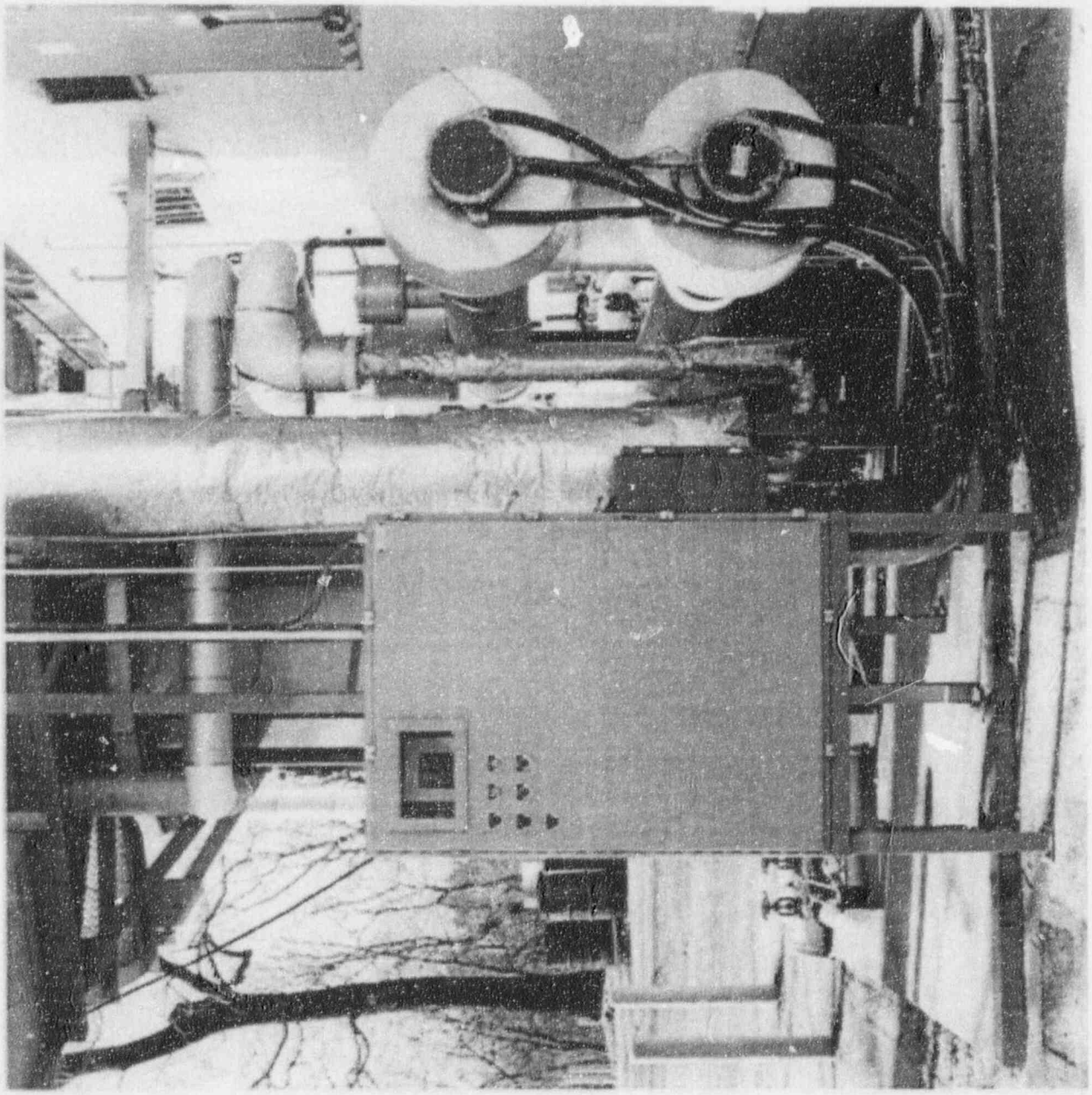

Figure 4-7 High-Pressure Electrical Heater and Power Control Cabinet

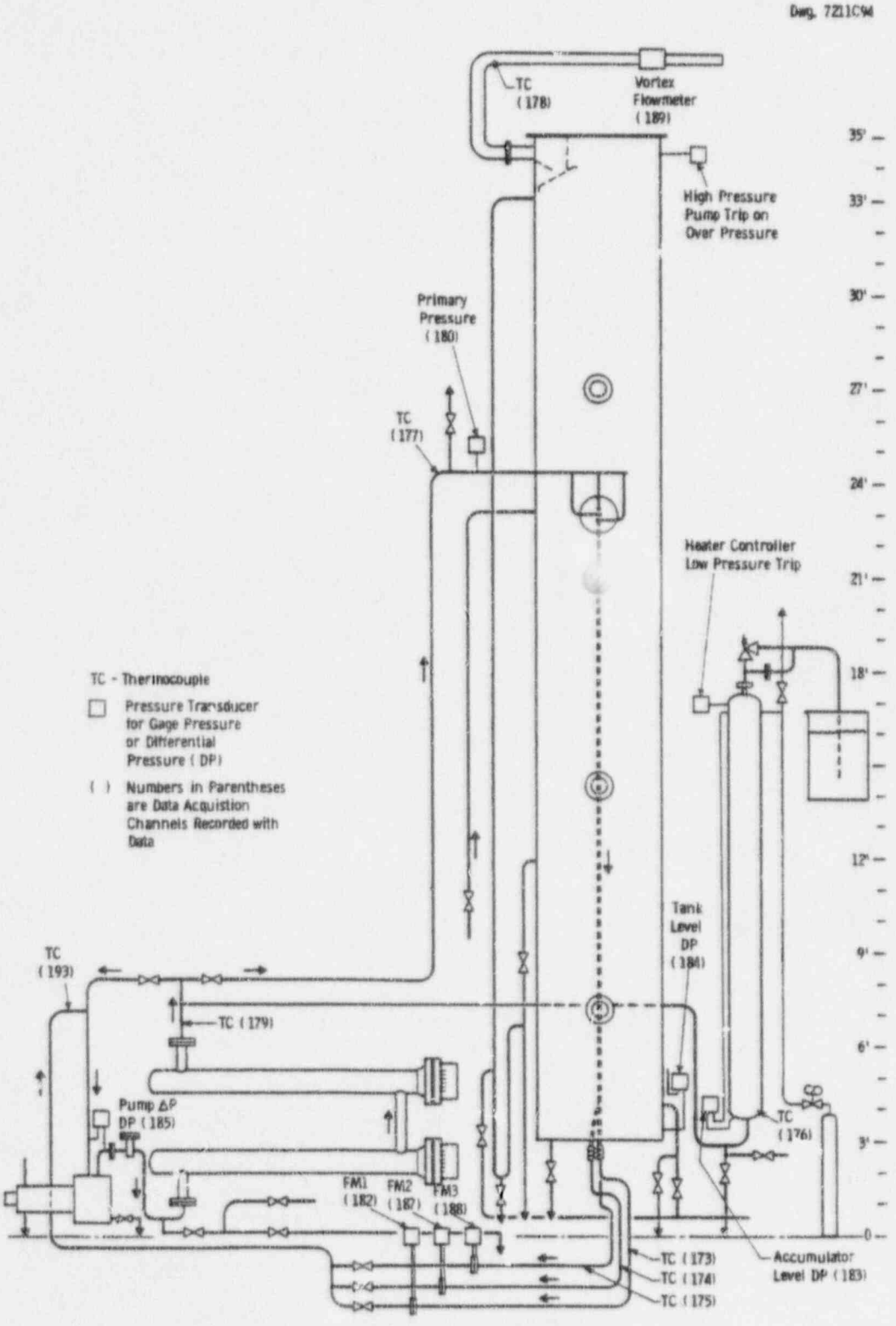

Figure 4-8 Instrumentation Outside the Heat Exchanger

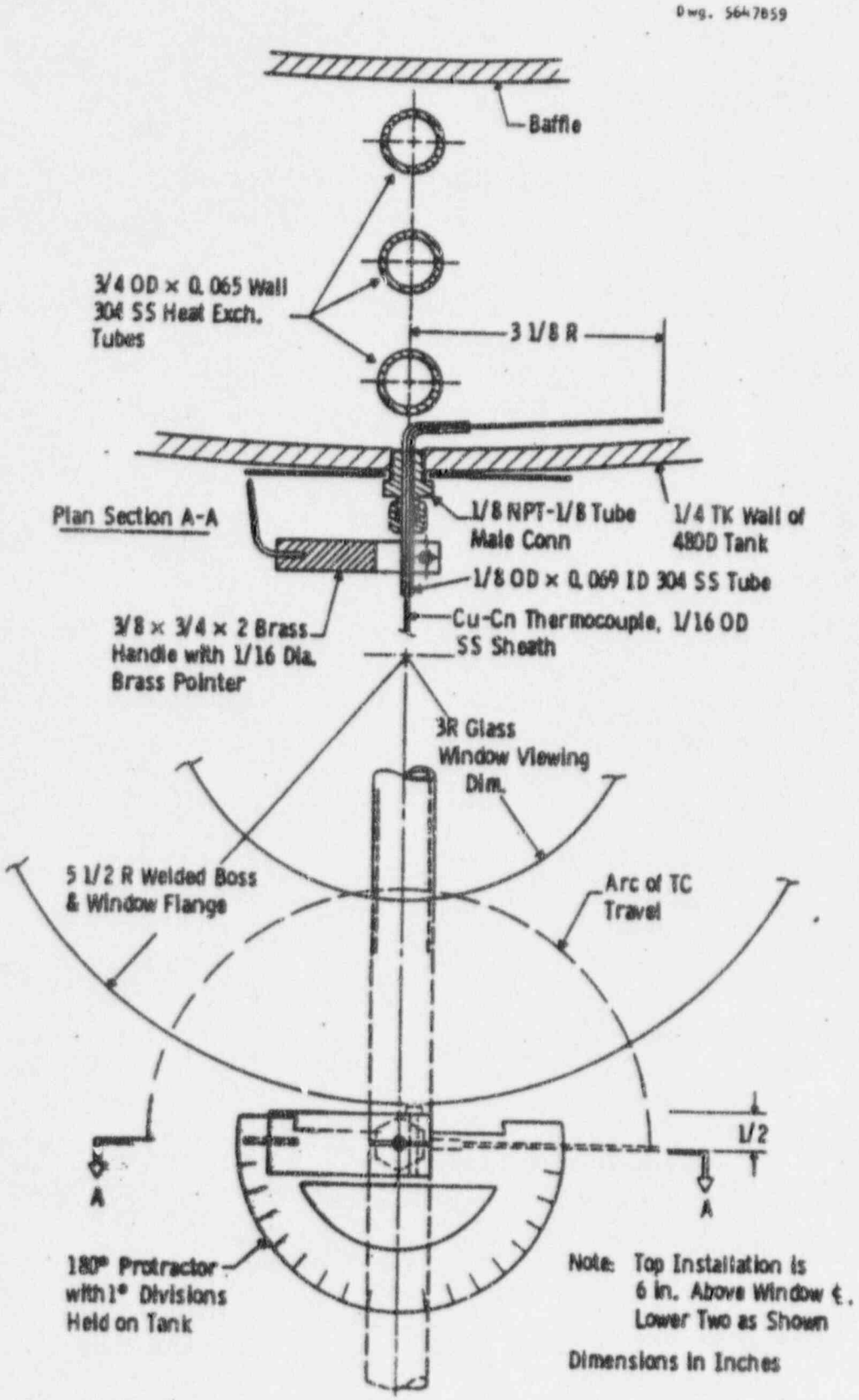

Figure 4-9 Rotating Thermocouple Traverses (3)

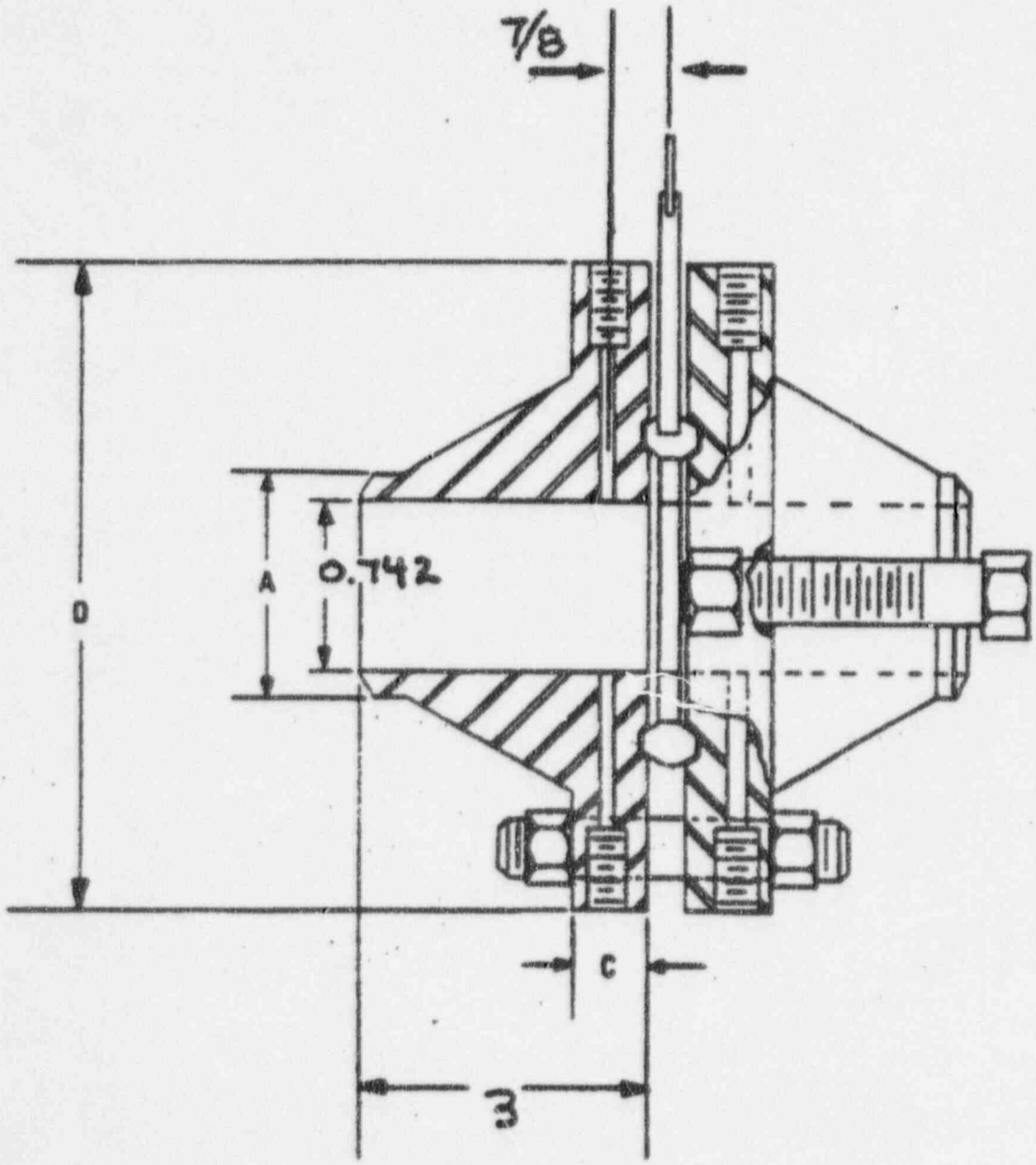

Figure 4-10 Orifice Assembly

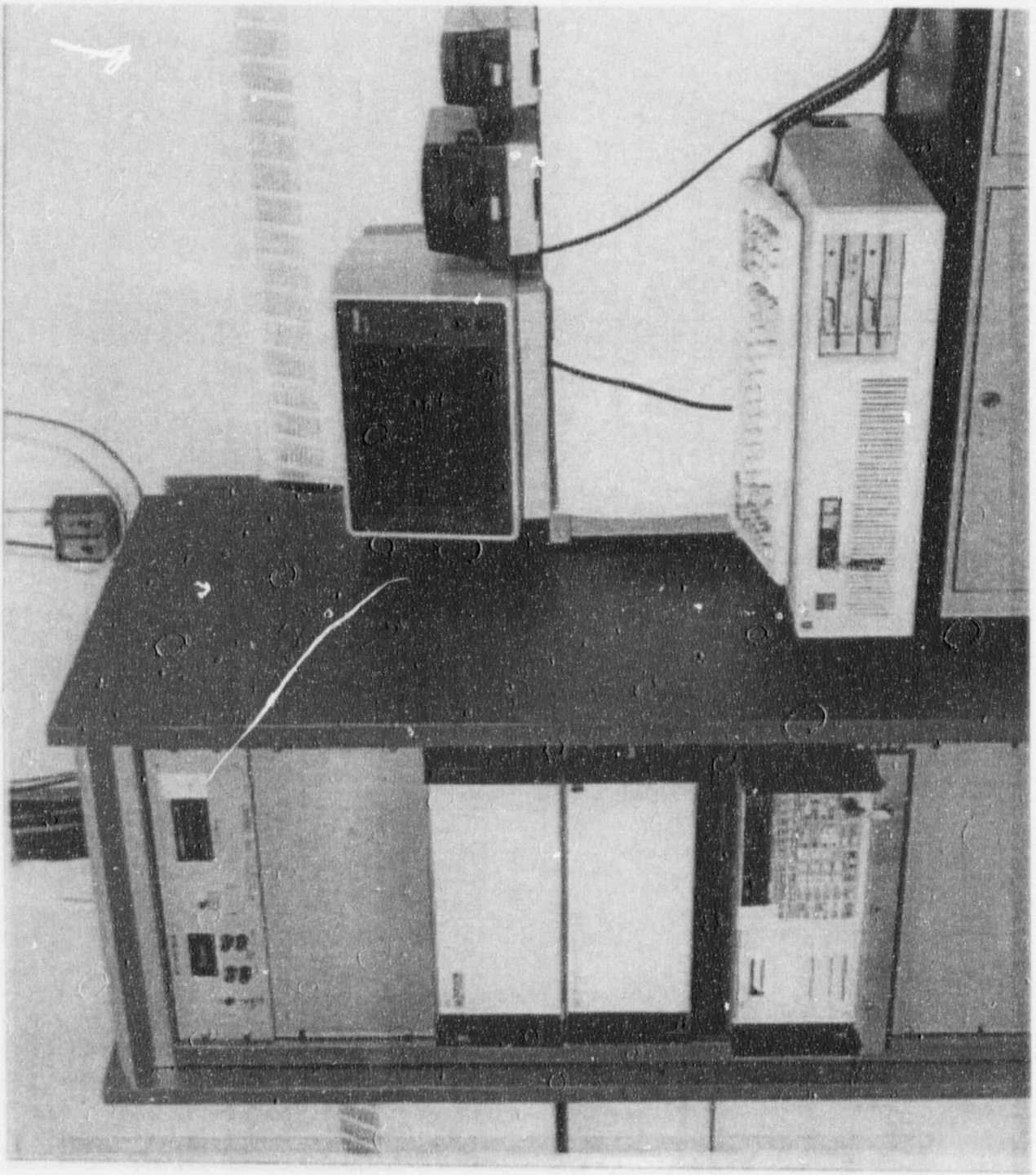

Figure 4-11 Data Acquisition and Recording Equipment

5.0 TEST MATRIX AND DESCRIPTION

The test matrix for both the phase I tests (performed in 1989) and the Phase II tests (performed in 1990) are included in Table 5-1. The test matrix consists of five types of tests as specified below:

Transient Tests – These tests were performed to determine the tank mixing behavior for various combinations of tube flow rate and inlet temperature. Transient tests were also performed to verify a correlation for the free convection heat transfer mechanism that occurs when the tank is subcooled.

Transient tests were performed by heating up the tank from ambient conditions to boiling with a fixed tube inlet temperature and tube flow rate. Data were initially recorded at short intervals (1 minute) for 20 minutes and then recorded at longer intervals (5 minutes) until the tank reached bulk boiling. Bulk boiling is defined as when all tank thermocouples at a level above the lowest tube primary side or wall thermocouple had readings of 212°F +/- 5°F.

Steady-State Tests – These tests were performed to develop the passive residual heat removal (PRHR) heat exchanger (HX) heat transfer correlation. Typically the tank was heated to boiling by using the pump, heater, and HX tubes. Once the tank bulk temperature was 212°F, the test was started. A tank bulk temperature of 212°F was defined as when all tank thermocouples at a level above the lowest tube primary side or wall thermocouple had readings of 212°F +/- 5°F.

After bulk boiling was achieved, the flow through the HX tubes was set by throttling the appropriate valves. The tank level was verified and makeup to the tank was provided if needed to re-establish the correct tank level. There were 10 data scans taken at each specified inlet temperature until the full range of inlet temperatures was covered. The range of inlet temperatures for each test is from a maximum of 650°F to 250°F at 50° intervals. The maximum inlet temperature for each test varied depending on the total tube flow rate due to the limited capacity of the heater.

Plume Tests – The purpose of these tests was to determine characteristics of the water-steam plume that exists around the HX tubes. These tests were conducted by heating the test tank up to boiling at a selected PRHR tube inlet temperature and flow rate. Once bulk boiling was achieved, the rotating thermocouples located at the three specified elevations were rotated to determine the physical dimensions of the plume at each elevation.

Configuration Tests – These tests were performed to confirm the applicability of the test results to the final PRHR physical configuration.

Configuration parameters tested included:

- Distance of the HX to the IRWST wall
- Distance between rows of tubes
- Water level above the tubes

Configuration tests were first run as transient tests and performed by heating up the tank from ambient conditions to boiling with a fixed tube inlet temperature and tube flow rate. Data were initially recorded at short intervals (1 minute) for 20 minutes and then recorded at longer intervals (5 minutes) until the tank reached bulk boiling. Bulk boiling is defined as when all tank thermocouples at a level above the lowest tube primary side or wall thermocouple had readings of 212°F +/-5°F.

At this point, plume data were taken as described earlier. Finally, the configuration tests were run as steady-state tests. There were 10 readings taken at each specified inlet temperature until the full range of inlet temperatures were covered. The range of inlet temperatures for each test was from a maximum of 650°F to 250°F at 50° intervals.

Uncovery Tests – These tests were performed to determine the thermal performance of the HX with the tank water level lowered to uncover the HX tubes. These tests were run with water levels equivalent to the top of the tubes, 25-percent tube uncovery, 50-percent tube uncovery, 75-percent tube uncovery, and 100-percent tube uncovery. The uncovery tests were run as steady-state tests with the tank level and tube inlet temperature held constant and the tank level set at the discreet levels. There were 10 data scans taken at each elevation for each test.

TABLE 5-1
PASSIVE RESIDUAL HEAT REMOVAL HEAT EXCHANGER TEST MATRIX

Phase I Tests

Steady-State Tests

Test	Flow/Tube	No. of Tubes	Inlet Temperature
SS3	5 gpm	3	425°F – 250°F
SS4	6 gpm	3	425°F – 250°F
SS5	7 gpm	3	425°F – 250°F
SS6	9 gpm	3	400°F – 250°F
SS7	10 gpm	3	400°F – 250°F

Transient Tests

Test	Flow/Tube	No. of Tubes	Inlet Temperature
TR1	7 gpm	3	417°F
TR4	9 gpm	3	405°F
TR7	6 gpm	3	420°F
TR11	6 gpm	1	630°F

Phase II Tests

Plume Tests

Test	No. of Tubes	Flow per Tube	Inlet Temperature	Comments
P01 (R)[1]	3	3 gpm	Max	Rotate TC 0-180°
P02 (R)	1	3 gpm	600°F	Rotate TC 0-180°
P03	3	6 gpm	Max	Rotate TC 0-180°
P04	1	6 gpm	600°F	Rotate TC 0-180°
P05	3	9 gpm	Max	Rotate TC 0-180°
P06	1	9 gpm	600°F	Rotate TC 0-180°

TABLE 5-1 (Continued)
PASSIVE RESIDUAL HEAT REMOVAL HEAT EXCHANGER TEST MATRIX

Configuration Tests				
Test	**No. of Tubes**	**Flow per Tube**	**Inlet Temperature**	**Comments**
C01 (R)	3	3 gpm	Max	No baffle
C02 (R)	3	3 gpm	Max	Back wall baffle 1 foot from tubes
C03 (R)	3	3 gpm	Max	Front baffle 1 foot from tubes
C04 (R)	3	3 gpm	Max	Insert baffle and back wall
C05	3	3 gpm	Max	Water level lowered 2 feet
Transient Tests				
Test	**No. of Tubes**	**Flow per Tube**	**Inlet Temperature**	**Comments**
T01	3	1 gpm	600°F	Water level 22 feet
T02	3	3 gpm	Max	Water level 22 feet
T03[3]	3	3 gpm	300°F	Water level 22 feet
T04	3	0.5 gpm	Max	Water level 22 feet

TABLE 5-1 (Continued)
PASSIVE RESIDUAL HEAT REMOVAL HEAT EXCHANGER TEST MATRIX

Steady-State Tests				
Test	**No. of Tubes**	**Flow per Tube**	**Inlet Temperature**	**Comments**
S01	3	9 gpm	Max.-250°F	(1)
S02 (R)	3	6 gpm	Max.-250°F	"
S03	3	3 gpm	Max.-250°F	"
S04 (R)	3	0.3 gpm	650°F-250°F	"
S05 (R)	3	1 gpm	650°F-250°F	"
S06 (R)	2	0.3 gpm	Max.250°F	"
S07 (R)(2)	1	9 gpm	Max.250°F	"
S08	1	6 gpm	650°F-250°F	"
S09	1	3 gpm	650°F-250°F	"
S10	1	0.3 gpm	650°F-250°F	"
S11(2)	1	1 gpm	650°F-250°F	"
S12 (R)(3)	2	6 gpm	Max.-250°F	"
S13 (R)	2	3 gpm	Max.-250°F	"
S14 (R)(3)	2	1 gpm	650°F-250°F	"
S15(5)	3	1 gpm	Max.-250°F	"
Uncovery Tests				
Test	**No. of Tubes**	**Flow per Tube**	**Inlet Temperature**	**Level**
U01	3	3 gpm	500°F	100%
U02 (R)	3	3 gpm	500°F	75%
U03 (R)	3	3 gpm	500°F	50%
U04 (R)	3	3 gpm	500°F	25%
U05	3	3 gpm	500°F	0%

Notes:

1) (R) indicates video recording performed for portions of this test.
2) Tests S07 through S11 were run using the middle tube.
3) Tests S12 through S14 were run using the two outside tubes.
4) The standard configuration consisted of the tubes 2 feet from the back wall, no baffle, and a water level of 22 feet. This configuration was determined after completion of the configuration tests.
5) Test S15 is a repeat of test S05. It was performed after all other medium-flow steady-state tests had been completed.
6) The configuration tests were run as both a transient test (heating the tank from ambient to bulk boiling), a steady-state test (varying the inlet temperature from the maximum down to 250°F), and a plume test.

6.0 DATA REDUCTION METHODS

This section describes the data handling that was performed on the PRHR test data and estimates the errors associated with the data and data reduction.

6.1 Data Reduction

The PRHR data acquisition files (see Subsection 4.5.5) contain complete sets of 201 channels taken at 1 to 5 minute intervals over the conduct of the test. Each data set contains a date and time stamp. A data reduction program reads the test data recorded in degrees Fahrenheit and millivolts, converts the millivolt data to the prescribed engineering units, and records the data in a tab delimited ASCII file (Appendix B). The correlations for conversion of the millivolt outputs are derived from a linear regression of the sensor calibration data and are presented in Table 6-1. The data reduction program also requires input of the test-specific information such as matrix test number, the orifice bore used (high, medium, or low flow, see Table 6-2), the time interval being evaluated, and the system pressure. The system pressure is input manually in the data reduction of the phase I data. Phase II data reduction uses output channel 180 for the system pressure.

The mass flow rate through each of the PRHR tubes was calculated from the orifice ΔPs by the following relationship:

$$\dot{m} = \left(\frac{\pi \, d^2 \, F_a}{4} \right) (K) \sqrt{2 \, g_c \, \rho_1 \, \Delta P} \qquad (6\text{-}1)$$

where:

- $\dot{m}$ = mass flow rate (lb/sec.)
- d = bore diameter (ft.)
- F_a = area expansion factor = $(1 - \alpha \, (T_f - 68))$
  where:
  - α = Thermal expansion coefficient (in./in./°F)
  - T_f = Fluid temperature (°F)
- K = flow coefficient
- g_c = 32.2 $(lbm/ft^3)/(lb_f sec.^2)$ gravitational constant
- ρ_1 = density of fluid upstream (lbm/ft^3)
- ΔP = differential pressure across the orifice (psf)
- D = pipe diameter (ft.)

The flow coefficient (K) is evaluated for flange tap orifices in accordance with Reference 5. The flow coefficient as a weak function of Reynolds number is programmed into the data reduction so that:

$$K = K_o + \frac{A}{R_D^5} \tag{6-2}$$

and

$$K_o = 0.5980 + 0.468\ (\beta^4 + 10\beta^{12}) \tag{6-3}$$

with

$$A = 0.87 + 8.1\beta^4 \tag{6-4}$$

where:

K_o = threshold flow coefficient value for any specific pipe diameter and β
R_D = pipe Reynolds number
A = constant function of D and β
β = beta factor ratio of bore diameter to pipe diameter

Table 6-2 presents the constants β, A, and K_o for each of the orifices used during the testing. The data reduction program calculates the Reynolds number based on the calculated flow rate using the pipe diameter and recalculates the flow coefficient until successive values of K are within 0.001. Fluid densities are based on the primary line temperatures from channels 173, 174, and 175 at the primary system pressure (channel 180) just prior to the orifice sections.

The temperatures for channel numbers 20 to 29 were reduced by 1.89°F based on an analysis of isothermal test data (see Figure 6-1). Comparison of the temperatures of the middle tube fluid above the 86" elevation were noticeably higher (1.97°F) than any of the surrounding temperatures. Review of the instrumentation wiring showed that all of the temperature readings in question came from the same thermocouple isothermal block.

A number of thermocouples (channels 17, 31, 35, 40, and 106) were not active during the two phases of the PRHR tests. The data for each of these channels were replaced by averaging the temperature data of the elevations above and below for all tests. In addition, the middle tube wall temperature recorded at elevation 6.417' (channel 44) was found to read significantly lower than adjacent thermocouples by as much as 30°F for tests S07 and S08 only. This condition was only noted in high water flow rate tests (S07 and S08) where the wall temperatures at elevation 7.917' exceeded 300°F.

The data for channel 44 were replaced by the average of channels 43 and 45 for these two tests only. Figure 6-2 shows an example of the noted behavior for test S07.

6.2 Calibration and Error Analysis

The PRHR test facility used the data acquisition system described in Subsection 4.5.5. The individual pressure transducers were calibrated prior to the start of testing for both the first and second phase of testing. Table 6-3 presents a summary of the instrumentation used and includes the standard deviation calculated from the linear regression of the sensor calibration data (σ). The data reduction coefficients generated from a linear regression analysis of the calibration data are presented in Table 6-1.

The type KK and TT thermocouples were not individually calibrated but were purchased as premium grade having a ±2°F (±1.1°C) tolerance from the standard. The output temperatures were a result of the Fluke data acquisition system compensated temperature modules, which provide direct temperature output through an internal linearization program. The internal conversion adds an additional uncertainty of ±0.6°F (±0.5°C).

Table 6-4 summarizes the overall error estimates of all the reduced data by applying the individual error estimates from the sensor and data acquisition system. Cable losses were assumed to be negligible because of short cable lengths. The overall estimate of error based on the worst case sensor uncertainty (calibration[1] or manufacturer's specifications) is determined as the square root sum of the squares of the individual contributions as indicated in Equation 6-5.

$$E = \pm \sqrt{\sum_{i=1}^{n} \Delta_i^2} \qquad (6\text{-}5)$$

where:

E = overall estimate of error

Δ_i = individual accuracy of the ith component

An estimate of the error associated in the calculation of the mass flow rate from the test data was obtained by evaluating Equation 6-6 for the flow Equation 6-1.

$$E_y = \pm \sqrt{\sum_{i=1}^{n} \left(\frac{\partial Y}{\partial X_i} \right)^2 (\Delta X_i)^2} \qquad (6\text{-}6)$$

[1] Standard deviation of the calibration data is assumed to be a 1σ and therefore the worst of 3σ or the manufacturer's specifications are used.

where:

Y = dependent variable
X_i = ith independent variable

The results indicate a standard deviation of ± 1.2 percent for flow measurement.

TABLE 6-1 DATA REDUCTION COEFFICIENTS					
Channel No.	Sensor	Phase I		Phase II	
		Coeff.	Constant	Coeff.	Constant
180	Sys Press.	9.35698	-742.388	9.3708605	-747.1532
182	FM1	0.33510805	-26.875665	0.3355	-27.021
183	Acc. Level	0.62774639	-50.282486	0.6541892	-51.77003
184	Tank Level	1.20944882	-97.723465	1.2972757	-103.6409
185	Pump DP	0.78184664	-62.547731	0.7835932	-62.54539
187	FM2	0.33406182	-26.724945	0.3356	-27.072
188	FM3	0.33428098	-26.745821	0.3342	-26.802
189	Vortex	6.25	-500	6.25	-500
200				50	0
201				50	0
182 (L)[1]	FM1			0.249086	-19.85112
187 (L)	FM2			0.2513521	-20.252
188 (L)	FM3			0.2539768	-20.43358

Notes:

(1) (L) indicates the low flow test setup where the ΔP cells were rescaled for 0 to 30 inches of water.

TABLE 6-2 FLOW ORIFICE CONSTANTS				
Flow Description	**Orifice Diameter (inches)**	β	**A**	**K_o**
Low	0.2457	0.3317	0.9681	0.6037
Medium	0.3258	0.4395	1.1722	0.6157
High	0.5397	0.7274	3.1377	0.8317

TABLE 6-3
LIST OF INSTRUMENTS

Location Transducer I.D.	Type of Transducer	Make/Model	Range	Manufacturer's Specified Accuracy	Standard Deviation of Calibration Correlation
Fluke DAS		Model 2240 SN 2385069	80 to 400 mV	±(0.02% reading + 0.015% range + 7 μV)	±0.02 mV
			0 - 40 volt	±(0.02% reading + 0.015% range + 7 μV)	±0.006 volts
			Thermocouple	±0.8°F (±0.5°C)	±0.6°F (±0.5°C)
Channel 1 to 52 Channel 173 to 179 Channel 190 to 193	Thermocouple (Type KK)	Marlin double precision	N/A	±2°F (±1.1°C)	NA
Channel 53 to 172	Thermocouple (Type TT)	Marlin double precision	N/A	±2°F (±1.1°C)	NA
Piping Pressure					
Channel 180	Pressure (Piezoresistive)	Rosemont 1GP9E22M1/SN 403727	0 -2500 psig	±0.25% of full scale	2.2 psig
182	Pressure (Piezoresistive)	Foxboro 843D/SN 23530	0 - 107 in. H_2O	±0.25% of full scale	0.01 in. H_2O
183	Pressure (Piezoresistive)	Foxboro SN 23528	0 - 207 in. H_2O	±0.25% of full scale	in. H_2O
184	Pressure (Piezoresistive)	Foxboro SN 23527	0 - 415 in. H_2O	±0.25% of full scale	0.14 in. H_2O
185	Pressure (Piezoresistive)	Foxboro SN 23529	0 - 250 psig	±0.25% of full scale	0.16 psi
187	Pressure (Piezoresistive)	Foxboro SN 20934	0 - 107 in. H_2O	±0.25% of full scale	0.04 in. H_2O
188	Pressure (Piezoresistive)	Honeywell SN 23561	0 - 107 in. H_2O	±0.25% of full scale	0.03 in. H_2O
188 (after 10/20/90)	Pressure (Piezoresistive)	Honeywell SN 23807	0 - 30 in. H_2O	±0.25% of full scale	0.19 in. H_2O
189	Vortex flowmeter	Foxboro SN 5422879	180 - 3170 lb/hr	±0.5% of full scale	NA
200	Watthour meter	S/N 2570	0 - 500 kw	±0.5% of full scale	NA
201	Watthour meter	S/N 2570	0 - 500 kwh	±0.5% of full scale	NA

TABLE 6-4
SUMMARY OF SPECIFICATION ERROR ESTIMATES

Sensor Description							DAS Accuracy		Total Accuracy Estimate	
Channel No.	ID	Type	Units E.U.	Span E.U.	Sensor Accuracy (%)	Sensor Accuracy E.U[5]	(%)	E.U	(%)	E.U.
Channel 180		Pressure	psia	0 -2500 psig	±0.33	±8.6	±0.05	±1.3	±0.33	±8.70
182	FM1	Pressure	inches H_2O	0 - 107 in. H_2O	±0.60	±0.66	±0.05	±0.05	±0.60	±0.66
182 (after 10/22/90)	FM1	Pressure	inches H_2O	0 - 30 in. H_2O	±0.03	±0.03	±0.07	±0.02	±0.08	±0.04
183		Pressure	inches H_2O	0 - 207 in. H_2O	±1.6	±3.3	±0.05	±0.09	±1.60	±3.30
184		Pressure	inches H_2O	0 - 415 in. H_2O	±0.12	±0.48	±0.04	±0.18	±0.13	±0.51
185		Pressure	psia	0 - 250 psig	±0.18	±0.75	±0.04	±0.11	±0.18	±0.76
187	FM2	Pressure	inches H_2O	0 - 107 in. H_2O	±0.75	±0.081	±0.05	±0.05	±0.75	±0.10
187 (after 10/22/90)	FM2	Pressure	inches H_2O	0 - 30 in. H_2O	±0.24	±0.06	±0.07	±0.02	±0.25	±0.06
188	FM3	Pressure	inches H_2O	0 - 107 in. H_2O	±1.2	±1.3	±0.05	±0.05	±1.20	±1.30
188 (after 10/20/90)	FM3	Pressure	inches H_2O	0 - 30 in. H_2O	±3.1	±0.6	±0.07	±0.02	±3.10	±0.60
Temperatures			°F	NA[1]		±2°F	NA	±0.8°F	NA	±2.15
200		Watt-hour Meter	kilowatts-hours	0 - 500 kwh	±0.5	±2.5	±0.02	±0.095	±0.50	±2.50
201		Watt-hour Meter	kilowatt-hours	0 - 500 kwh	±0.5	±2.5	±0.02	±0.095	±0.50	±2.50

Notes:

(1) NA = not applicable; na = not available
(2) Estimate
(3) Manufacturer data not available error estimate based on model - C252230
(4) Based on performance evaluation of channels 121 through 136
(5) Worst case from calibration data

a,b,c

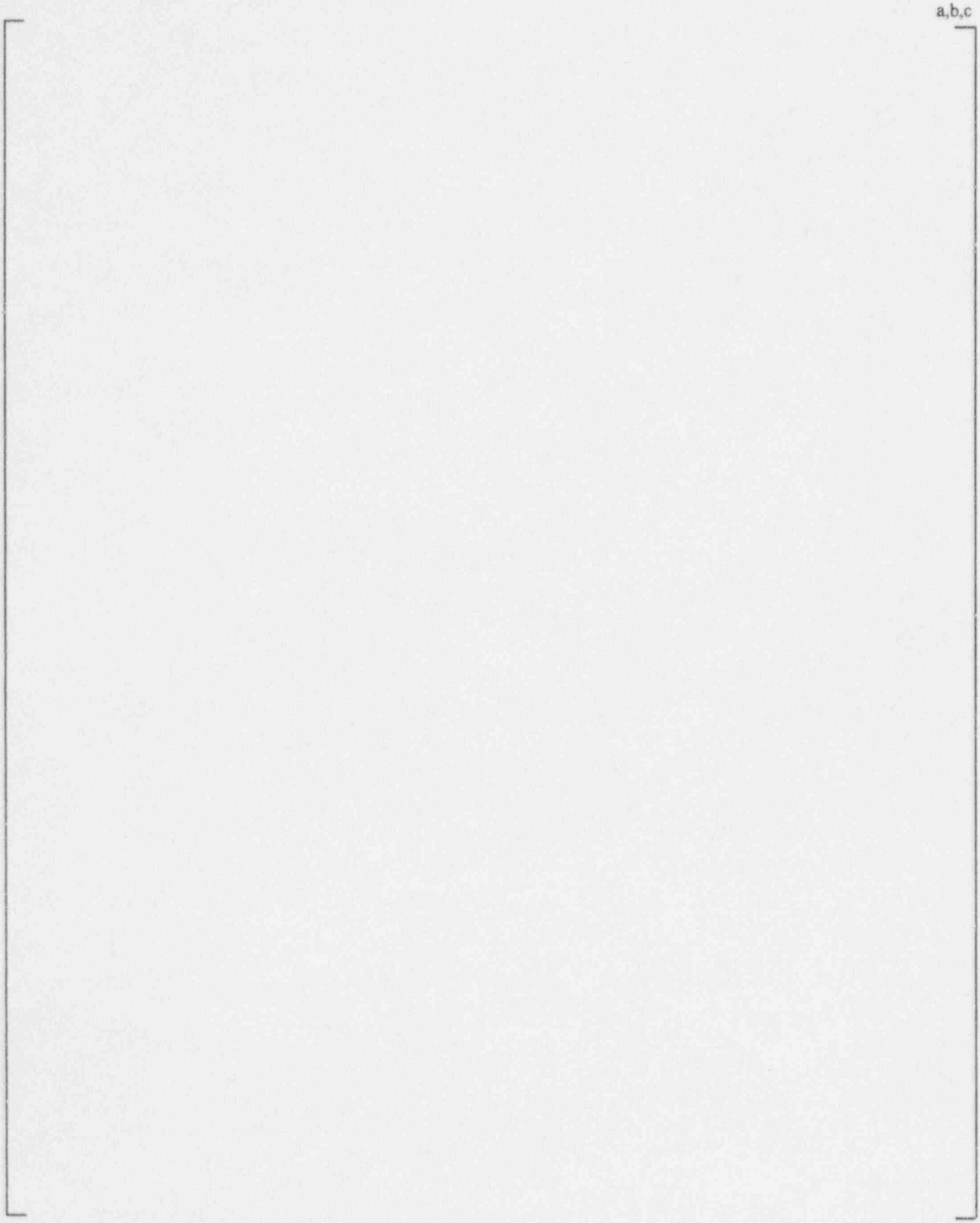

Figure 6-1 Comparison of Tube 1 and Tube 2 After 48 Hours No Flow

a,b,c

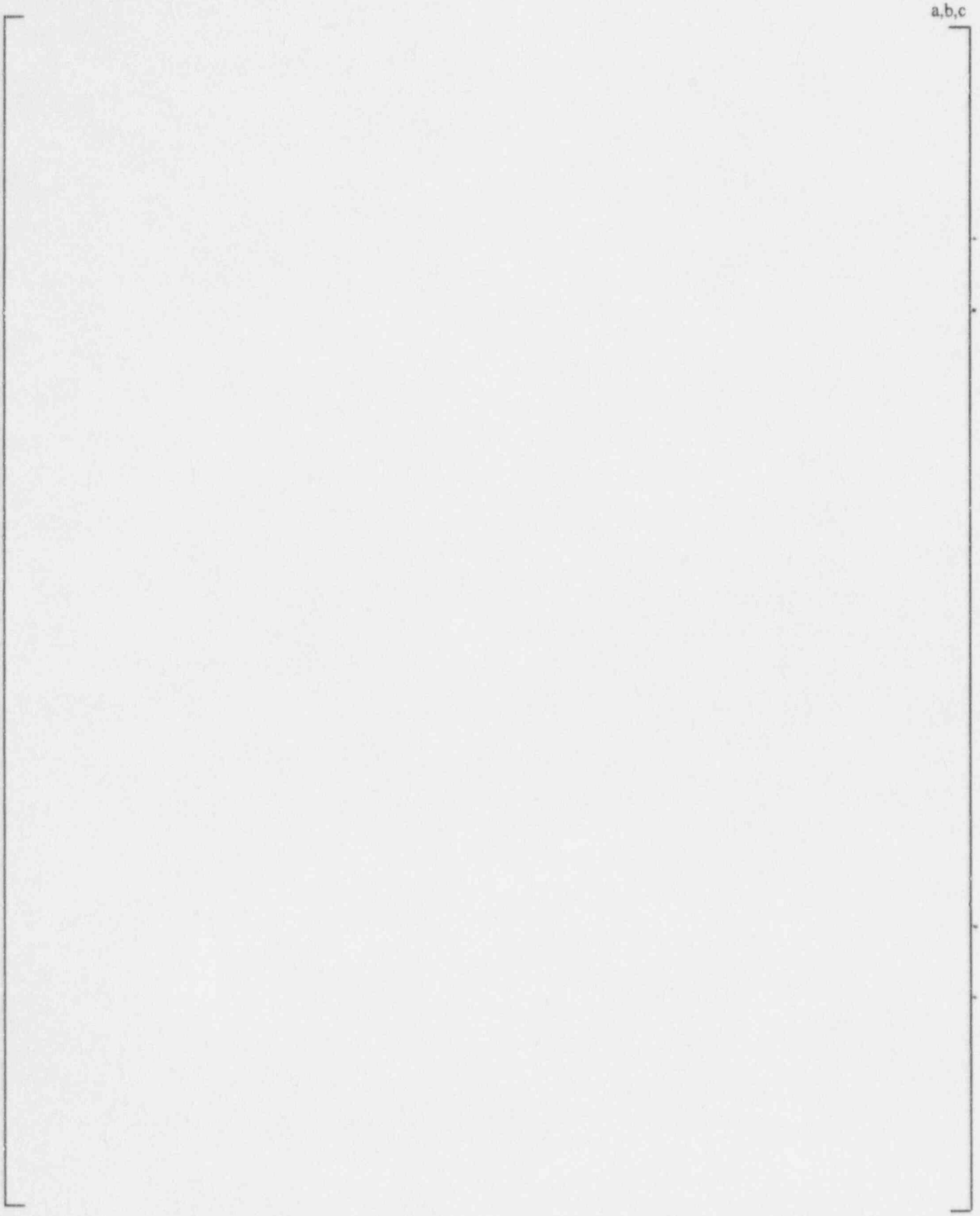

Figure 6-2 History of Tube Temperatures for Test S07

7.0 DATA ANALYSIS METHODS

This section describes the methods used to analyze the test data from the phase I and II tests to calculate local and overall tube heat transfer performance of the passive residual heat removal (PRHR) heat exchanger (HX).

The data reduction program includes several heat transfer correlations as well as a velocity profile calculation for the fluid on the primary side of the tube. The program takes raw test data, calculates the wall heat flux, inside wall temperature, and outside wall temperature, and compares the measured heat transfer with the heat flux predicted by several selected correlations.

As described earlier, both steady-state and transient tests were conducted. The steady-state tests were performed for a series of tube flows and initial primary-side temperatures and a constant tank temperature. The transient tests allowed both the primary-side temperature and the tank water temperature to vary. The transient tests were long transients (minutes, not seconds) so that a quasi-steady-state approach could be used to interpret the test data. In addition, tests with tube bundle uncovery were also performed to simulate boildown of the IRWST.

Figure 7-1 shows a sketch of the instrumentation used to calculate the tube heat flux, overall heat transfer, and outside heat transfer coefficient. The primary measurements included the tube flow rates, primary fluid axial temperature distribution, tube outside wall temperatures, and the tank temperatures, which were measured at several locations and elevations within the tank.

The primary fluid axial temperature profile in the water tubes was measured at 18-inch increments using the thermocouples inside the tube. The thermocouples came in from both the top and bottom of the tube to minimize any blockage of the tube flow area.

The axial primary fluid temperatures were used to calculate the change in primary fluid heat content over the length of the PRHR tubes. The thermocouple temperature readings were converted to local fluid enthalpy values using the steam tables. A steady-state energy balance on the primary side was expressed as:

$$q''_{w_i} = \frac{\dot{m}_i}{\pi D_i} \frac{dH_{f_i}}{dx} \qquad (7\text{-}1)$$

where:

q''_{w_i} = local wall heat flux (Btu/hr-ft.^{2})

$\dot{m}_i$ = tube mass flow rate (lbm/hr)

H_{f_i} = local primary fluid enthalpy at position i as determined from the primary fluid temperature measurement (Btu/lbm)

x = elevation along the primary tube (ft.)

D_i = inside tube diameter (ft.)

For improved accuracy, the primary fluid enthalpies at each elevation were curve-fitted to a third-order polynomial, and the resulting curve was differentiated to obtain the wall heat flux over different axial sections as shown in Equation 7-1. The use of the fitted enthalpies for the heat flux calculations, rather than actual temperature data reduces the uncertainty of averaging the specific heat over the 18-inch length in the test section. Specific heat variations can become significant at high primary-side temperatures. Curve-fitting the primary fluid enthalpies results in smoother calculated wall heat fluxes since the individual fluid enthalpy variations are minimized particularly when taking differences. Figure 7-2 shows a typical plot of the measured primary fluid enthalpies with the fitted expression and shows excellent agreement with the test data. Figure 7-3 shows the resulting wall inside heat flux calculated from the fit, which again shows a smooth continuous curve as might be expected.

The heat flux values calculated using the third-order enthalpy fit were checked against an overall heat balance. The calculated local heat flux values were integrated over the length of the PRHR tubes and were compared to the total tube heat loss based on the tube flow weighted difference of the inlet to exit temperature degrees. The agreements between the summed local heat flux values and the overall tube energy balance was typically 3 percent. This confirms the accuracy of the fit used to determine the local heat flux values.

The use of Equation 7-1 assumes a steady-state process. As explained above, while some of the tests were transient, the time period for the transient was much longer than the transient time of the primary system water as it flowed in the tubes so that use of Equation 7-1 is acceptable for these quasi-steady-state situations.

Using the calculated wall heat flux from the primary fluid enthalpies, the radial temperature distribution can next be calculated at each instrumented position. To calculate the inside wall temperature, an appropriate inside-tube heat transfer correlation was determined based on the tube geometry, flow, and fluid properties. The correlations by Petukhov-Popov [Reference 6] and Dittus-Boelter [Reference 7] were used to calculate the inside wall convection coefficients. Kreith and Bohm [Reference 8] reviewed the different turbulent convection heat transfer coefficients and recommended Petukhov-Popov since it had less uncertainty than Dittus-Boelter or other similar correlations.

In addition, since large temperature gradients existed across the boundary layer of the primary fluid, a viscosity correction was applied to both the Dittus-Boelter and Petukhov-Popov correlations. The factor is a property ratio correction and is applied to the viscosity, as recommended by Kays [Reference 9]:

$$\mu = \mu_{cp} \left(\mu_o / \mu_{mean}\right)^{0.21} \qquad (7\text{-}2)$$

where:

μ_{cp} = constant property viscosity (lbm/ft.-hr)
μ_o = viscosity at the wall temperature, (lbm/ft.-hr)
μ_{mean} = mean fluid viscosity (lbm/ft.-hr)

The corrected viscosity is used in the calculation of the tube Reynolds number.

A second correction factor is also applied to account for local velocity and fluid temperature profile effects. The liquid temperature is measured at the centerline of the tube, which is the hottest location in the tube. The correct temperature to use for the energy balance given in Equation 7-1 is the bulk fluid temperature, which is a flow-weighted average temperature. Based on the mass flow rates inside the HX tubes, the flow is in a turbulent flow regime. The turbulence will result in bulk fluid temperatures close to but not equal to the thermocouple readings taken at the centerline of the tubes.

Two methods of calculating the bulk fluid temperature were investigated. The first approach is based on a normalized 1/nth power velocity profile. It is assumed that the temperature distribution is directly proportional to the normalized velocity distribution, as:

$$\left(\frac{T_w - T(r)}{T_w - T_c}\right) \approx \left(\frac{V(r)}{V(R)}\right) \approx \left(\frac{r}{R}\right)^{\frac{1}{n}} \tag{7-3}$$

where:

T(r) = fluid temperature at radial position r (°F)
T_w = fluid temperature at wall (°F)
T_c = fluid temperature measured in the center of fluid stream (°F)
V(r) = local velocity in the tube at radius r (ft./hr)
V(R) = centerline velocity in the tube (ft./hr)
r = local radial position in the tube (ft.)
R = tube inside radius (ft.)
n = power fit for velocity profile

The ratio of the wall-to-bulk temperature to the wall-to-centerline temperature can then be calculated as:

$$\frac{T_w - T_b}{T_w - T_c} = \frac{\int_0^R \left(\frac{r}{R}\right)^{1/n} \left(\frac{T_w - T(r)}{T_w - T_c}\right) rdr}{\int_0^R \left(\frac{r}{R}\right)^{1/n} rdr} \tag{7-4}$$

which is integrated to fit the bulk temperature, T_b (°F). The resulting temperature ratio, assuming a 1/n law velocity profile is given as:

$$\frac{T_w - T_b}{T_w - T_c} = \frac{2n+1}{2n+2} = 0.9375 \text{ (for } n=7) \qquad (7\text{-}5)$$

Equation 7-5 indicates that the temperature profile is rather flat and the measured centerline temperature is approximately equal to the bulk temperature. The appropriate value for n, as a function of Reynolds number, is given in Schlichting [Reference 10].

A value for the heat transfer coefficient on the inside of the PRHR tube is calculated based on fluid properties defined by the bulk temperature. A new inner wall temperature is calculated from the steady-state heat balance. The new inner wall temperature is then used to calculate a new bulk fluid temperature. The current and previous values for the bulk fluid temperature are compared and once acceptably close, the revised temperatures and heat transfer coefficient are passed back to the main program.

An alternate method was also used to determine the bulk fluid temperature inside the tubes via an interpolation of tabular data based on the universal logarithmic velocity profile. The appropriate coefficient is determined from a look-up table provided in the PRHR data reduction and analysis program that is based on the Reynolds number for the flow inside the tube from Knudsen and Katz [Reference 11]. The same iterative method of calculating a revised inside wall heat transfer coefficient and bulk fluid temperature was used as previously described.

Both methods indicate that the temperature profile was flat and the center line and bulk fluid temperatures are nearly equal. The revised wall and bulk fluid temperatures are calculated as well as the revised inner tube heat transfer coefficient. From the revised inner wall temperature, the outer wall temperature can then be calculated.

The hydraulic diameter used in the analysis of the data was the tube inside diameter since accounting for the thermocouple leads overestimated the wetted parameter effect that would contribute to the frictional pressure drop but not the wall heat transfer effects. The blockage effect on the flow area in the tube was included in the analysis by reduction of the flow area. The blockage area was assumed constant over the entire tube length. The inside wall area heat flux from the enthalpy balance provides an estimate of the inside wall temperature, $T_{w_i}(x)$:

$$T_{w_i}(x) = Tp_i(x) - q''_{w_i}(x)/h_i(x) \qquad (7\text{-}6)$$

where:

$Tp_i(x)$ = measured primary fluid temperature at elevation i (°F)

$h_i(x)$ = calculated inside primary-side heat transfer coefficient for elevation i (Btu/hr-ft.^{2}-°F)

$T_{w_i}(x)$ = calculated inside tube wall temperature for elevation i (°F)

where the inside tube wall heat transfer coefficient, h_i, is obtained from the Petukhov-Popov or Dittus-Boelter correlations. Using the inside wall temperature, the temperature drop across the tube wall can then be calculated using the steady-state heat conduction solution for cylindrical coordinates. The calculated outside wall temperature becomes:

$$T_{w_o}(x) = T_{w_i}(x) - \frac{q''_{w_i}(x) D_i}{2k(x)} \text{ Ln } (\frac{D_o}{D_i}) \qquad (7\text{-}7)$$

where:

D_o = outside tube diameter (ft.)
$k(x)$ = tube thermal conductivity (Btu/hr-ft.-°F)

where the tube wall conductivity, k(x), is a function of temperature. Direct measurements of the tube inside diameters, outside diameter, and wall thickness were made and used in the heat flux and heat transfer calculations. The value for the tube wall conductivity was also confirmed by comparisons to published literature on stainless steels.

The tube wall outside temperature was also directly measured using 0.020-inch thermocouples, which were silver soldered into the 0.025-inch deep grooves cut in the tube. The measured wall temperatures ideally should represent a point 0.01 inches below the cladding surface.[1] Using the calculated wall heat flux from the primary fluid measurements (Equation 7-1) and correcting it for area changes, the cylindrical conduction equation can be rewritten to extrapolate the measured wall thermocouple value to the true edge of the tube. Since the groove is filled with silver braze, the thermal conductivity of silver braze, k_s, is used in estimating the outside wall temperature of the tube from the outside wall temperature measurements. That is:

$$T_{W_{oe}}(x) = T_{W_{om}}(x) - q''_{W_i}(x) \left(D_o - \frac{0.02}{12}\right) \frac{\text{Ln}\left[\left(\frac{D_o}{\left(D_o - \frac{0.02}{12}\right)}\right)\right]}{(2 \cdot k_s)} \qquad (7\text{-}8)$$

where:

$T_{W_{om}}(x)$ = measured wall temperature at D_o -0.02 inches (°F)

[1] It is assumed that the thermocouple centerline measures the temperature at its position and the top of the thermocouple is flush with the outside surface of the tube.

$T_{W_{oe}}(x)$ = wall surface temperature, which is extrapolated using the wall heat flux (°F)

k_s = thermal conductivity of silver braze (Btu/hr-ft.-°F) [Reference 12]

In the original analysis of the test data, the extrapolation of the wall thermocouple used the conductivity of the stainless steel tube wall in Equation 7-8. However, after correcting the flows, the heat flux values at the top of the tube bundle increased significantly so that the value of the correction, as calculated using the stainless steel conductivity, became unrealistically large. As a result, the high heat flux regions on the tube had a lower $T_w - T_{sat}$ value as compared to lower heat flux points on the tube. That is, the data no longer displayed an increasing wall superheat trend with increasing wall heat flux. The correction resulted in a non-physical behavior of the data. Since silver braze was used to fill the thermocouples in the grooves of the tube, the conductivity of the silver braze was used in the extrapolation of the thermocouple reading to the outside surface of the tube wall. This results in a smaller difference of the measured buried wall thermocouple reading when compared to the extrapolated wall surface temperature. Using this correction method, the resulting boiling curves show the expected trends of increased wall superheat as the heat flux increases.

The measured wall temperatures, as extrapolated to the tube surface by Equation 7-8, were used since this presented a more consistent set of data for the tests. Table 7-1 gives examples of the calculated wall heat fluxes, temperatures, inside heat transfer coefficients, and wall temperatures for a typical test.

The local tank fluid temperature is obtained by averaging the local thermocouple measurements 3 inches, 6 inches, and 12 inches in front of the tube and 6 inches behind the tube at each elevation of interest. These thermocouples are shown in Figure 7-1.

The local saturation temperature was calculated at each thermocouple elevation and used to obtain the wall superheat $T_{wall} - T_{sat}$ to develop the boiling curve for the test data. The temperature traverses from the plume tests showed that the local liquid temperature was at or above the bulk saturation temperature at the particular elevation. This showed that a plume of hot liquid was present around the tubes when the tubes had sufficient wall superheat to boil. Therefore, correlating the data as a boiling curve (q''_{w_o} vs $(T_{wall} - T_{sat})$) was used. Several tests were videotaped, which showed boiling on the tube surface.

Using the fitted primary fluid temperatures and calculated heat flux, this heat flux can be integrated and compared to the overall tube heat duty as calculated using the inlet and exit thermocouples, as discussed earlier.

The overall heat duty can be calculated from the primary fluid temperatures and the calculated heat flux. The heat flux can be integrated and compared to the overall tube heat duty, as calculated from the inlet and exit temperatures.

TABLE 7-1
EXAMPLES OF PRHR DATA FROM STEADY-STATE TEST

Elevation (ft.)	Primary Tube Temperature (°F)	Inside Wall Heat Flux (Btu/hr-ft.^{2})	Temperatures		
			Calculated Inside Wall (°F)	Extrapolated Measured Outside Wall (°F)	Tank Fluid (°F)
18.42	[				] a,b,c
16.92					
15.42					
13.92					
12.42					
10.92					
9.42					
7.92					
6.42					
4.92					
3.42					
1.92	]				

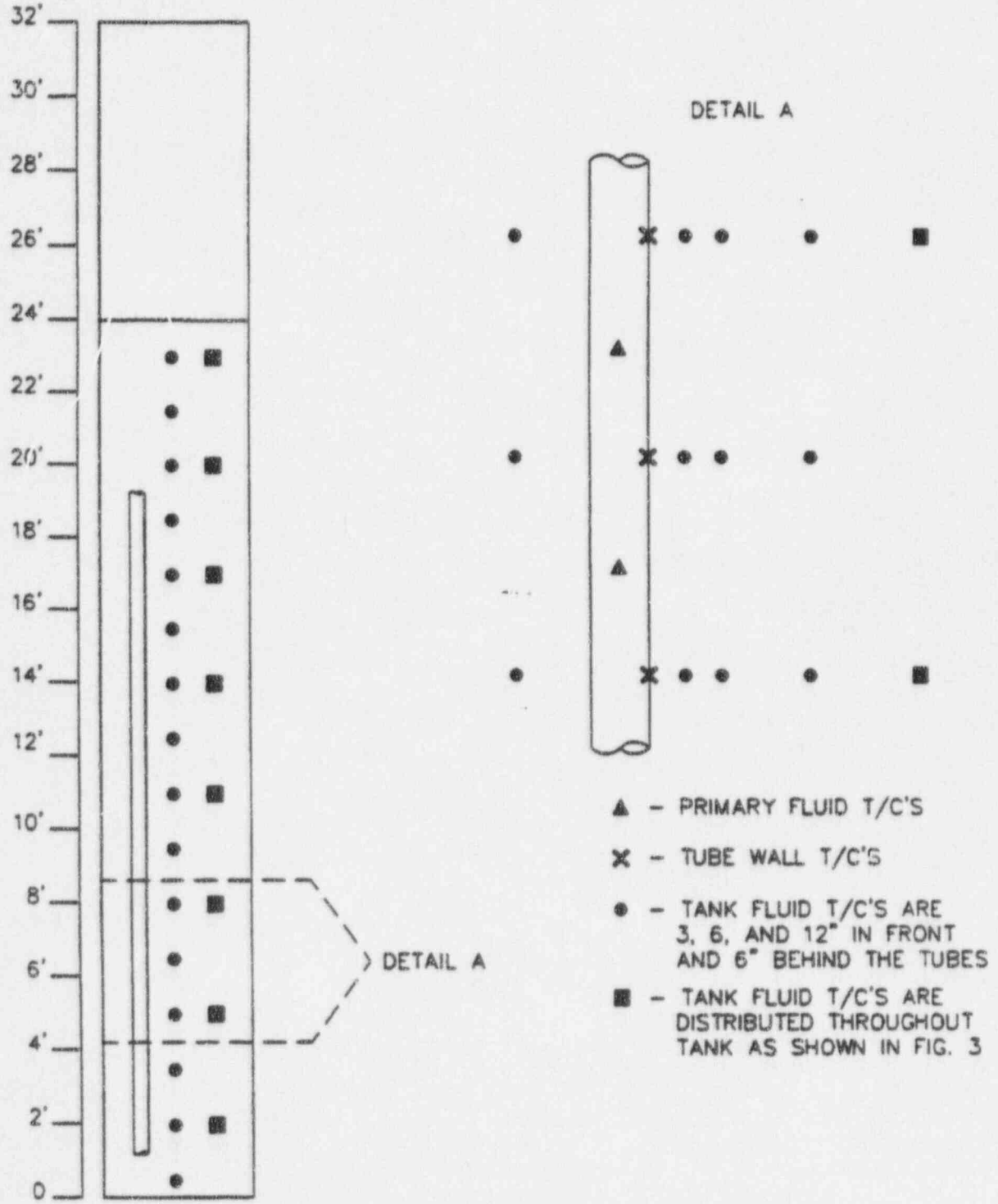

Figure 7-1 Instrumentation Locations and Layout to Calculate Local Tube Wall Heat Fluxes

a,b,c

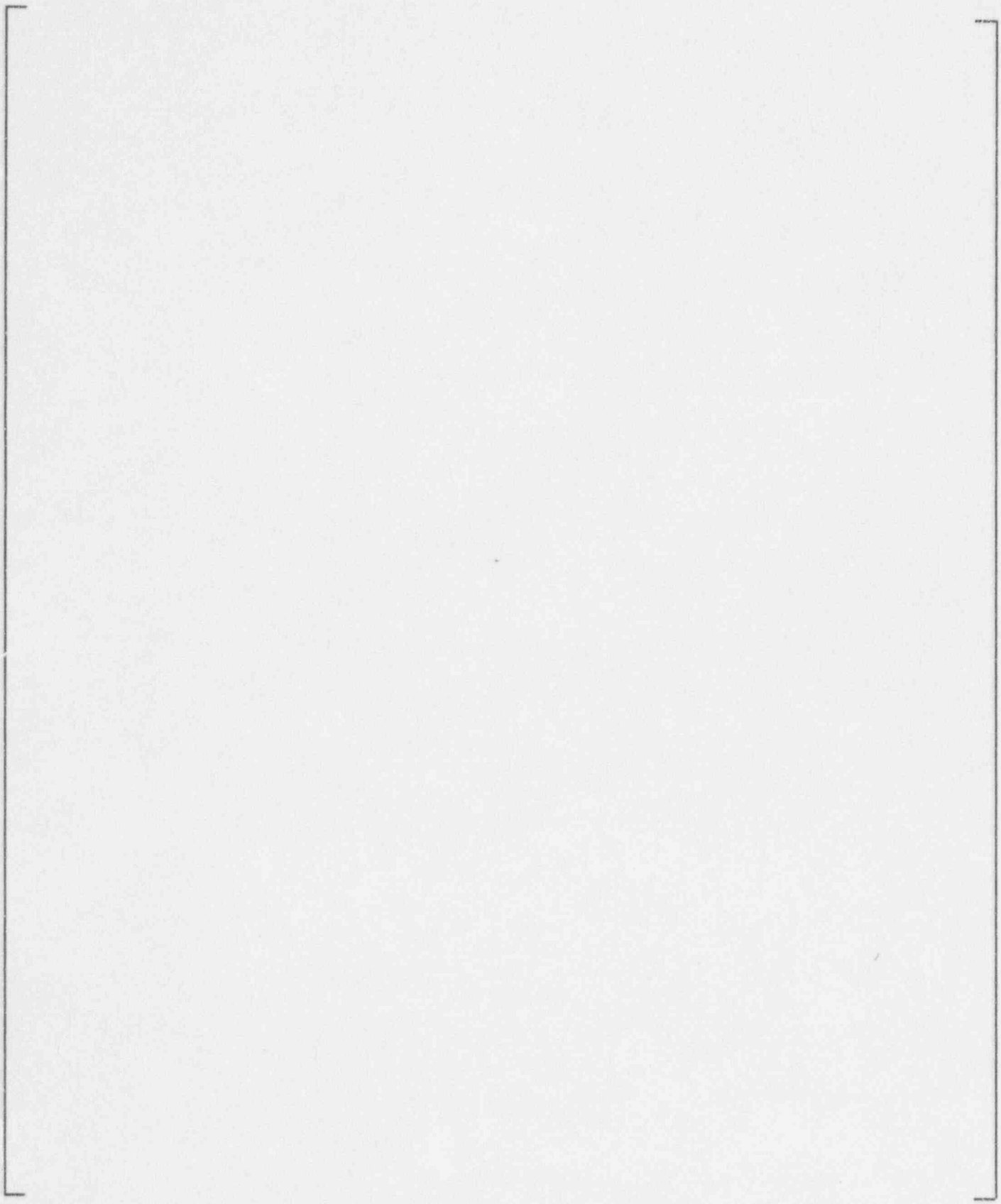

Figure 7-2 Measured and Fitted Primary Fluid Enthalpy Data

a,b,c

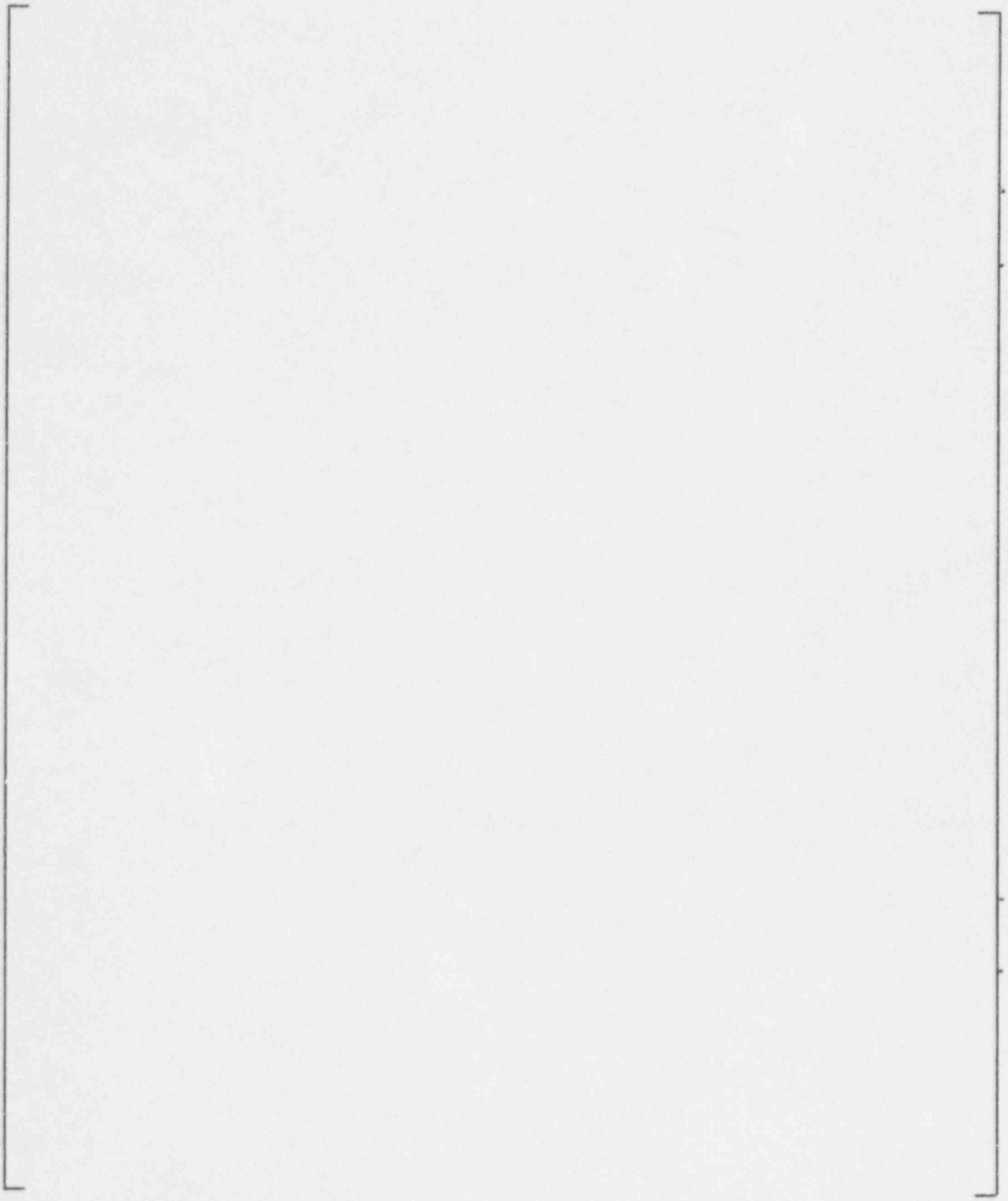

Figure 7-3 Calculated Wall Heat Flux From Fitted Data

8.0 TEST RESULTS

The test data from the different test categories and observations relevant to the expected performance of the passive residual heat removal (PRHR) heat exchanger (HX) are discussed below.

8.1 Configuration Tests

The purpose of the configuration tests was to confirm the applicability of the test results to the final PRHR physical configuration and to determine the reference configuration for the remaining tests. Specifically, the tests were performed to determine the effects of the following configuration parameters:

- Distance of the HX to the in-containment refueling water storage tank (IRWST) wall
- Distance between rows of tubes
- Water level above the tubes

Five configuration tests were performed (C01, C02, C03, C04, and C05) at approximately the same flow rate of 3 gpm (3.3 to 3.6 gpm). Configuration tests C01 though C04 involved varying the location of the HX tubes to a back wall and placing a baffle in front of the tubes. Figure 8-1 shows the four configurations tested. Configuration test C05 was performed at a lower tank water level. The following is a description of each test:

Configuration 1 Configuration test C01 was termed the baseline configuration. The tubes were located in the annulus between the baffle and the tank wall, 2 feet in front of the back wall of the baffle. The water level was 4 feet above the tubes (see Figure 8-1). This is the same configuration used for the Phase I tests.

Configuration 2 In configuration test C02, the tubes were located only 1 foot in front of the back wall. This test was used to investigate the effect of locating the PRHR HX closer to the IRWST walls.

Configuration 3 In configuration test C03, the tubes were located 2 feet from the back wall; however, a baffle was inserted 1 foot in front of the tubes, beginning at an elevation equal to the top of the tubes and extending down to an elevation 16 inches above the bottom of the tank. The baffle was used to simulate a row of tubes 2 feet away from the PRHR HX tubes.

Configuration 4 In configuration test C04, the tubes were located 1 foot from back wall, and the baffle was inserted 1 foot in front of the tubes. This test was also used to determine any effects of another row of tubes placed 2 feet away.

Configuration 5 Configuration test C05 was performed with the same configuration as C02; however, the test was performed with the water level lowered 2 feet. The purpose of this test was to determine the effect of water level above the tubes on the time from PRHR initiation to steam release from the IRWST.

The following observations from the configuration tests can be made:

- In general, heat transfer characteristics were similar for all configurations but appeared to be slightly enhanced with the addition of the front baffle for the high-temperature cases and by inserting a back wall closer to the tubes for the lower temperature test runs. Table 8-1 presents a summary of the various steady-state test conditions established during the tests. C05 results are transient data in that no steady-state conditions were established as the test was performed. Table 8-2 illustrates the difference in configurations by a comparison of the overall heat losses from tubes 1 and 2 from the data normalized by the total tube flow. The heat transfer was slightly enhanced as the back baffle (C02) or the front baffle were moved closer to the tubes because of the increased fluid buoyancy around the tubes caused by the higher fluid temperature and boiling. The increased buoyancy drove flow up along the tubes, resulting in higher local velocities and greater natural circulation heat transfer. The higher flow along the tubes made the heated tubes act as a pump, which promoted increased mixing in the tank. Figures 8-2 through 8-5 show the outside wall heat flux versus estimated outside wall temperature minus saturation temperature for configuration tests C01 through C04. Each data point represents the heat flux at a discreet point on the HX tube.

- Tank mixing appeared to be improved with the baffle placed in front of the tubes as discussed above. Figure 8-6 is a plot of the average tank temperature against time for the five configuration tests, while Table 8-3 presents the tank heatup rates for the five tests. The tank water heated up at approximately the same rate for all configurations from the start of the test to the beginning of tank steaming; however, the configurations with the baffle placed in front of the tubes (C03, C04) heated up faster from the point of first steaming to bulk boiling. Since the heat input into the tank water from the tubes was similar for all configurations, the results imply that the tank water mixed better for those tests with the baffle. Furthermore, the amount of steam released from tests C03 and C04, from the time of first steaming to the time of bulk boiling, should be less because the heat input to the tank was used to raise the bulk tank water temperature.

8.2 Plume Tests

A series of plume tests were performed, as described in Section 5.0. In addition, plume data were taken for the various configuration tests described earlier. Selected results of these tests are presented in Figures 8-7 through 8-13. A mechanical obstruction at the top level prevented a complete profile from being obtained. The plots are of the maximum recorded plume temperatures at locations around the outside tube for various tube flow rates, number of tubes operating, and tank configurations. The

shape of the measured plume around the tube was similar in all cases. The highest tank temperature recorded was 228°F, which occurred at the lowest elevation. This was expected because the saturation temperature at the lowest elevation was highest due to the head of the tank water.

A comparison of the plots for tests P01 and C02 show that the shape of the plume of tube 1 was not affected by the operation of the other tubes. These results indicate that the tube pitch selected was adequate and that heat transfer did not improve significantly by increasing the tube pitch. This is confirmed by the results of selected steady-state tests. A comparison of the plots for tests P01, P03, and P05 show that the shape of the plume was also unaffected by the primary-side tube flow rate. The bottom elevation of P03 is not shown because of its low temperature <195°F.

A comparison of plots for test P01 and C02 show that the shape of the plume was largely unaffected by the placement of the back wall 1 foot closer to the tubes. The measurement of the plume was limited to 3 inches on either side of the outside tube at the wall of the vessel. A comparison of the plots of C03 and C04, which relocate a baffle to within a foot in front of the row of tubes, show that the plume temperatures are generally higher than those observed during the tests without baffles in front of the tubes. The plume tests show that the major portion of the buoyant plume does exist in a relatively confined area around a given tube and buoyancy is limited to the immediate area around the tubes on the order of $\pm$ 1.0 inches on either side of the tube centerline. The buoyant plume does become sightly larger along the tube toward the top of the tank. The plume data indicate that the zone of influence of temperature effects is limited to approximately $\pm$ 2.0 inches on either side of the tube centerline based on the plume test and configuration test temperature profiles.

Since the PRHR rows are on a 3 inch square pitch, this does not exclude some thermal interaction but would limit interaction because the primary plume is less than 1.5 inches from the tube centerline. Therefore the vertical tubes can be assumed to behave independently. Thus, the data from this series of tests also apply to multi-headered tube arrays. This observation combined with the similar heat fluxes for tests C03 and C04 indicate that there should be limited interactions between rows of HX tubes when the distance between the rows is 3 inches or more. Observation of the test video tapes indicates that the plume is localized along the tube during the high heat flux.

As a result of the plume and configuration tests, the standard configuration for the steady-state transient and uncovery tests was with the tubes 2 feet from the back wall, no baffle, and the water level lowered 2 feet. This configuration was chosen because of the following reasons:

- The baseline configuration (C01) demonstrated the heat flux and tank mixing to be lowest. This, combined with the fact that the plume was limited in size for the cases with the baffle (C03 and C04), shows that test results obtained for tests run with this configuration will be conservative.

- The water level was chosen to be 2 feet above the tubes. This option was selected due to the current HX tube length of 20 feet, and therefore the IRWST water level was only 2 feet above the top of the tubes. Since the results of test C05 showed no appreciable difference in the time

to measurable steam formation between C05 and C01 or C02, the aforementioned water level was chosen.

8.3 Steady-State Tests

For the steady-state tests, the tank of water was allowed to heat up to 212 ± 5°F. Once the tank was heated, a series of tests was performed for a given primary tube flow rate and pressure. Initially the primary inlet temperature was fixed at the highest value (up to 650°F) possible with the system heater. The primary fluid mass flow was held constant and the primary inlet temperature was decreased in approximately 50°F increments. Once a steady state was reached, several data scans (mostly 10) were taken at every temperature plateau. These scans were reduced and averaged to obtain the wall heat flux. Table 8-4 provides an overall summary of the tests that were performed during phase I and II. The heat losses indicated are estimated on the basis of the curve-fitted temperature and enthalpy data presented in Section 7.0.

Figure 8-14 shows measured temperature data from a steady-state test (test S02). The measured primary tube temperatures, wall temperatures, and average fluid temperatures are shown on the figure. With the tank temperature near the boiling point (at atmospheric pressure), the heat transfer process is a combination of vertical free convection and weak boiling at the tube surface.

Figures 8-15 to 8-17 shows the boiling regime on the outside of the PRHR tubes at different elevations. Weak boiling is observed at the bottom of the tubes, while more developed boiling is observed at the top of the PRHR.

Figure 8-18 shows the calculated heat flux on the outside of the PRHR tubes, using the energy balance from Equation 7-1 for a series of primary-side fluid temperatures. The data for each individual test are represented as a string of data points with the lowest heat flux and the smallest tube wall superheat ($T_{wall} - T_{sat}$) values at the bottom of the PRHR tube. The high heat flux points have larger tube wall superheats and occur at the top of the tube where the hot primary fluid enters. Each set of data is for a different primary-side temperature, as well as different primary-side flows. The data show a combination boiling and free convection heat transfer. At low primary fluid temperatures, the heat transfer is dominated by free convection. As the primary temperature and the wall superheat increases, the heat transfer mode changes to boiling.

Figures 8-19 through 8-21 show the estimated outside wall heat fluxes for tests S11, S14, and S05 at inlet temperatures from 650°F to 250°F, which were all performed at 1 gpm. These figures show that the heat flux was unaffected by the number of tubes operating. The data are similar for all three tests, regardless of whether one tube, two tubes, or three tubes were operating, respectively. This confirms that the selected tube pitch (1.5 inches centerline to centerline) is adequate so that tube-to-tube interactions are minimized and that no benefit would be realized from increasing the tube pitch.

Comparisons of the overall tube heat duty are shown in Figure 8-22 for the different test conditions. As expected, higher primary-side initial temperatures and higher flow result in increased heat transfer (Btu/hr) to the simulated IRWST.

8.4 Transient Tests

The transient tests were conducted with the tank initially at or near room temperature. The tank was heated by flow through the three primary tubes until bulk pool boiling occurred. Table 8-5 provides the nominal test conditions for each of the transient tests. Test TR-1 was performed, but the data were not retrievable and are not reported herein.

The tests record the temperature distribution in the simulated IRWST and thereby provide a measure of the mixing within the tank. Figure 8-23 shows the location of vertical thermocouple rakes installed in the tank. Each rake is equipped with a number of thermocouples installed at various elevations (see Table 4-3). Figure 8-24 shows the response of the tank fluid thermocouples mounted at position "D" in the center of the tank for test T02. The elevations at the top of the tubes are shown to heat up first and the lower elevations were delayed and heated up as the overall tank temperature increased to a bulk boiling condition. This stratified thermal condition was established with the PRHR HX acting as a thermal pump. The tank water was heated along the tubes, first by natural convection, and later by weak boiling. The heated plume, which surrounded the PRHR tubes, flowed up to the top of the tank as a hot fluid layer. The PRHR HX was an effective thermal pump, which quickly heated the tank water. At 9500 seconds, when the uppermost elevation is at 212°F, there is a 70°F vertical gradient between the top tank elevation (23.917 feet) and elevation (4.917 feet). Figure 8-25 shows the water mixing in the tank by illustrating the response over the tank cross section at the 13.92-foot elevation during test T02. The small range of temperatures indicate that the tank is well mixed throughout the test. Tables 8-6 through 8-9 show the tank fluid temperatures at different times during the test, indicating the uniformity of the heating throughout the tank.

8.5 Uncovery Tests

All the tests described in Section 8.1 to 8.4 had the PRHR HX covered with a single- or two-phase mixture. A specific series of tests was also performed for which the simulated PRHR and IRWST were uncovered to different levels (75 percent, 50 percent, and 25 percent) to see the effect on the HX performance and heat transfer.

The tube bundle uncovery data were reduced using the same set of equations for the heat flux and wall temperature as described above. Figures 8-26 and 8-27 show the comparison of the fitted primary fluid temperatures and the measured outside wall temperature for both instrumented tubes for test U02 with approximately 25 percent of the tube bundle uncovered. The outside wall temperatures below the two-phase level in the tank data present a clear indication of good cooling (nucleate boiling) and poor cooling (steam cooling) above the two-phase mixture height. The primary fluid temperatures show the same behavior, and the change in the slope of the curve represents the good cooling. Similar

comparisons for the tube wall temperatures for test U04 with 75-percent uncovery are shown in Figures 8-28 and 8-29. For these tests, more of the tube was at the primary tube side temperature.

The PRHR tube bundle uncovery tests were similar to rod bundle uncovery tests. A dryout front existed, below which nucleate boiling occurred. Above the dryout front the heat transfer was primarily steam cooling with small entrained droplets. The spacing (18-inches) of the heat fluxes calculated from the primary-side thermocouples averaged the heat transfer effects across the interface so a dryout front could not be detected from this data. However, the wall temperature measurements more easily detect the front as it passes the thermocouple location.

TABLE 8-1
SUMMARY OF CONFIGURATION TESTS

Tests	Active Tubes	Orifice[1]	Pressure	Temperature	Tube 1		Tube 2	
					Mass Flow	Qdata	Mass Flow	Qdata
			psia	°F	(lb/sec)	(Btu/hr)	(lb/sec)	(Btu/hr)
C01	1, 2, 3	M	[					a,b,c]
	1, 2, 3	M						
	1, 2, 3	M						
	1, 2, 3	M						
	1, 2, 3	M						
	1, 2, 3	M						
C02	1, 2, 3	M						
	1, 2, 3	M						
	1, 2, 3	M						
	1, 2, 3	M						
	1, 2, 3	M						
C03	1, 2, 3	M						
	1, 2, 3	M						
	1, 2, 3	M						
	1, 2, 3	M						
	1, 2, 3	M						
	1, 2, 3	M						
C04	1, 2, 3	M						
	1, 2, 3	M						
	1, 2, 3	M						
	1, 2, 3	M						
	1, 2, 3	M						
	1, 2, 3	M						

TABLE 8-1 (Continued)
SUMMARY OF CONFIGURATION TESTS

Tests	Active Tubes	Orifice[1]	Pressure	Temperature	Tube 1		Tube 2	
					Mass Flow	Qdata	Mass Flow	Qdata
			psia	(°F)	(lb/sec)	(Btu/hr)	(lb/sec)	(Btu/hr)
C05	1, 2, 3	M	[					a,b,c]
	1, 2, 3	M						
	1, 2, 3	M						
	1, 2, 3	M						
	1, 2, 3	M						
	1, 2, 3	M						

Notes:

(1) Refer to Table 6-2, "H" refers to high flow orifice, "M" refers to medium flow orifice, and "L" refers to low flow orifice.

TABLE 8-2
EFFECT OF VARIOUS CONFIGURATIONS

Test Identification	Temperature (°F)					
	500	450	400	350	300	250
C01	164[1]	131	92	58	33	11
C02	166	129	90	61	36	—
C03	167	136	100	63	32	21
C04	165	124	92	63	49	24

Notes:

(1) The values indicated are the ratio of total heat loss from tubes 1 and 2 divided by the total mass flow from tubes 1 and 2 expressed in Btu/lb.

TABLE 8-3
TANK HEATUP RATE

Test	From Start to First Steaming	From First Steaming to Bulk Boiling	From Start to Bulk Boiling
C01	[		]
C02			
C03			
C04			
C05	[		]

a,b,c

TABLE 8-4
SUMMARY OF STEADY-STATE PASSIVE RESIDUAL HEAT REMOVAL TESTS

Test Identification	Active Tubes	Orifice[1]	Pressure (psia)	Temperature (°F)	Tube 1 Mass Flow (lb/sec.)	Tube 1 Heat Loss (Btu/hr)	Tube 2 Mass Flow (lb/sec.)	Tube 2 Heat Loss (Btu/hr)
SS03[2]	1, 2, 3	H						
	1, 2, 3	H						
	1, 2, 3	H						
	1, 2, 3	H						
	1, 2, 3	H						
	1, 2, 3	H						
	1, 2, 3	H						
	1, 2, 3	H						
	1, 2, 3	H						
	1, 2, 3	H						
	1, 2, 3	H						
	1, 2, 3	H						
SS04[2]	1, 2, 3	H						
	1, 2, 3	H						
	1, 2, 3	H						
	1, 2, 3	H						
	1, 2, 3	H						
	1, 2, 3	H						
	1, 2, 3	H						
	1, 2, 3	H						
SS05[2]	1, 2, 3	H						
	1, 2, 3	H						
	1, 2, 3	H						
	1, 2, 3	H						
	1, 2, 3	H						
	1, 2, 3	H						
	1, 2, 3	H						
SS06[2]	1, 2, 3	H						
	1, 2, 3	H						
	1, 2, 3	H						
	1, 2, 3	H						
	1, 2, 3	H						
	1, 2, 3	H						
	1, 2, 3	H						
SS07[2]	1, 2, 3	H						
	1, 2, 3	H						
	1, 2, 3	H						
	1, 2, 3	H						
	1, 2, 3	H						
	1, 2, 3	H						
	1, 2, 3	H						
S01	1, 2, 3	H						
	1, 2, 3	H						
	1, 2, 3	H						
	1, 2, 3	H						

a,b,c

TABLE 8-4 (Continued)
SUMMARY OF STEADY-STATE PASSIVE RESIDUAL HEAT REMOVAL TESTS

Test Identification	Active Tubes	Orifice[1]	Pressure (psia)	Temperature (°F)	Tube 1 Mass Flow (lb/sec.)	Tube 1 Heat Loss (Btu/hr)	Tube 2 Mass Flow (lb/sec.)	Tube 2 Heat Loss (Btu/hr)
S02	1, 2, 3	M						
	1, 2, 3	M						
	1, 2, 3	M						
	1, 2, 3	M						
	1, 2, 3	M						
S03	1, 2, 3	M						
	1, 2, 3	M						
	1, 2, 3	M						
	1, 2, 3	M						
	1, 2, 3	M						
	1, 2, 3	M						
	1, 2, 3	M						
S04	1, 2, 3	L						
	1, 2, 3	L						
	1, 2, 3	L						
	1, 2, 3	L						
	1, 2, 3	L						
	1, 2, 3	L						
	1, 2, 3	L						
	1, 2, 3	L						
	1, 2, 3	L						
S05	1, 2, 3	M						
	1, 2, 3	M						
	1, 2, 3	M						
	1, 2, 3	M						
	1, 2, 3	M						
	1, 2, 3	M						
	1, 2, 3	M						
	1, 2, 3	M						
	1, 2, 3	M						
	1, 2, 3	M						
	1, 2, 3	M						
	1, 2, 3	M						
S06	1, 3	L						
	1, 3	L						
	1, 3	L						
	1, 3	L						
	1, 3	L						
	1, 3	L						
	1, 3	L						
	1, 3	L						
	1, 3	L						

a,b,c

TABLE 8-4 (Continued)
SUMMARY OF STEADY-STATE PASSIVE RESIDUAL HEAT REMOVAL TESTS

Test Identification	Active Tubes	Orifice[1]	Pressure (psia)	Temperature (°F)	Tube 1 Mass Flow (lb/sec.)	Tube 1 Heat Loss (Btu/hr)	Tube 2 Mass Flow (lb/sec.)	Tube 2 Heat Loss (Btu/hr)
S07	2	H						
	2	H						
	2	H						
	2	H						
	2	H						
	2	H						
	2	H						
	2	H						
	2	H						
S08	2	H						
	2	H						
	2	H						
	2	H						
	2	H						
	2	H						
	2	H						
	2	H						
	2	H						
S09	1	M						
	1	M						
	1	M						
	1	M						
	1	M						
	1	M						
	1	M						
	1	M						
S10	2	L						
	2	L						
	2	L						
	2	L						
	2	L						
	2	L						
	2	L						
	2	L						
	2	L						
S11	1	M						
	1	M						
	1	M						
	1	M						
	1	M						
	1	M						
	1	M						
	1	M						
	2	M						
	2	M						
	1	M						

a,b,c

TABLE 8-4 (Continued)
SUMMARY OF STEADY-STATE PASSIVE RESIDUAL HEAT REMOVAL TESTS

Test Identification	Active Tubes	Orifice[1]	Pressure	Temperature	Tube 1		Tube 2	
					Mass Flow	Heat Loss	Mass Flow	Heat Loss
			(psia)	(°F)	(lb/sec.)	(Btu/hr)	(lb/sec.)	(Btu/hr)
S12	1, 2	H						
	1, 2	H						
	1, 2	H						
	1, 2	H						
	1, 3	H						
	1, 3	H						
	1, 3	H						
	1, 3	H						
	1, 3	H						
S13	1, 2	M						
	1, 2	M						
	1, 2	M						
	1, 2	M						
	1, 2	M						
	1, 2	M						
	1, 2	M						
	1, 2	M						
	1, 2	M						
	1, 3	M						
	1, 3	M						
	1, 3	M						
	1, 3	M						
S14	1, 2	M						
	1, 2	M						
	1, 2	M						
	1, 2	M						
	1, 2	M						
	1, 2	M						
	1, 2	M						
	1, 2	M						
	1, 2	M						
	1, 3	M						
	1, 3	M						
	1, 3	M						
	1, 3	M						
S15	1, 2, 3	M						
	1, 2, 3	M						
	1, 2, 3	M						
	1, 2, 3	M						
	1, 2, 3	M						
	1, 2, 3	M						
	1, 2, 3	M						
	1, 2, 3	M						
	1, 2, 3	M						

a,b,c

Notes:
(1) Refer to Table 6-2, "H" refers to high flow orifice, "M" refers to medium flow orifice, and "L" refers to low flow orifice.
(2) Phase 1 tests.

TABLE 8-5
SUMMARY OF THE PASSIVE RESIDUAL HEAT REMOVAL TRANSIENT TESTS

Test Name	Orifice Used[1]	Duration (sec.)	Pressure (psia)	Inlet Temperature (°F)	Flow Rate (lb/sec.)
TR-4[2]	H				
TR-7[2]	H				
TR-11[2]	H				
T-01	M				
T-02	M				
T-03	M				
T-04	L				

a,b,c

Notes:

(1) Refer to Table 6-2, "H" refers to high flow orifice, "M" refers to medium flow orifice, and "L" refers to low flow orifice.

(2) Phase I tests.

TABLE 8-6
INITIAL PASSIVE RESIDUAL HEAT REMOVAL TANK TEMPERATURES FOR TEST T02

Elevation	Location in Tank							
	C	D	E	F	G	H	J	K
28.000								
26.000								
23.917								
22.917								
21.417								
19.917								
18.417								
16.917								
15.417								
13.917								
12.417								
10.917								
9.417								
7.917								
6.417								
4.917								
3.417								
1.917								
0.417								

a,b,c

TABLE 8-7
PASSIVE RESIDUAL HEAT REMOVAL TANK TEMPERATURES FOR TEST T02 AFTER 5172 SECONDS

Elevation	Location in Tank							
	C	D	E	F	G	H	J	K
28.000	78.3	79.5	73.9	75.5	75.2	75	76.1	82.9
26.000	78.7	81.3	71.8	72.2	71.9	69.7	75.1	83.6
23.917	81	87.3	83.1	77	77.5	77.9	71.4	80.1
22.917	87.7	96	91.5	82.7	82	86.3	80.8	75.2
21.417			147.6	155.9	151.3	146.9		
19.917	147.2	146.8	142.9	146.8	145.8	145.5	145.7	145.7
18.417			139	144.75	144.6	144.4		
16.917	142.6	142.2	134.9	142.7	142.7	141.9	142	142
15.417			136.5	135.6	135.6	138.5		
13.917	134.3	133.7	129.5	132.4	131.4	133.5	133.6	133.3
12.417			125.4	122.7	127.4	127.3		
10.917	120.3	119.9	117	120.6	121.1	121.1	120.1	119.8
9.417			114.4	115.2	112.2	113.1		
7.917	107.8	107.4	105.7	104.6	106	108	107.2	107.2
6.417			102.9	100.7	101.9	102		
4.917	96.7	96.5	96	97.4	97.5	97.5	96.6	96.7
3.417			90	89.2	90	90.2		
1.917	77.9	78	78	78	78	77.7	76.7	77.4
0.417			62.6	62.2	62.7	62.4		

TABLE 8-8
PASSIVE RESIDUAL HEAT REMOVAL TANK TEMPERATURES
FOR TEST T02 AFTER 7983 SECONDS

Elevation	Location in Tank							
	C	D	E	F	G	H	J	K
28.000								
26.000								
23.917								
22.917								
21.417								
19.917								
18.417								
16.917								
15.417								
13.917								
12.417								
10.917								
9.417								
7.917								
6.417								
4.917								
3.417								
1.917								
0.417								

a,b,c

TABLE 8-9
PASSIVE RESIDUAL HEAT REMOVAL TANK TEMPERATURES
FOR TEST T02 AFTER 14178 SECONDS

Elevation	Location in Tank							
	C	D	E	F	G	H	J	K
28.000								
26.000								
23.917								
22.917								
21.417								
19.917								
18.417								
16.917								
15.417								
13.917								
12.417								
10.917								
9.417								
7.917								
6.417								
4.917								
3.417								
1.917								
0.417								

a,b,c

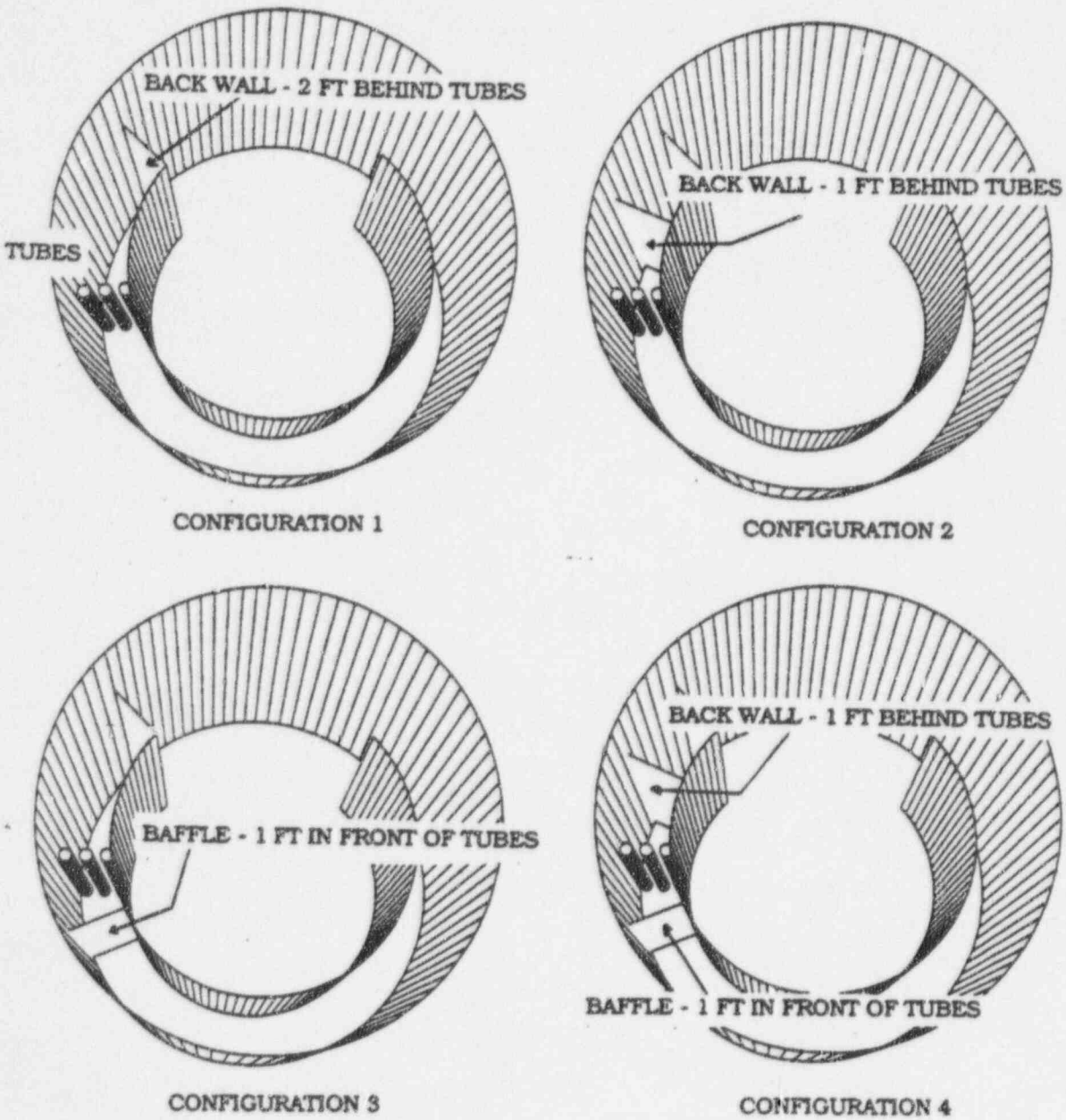

Figure 8-1 Passive Residual Heat Removal Heat Exchanger Configuration Tests

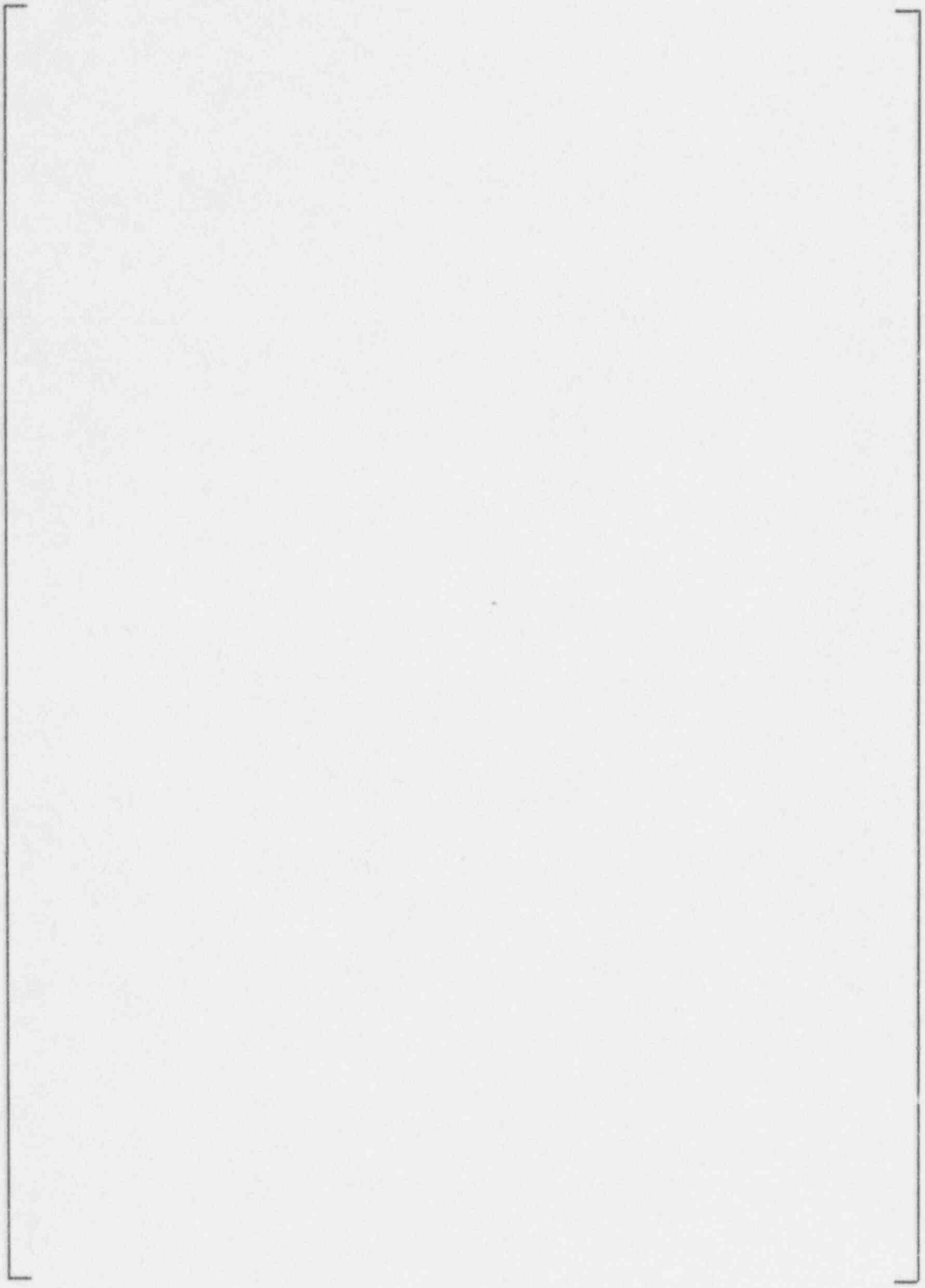

(a,h,c)

Figure 8-2 Local Wall Heat Flux for Configuration 1 (Test C01)

(a,b,c)

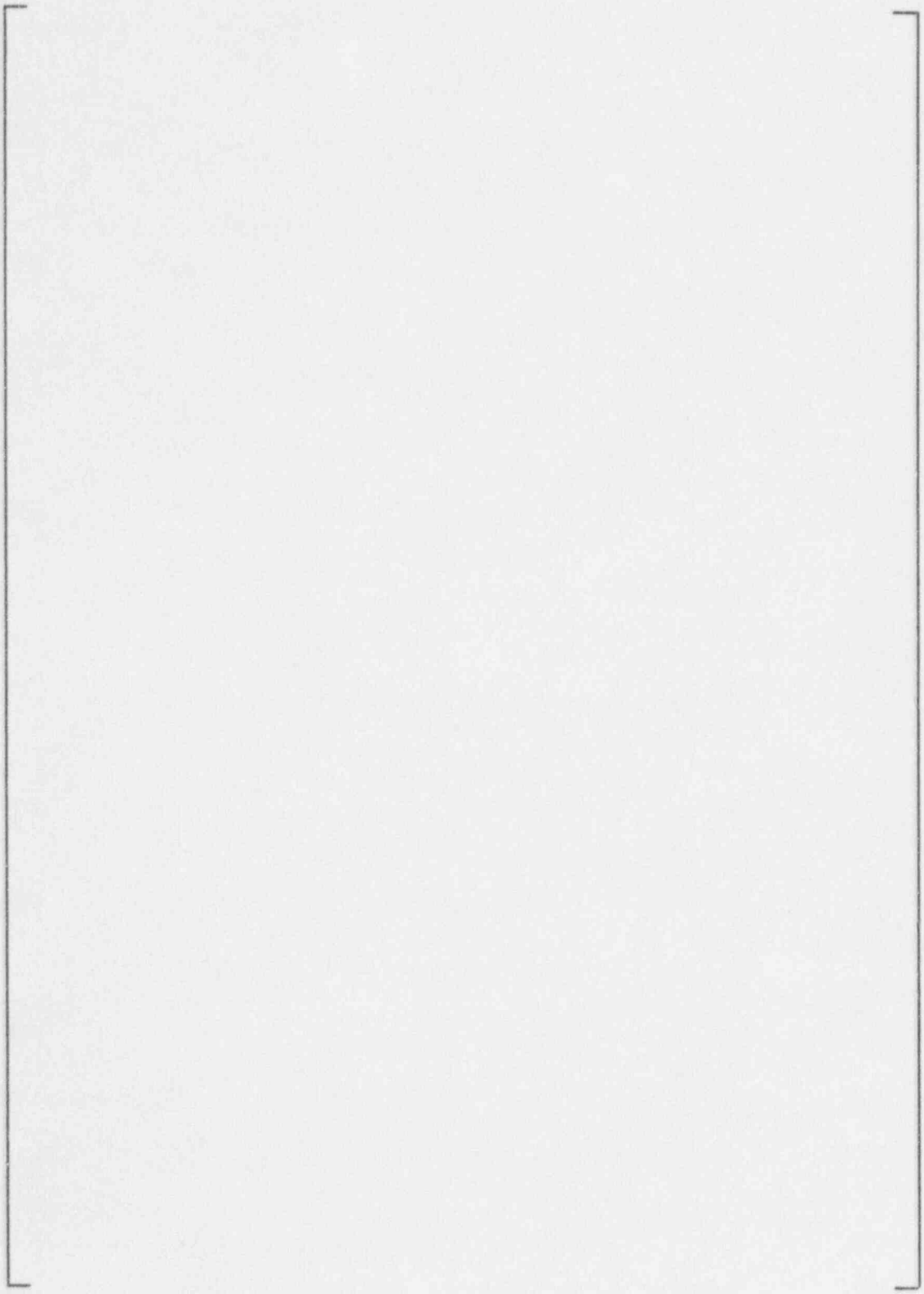

Figure 8-3 Local Wall Heat Flux for Configuration 2 (Test C02)

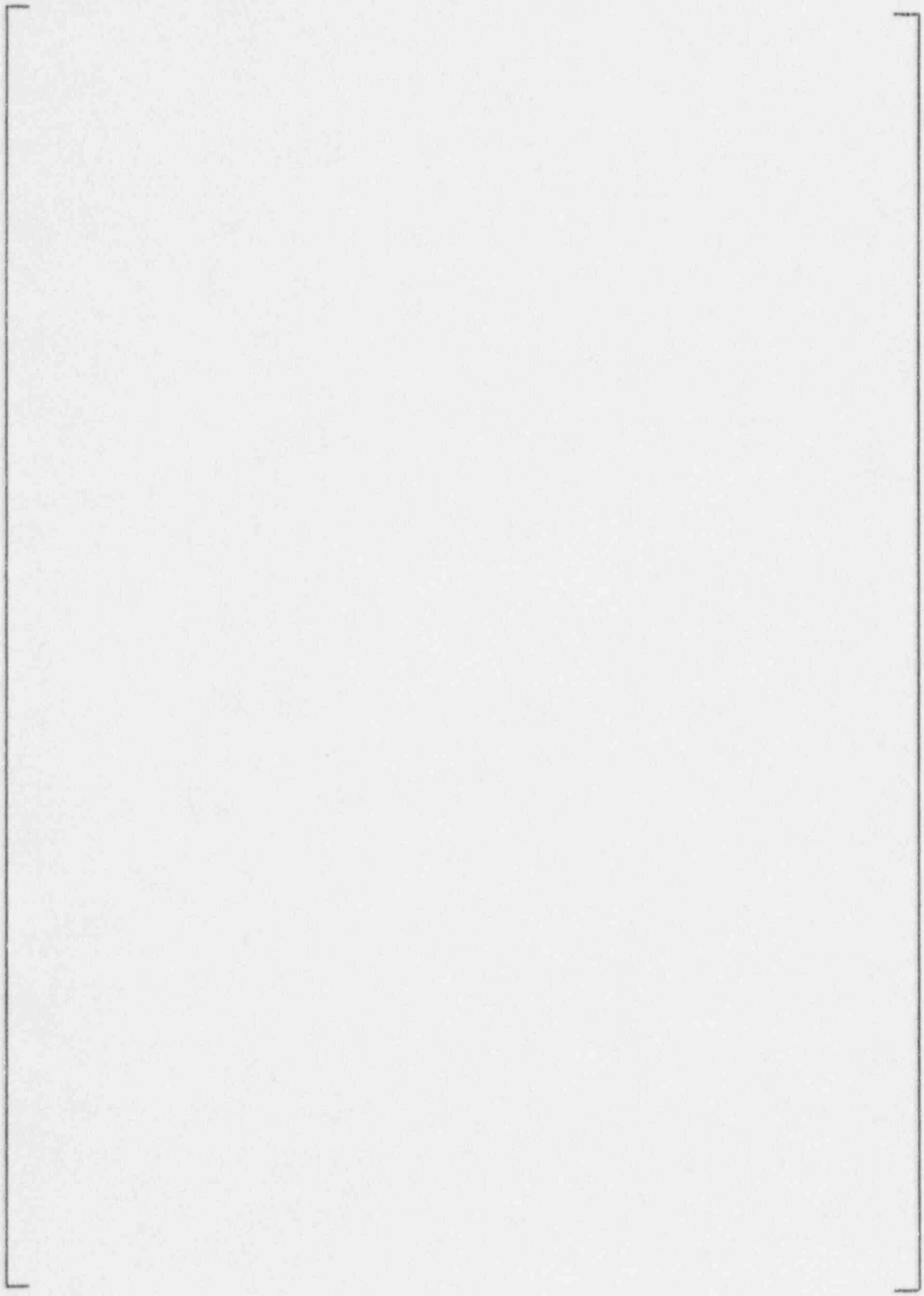

(a,b,c)

Figure 8-4 Local Wall Heat Flux for Configuration 3 (Test C03)

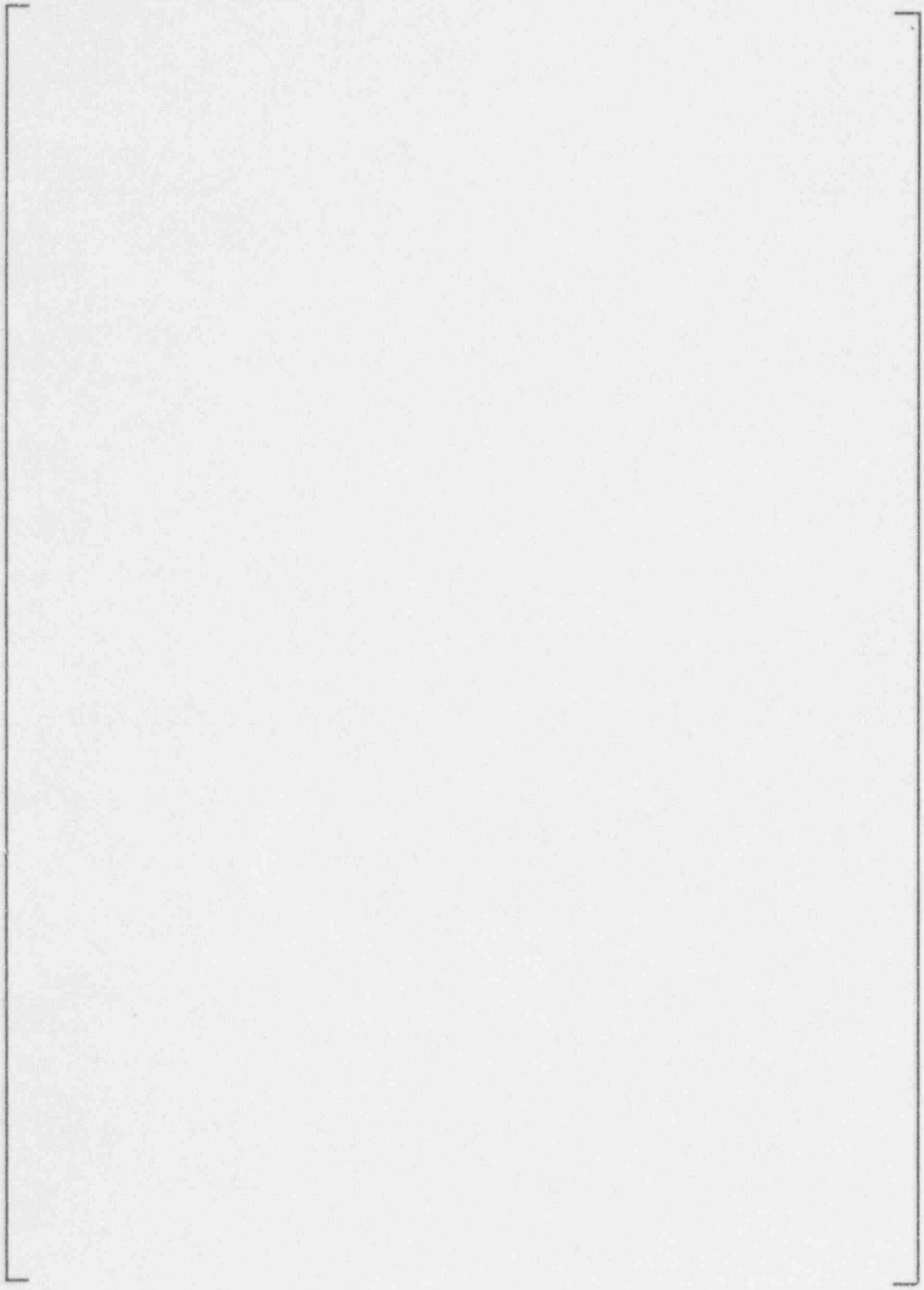

(a,b,c)

Figure 8-5 Local Wall Heat Flux for Configuration 4 (Test C04)

[ ] (a,b,c)

Figure 8-6 Transient Tank Heatup

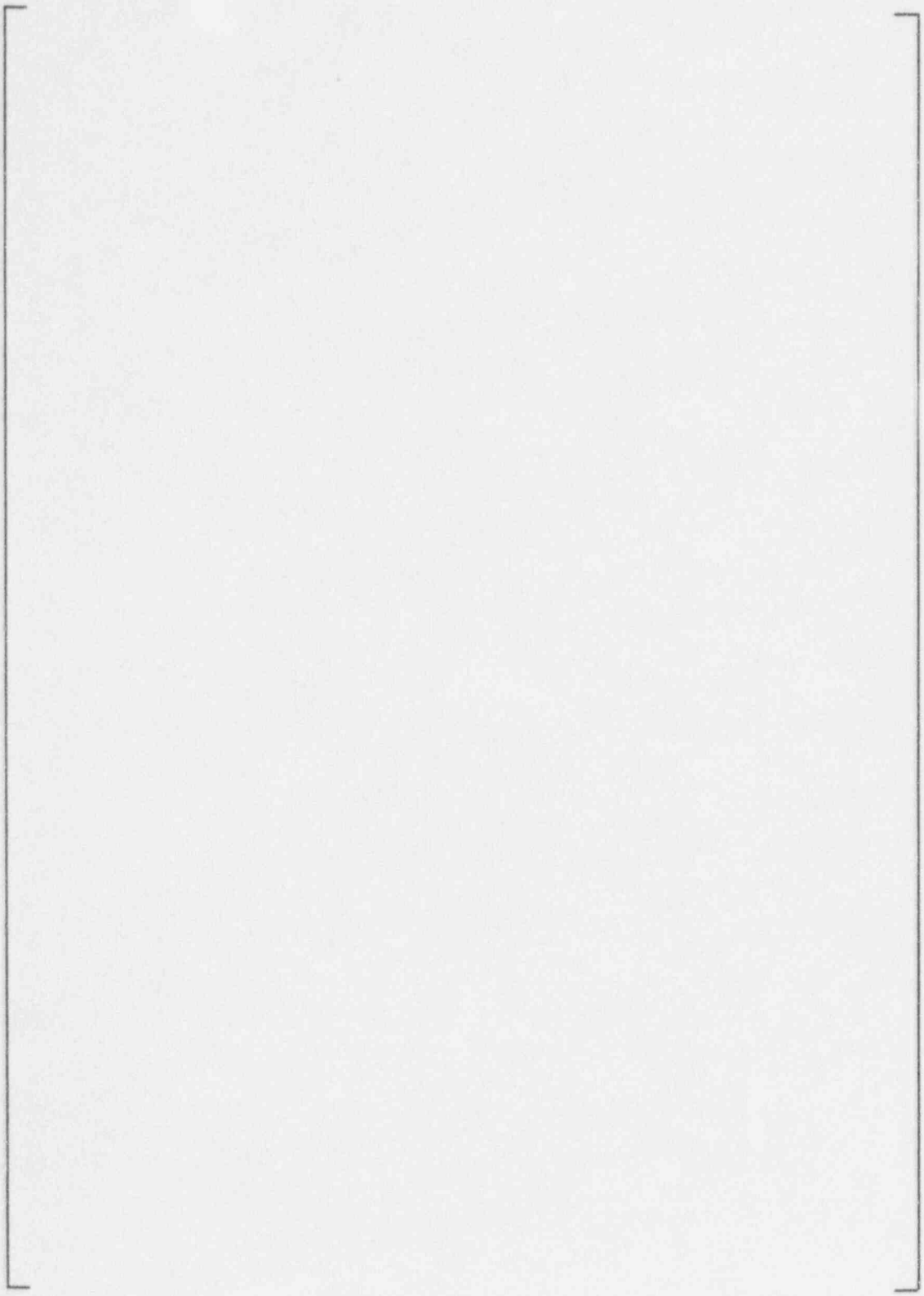

(a,b,c)

Figure 8-7 Plume Temperature Traverse for Plume Test P01

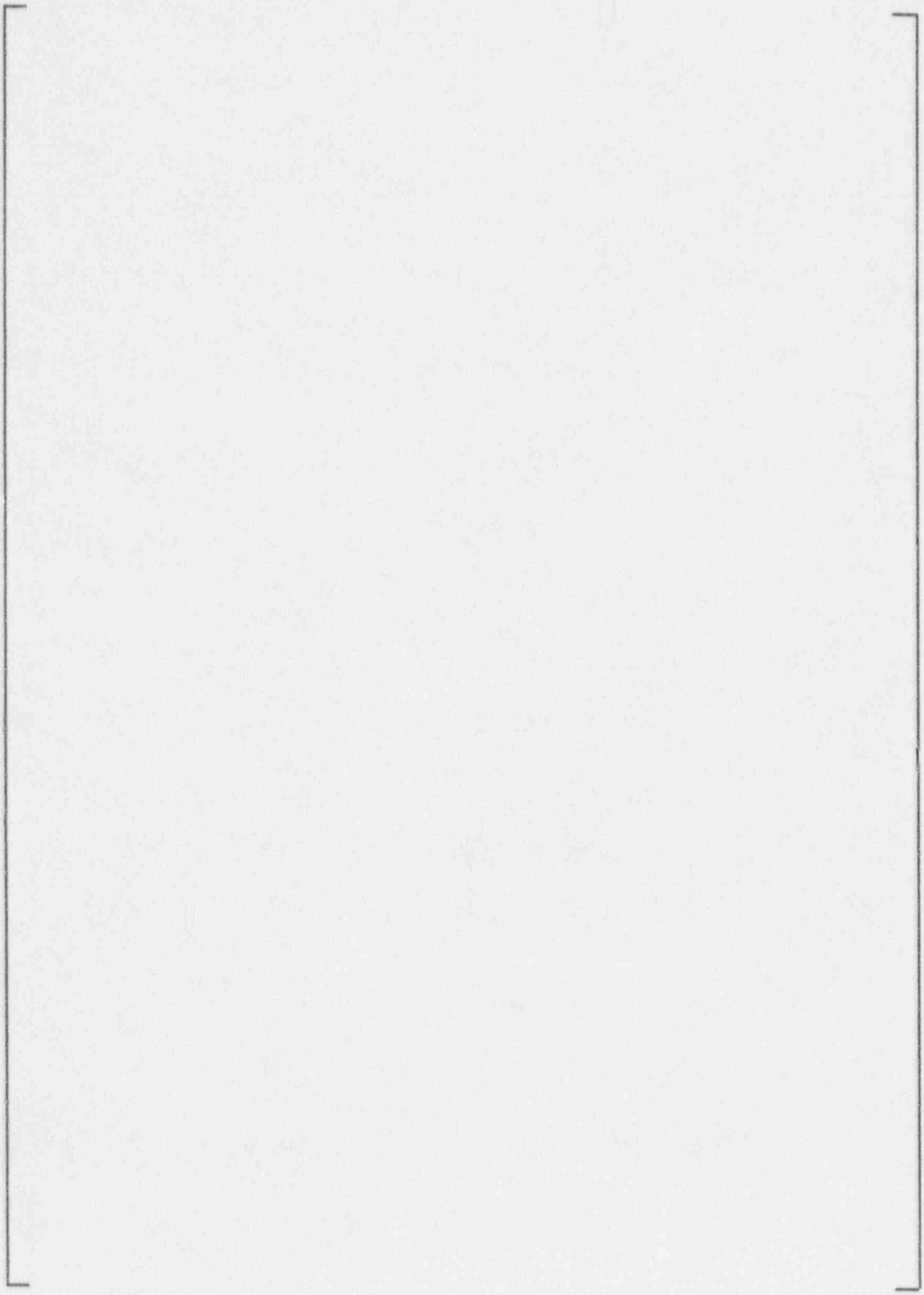

(a,b,c)

Figure 8-8 Plume Temperature Traverse for Plume Test P02

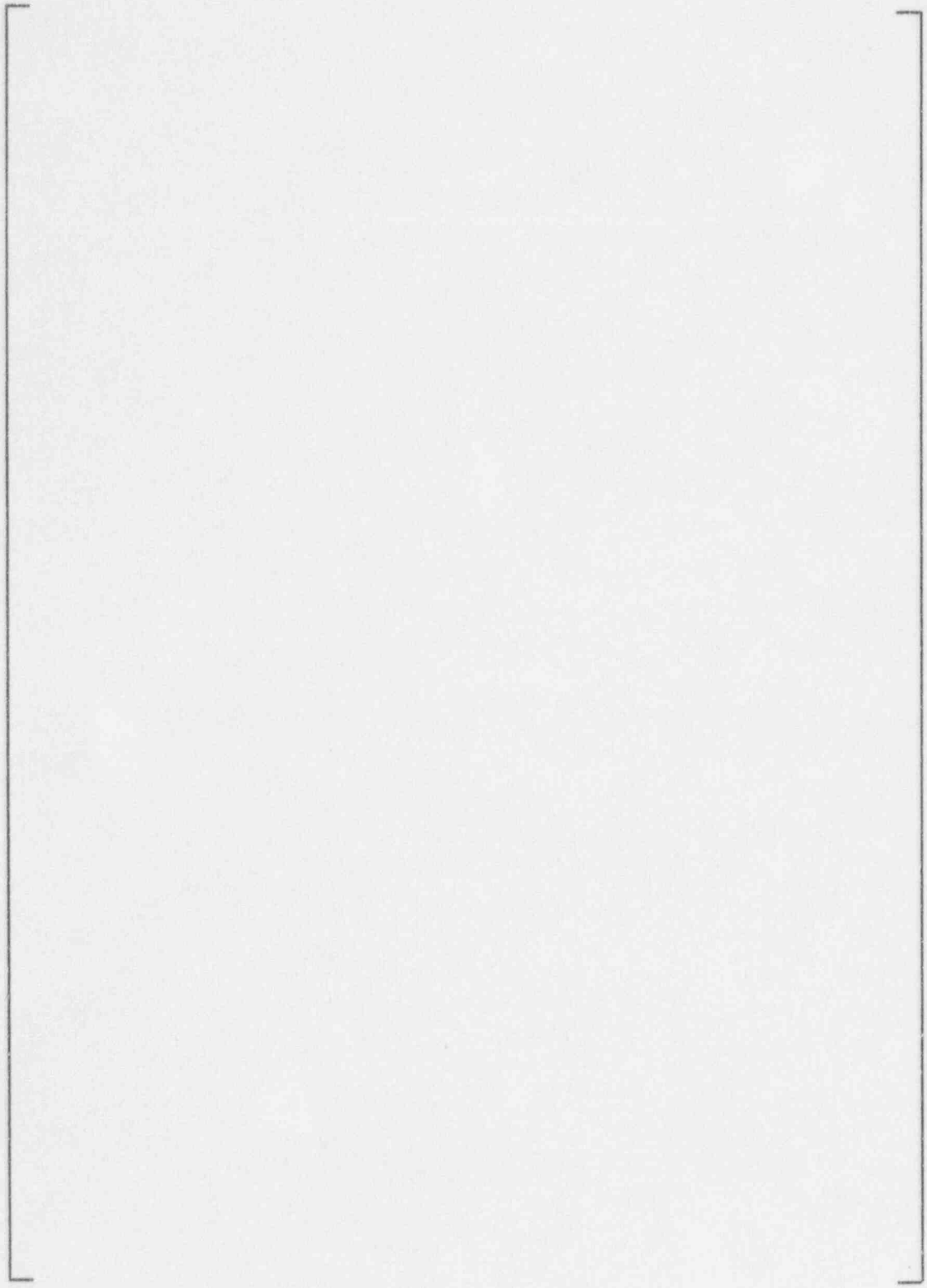

(a,b,c)

Figure 8-9 Plume Temperature Traverse for Plume Test P03

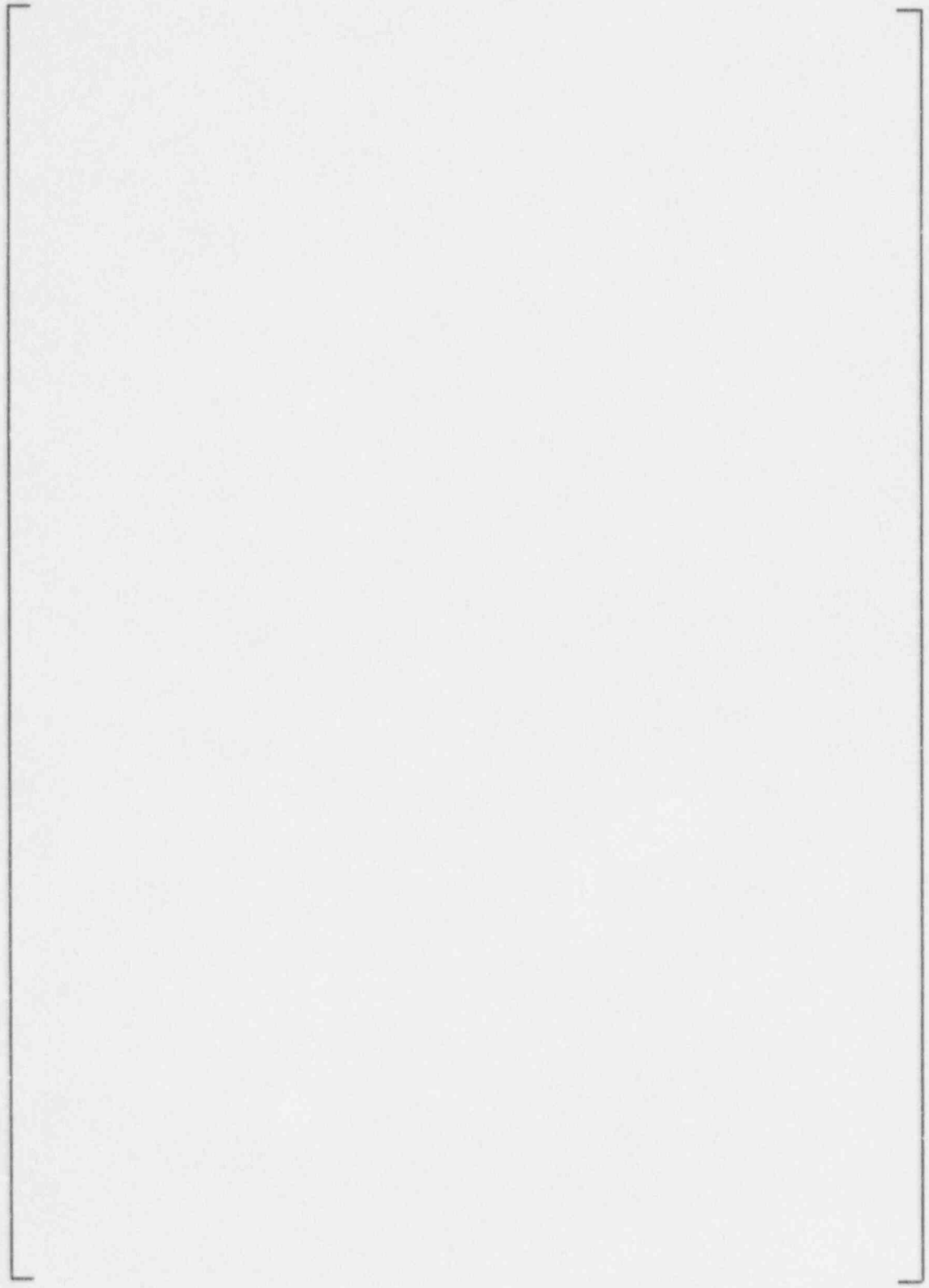

(a,b,c)

Figure 8-10 Plume Temperature Traverse for Plume Test P05

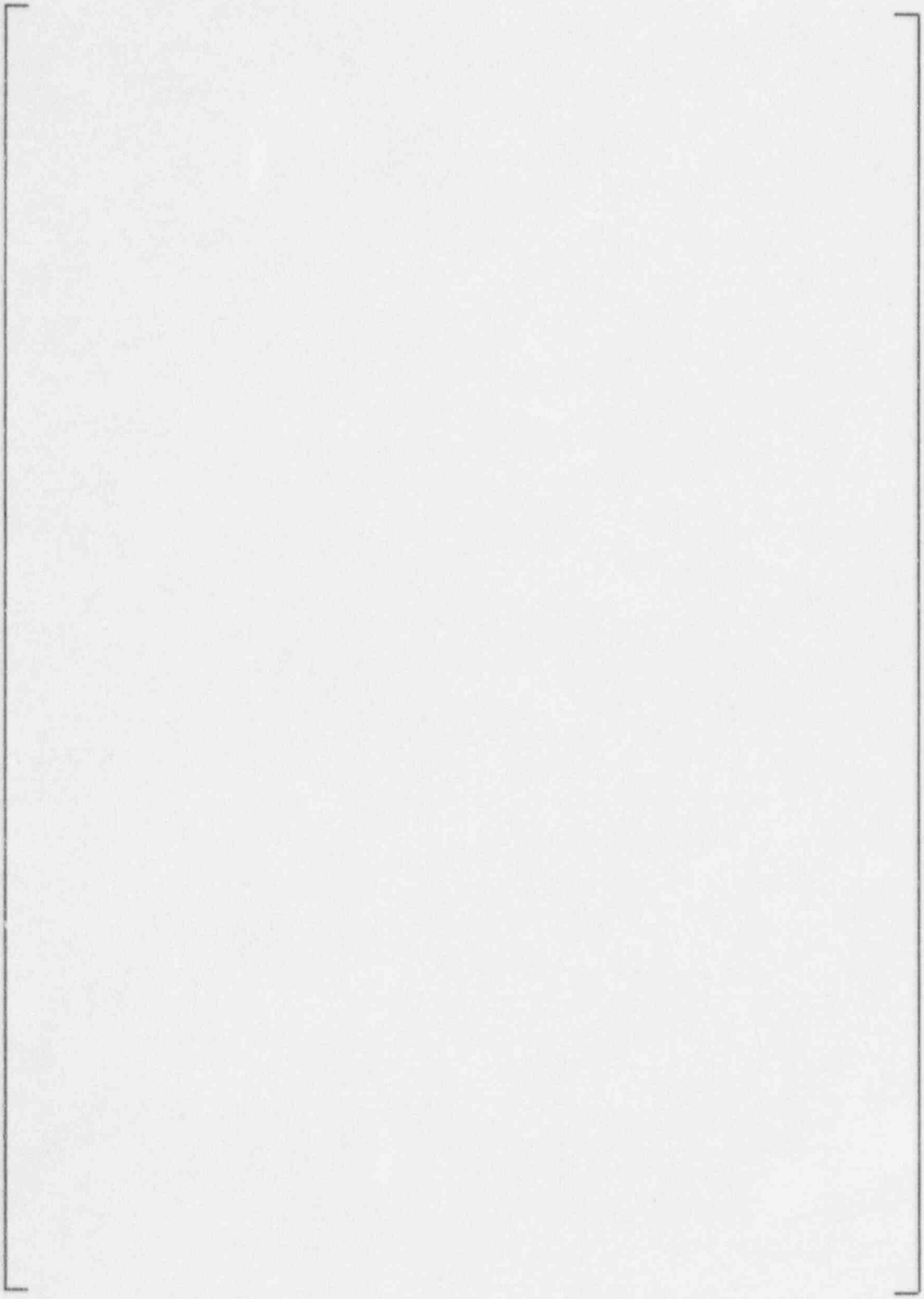

(a,b,c)

Figure 8-11 Plume Temperature Traverse for Configuration Test C02

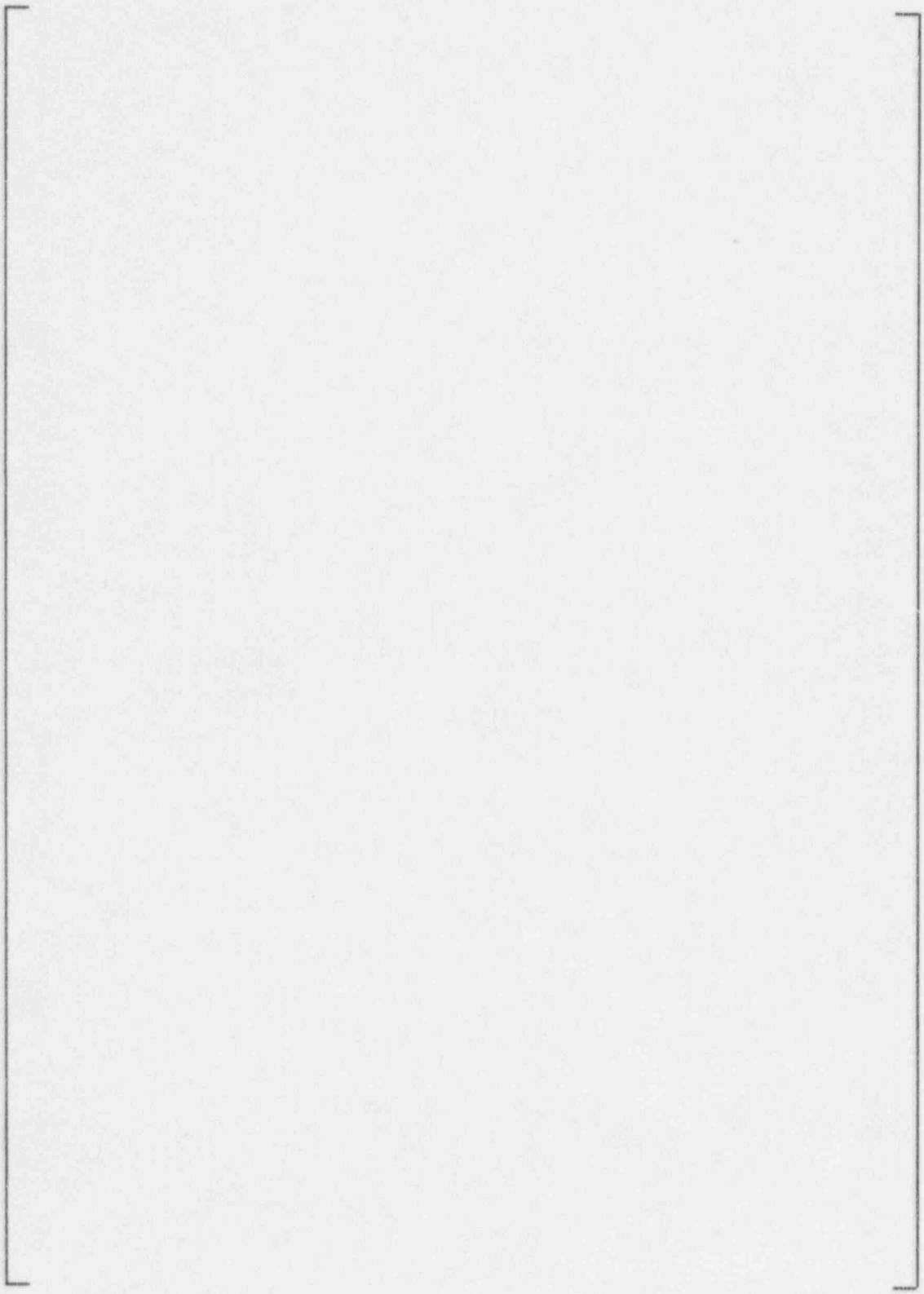

(a,b,c)

Figure 8-12 Plume Temperature Traverse for Configuration Test C03

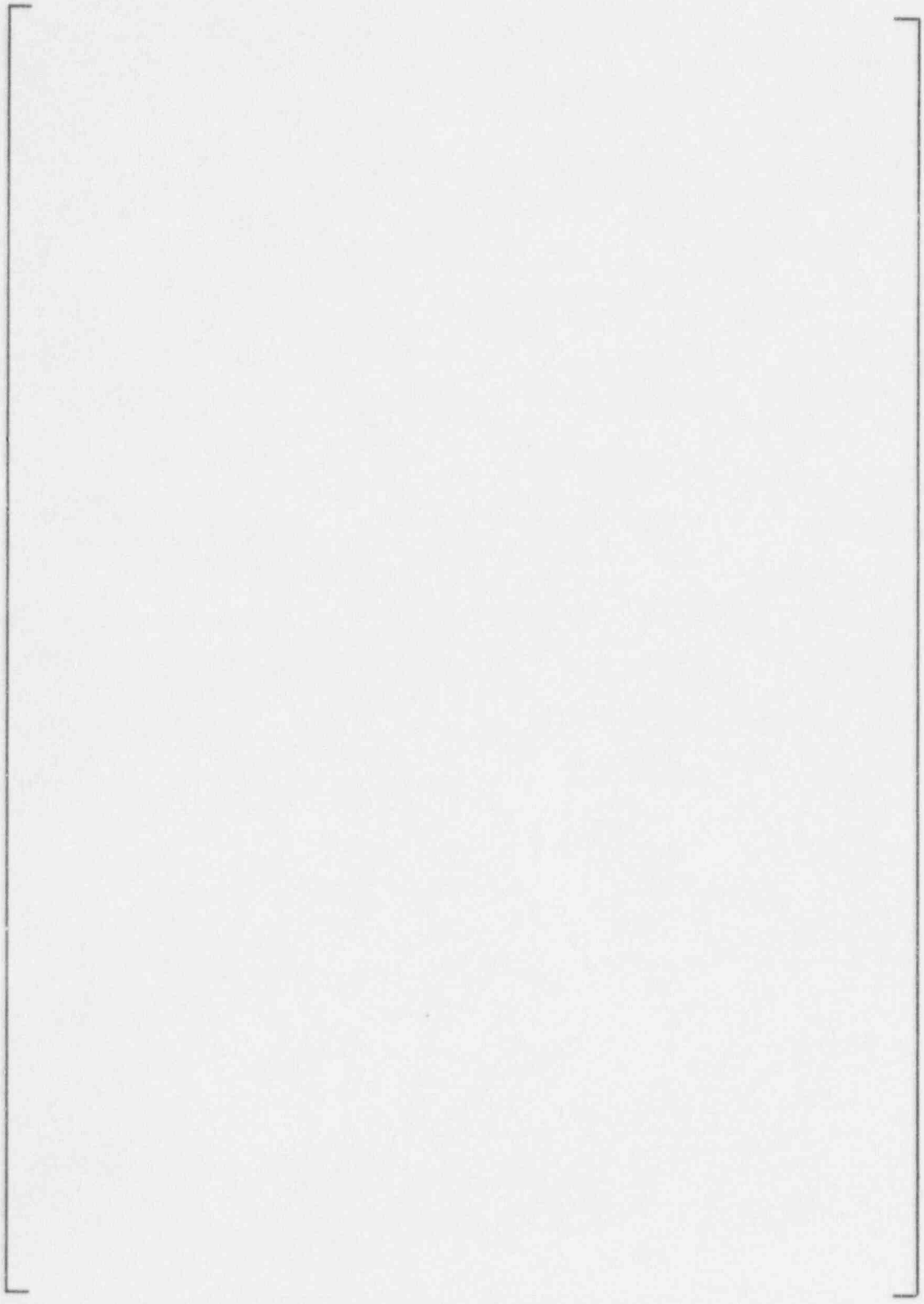

(a,b,c)

Figure 8-13 Plume Temperature Traverse for Configuration Test C04

a,b,c

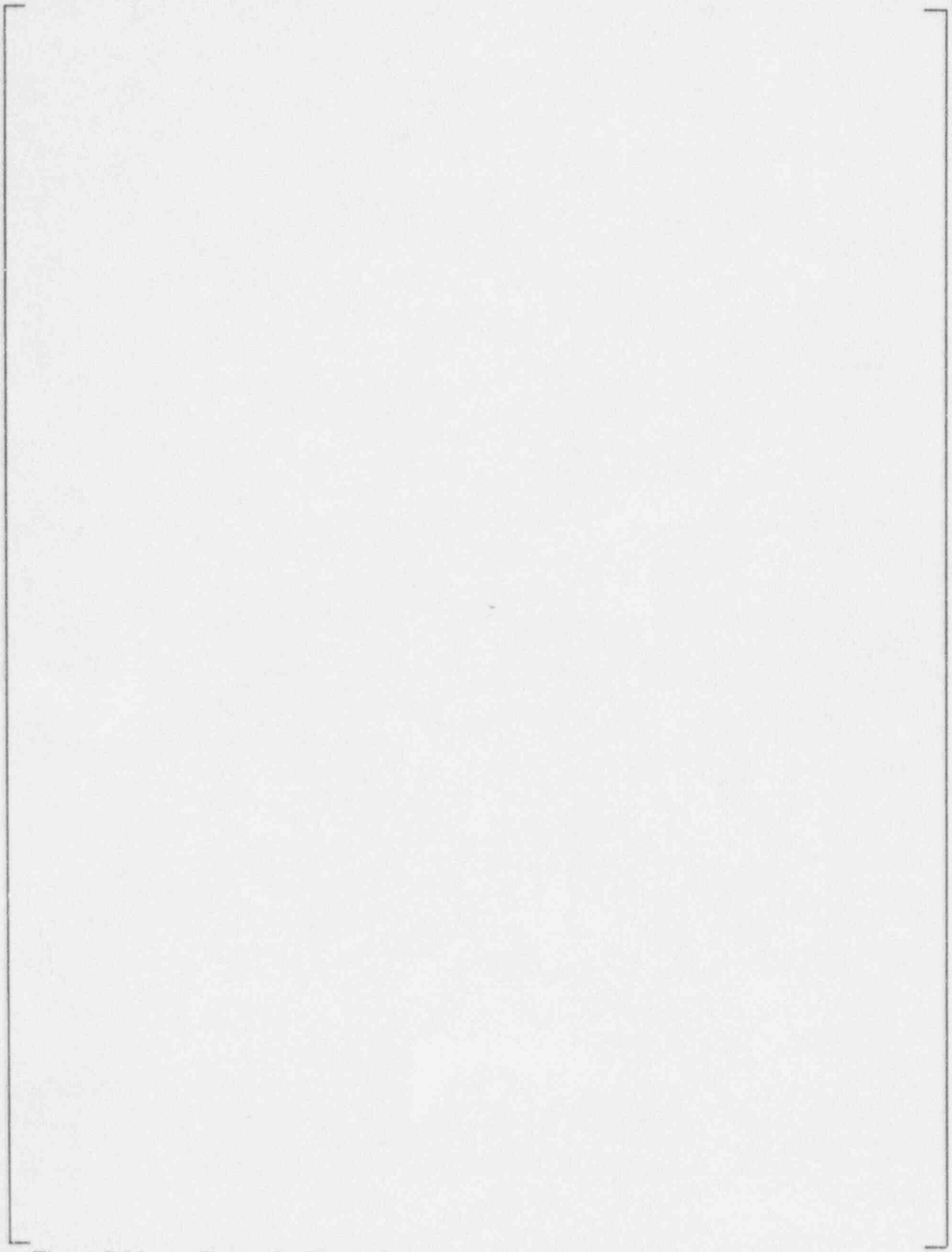

Figure 8-14 **Composite Plot of Primary Fluid, Wall Temperature, and Tank Temperature Data for Tests S02 Tube 1**

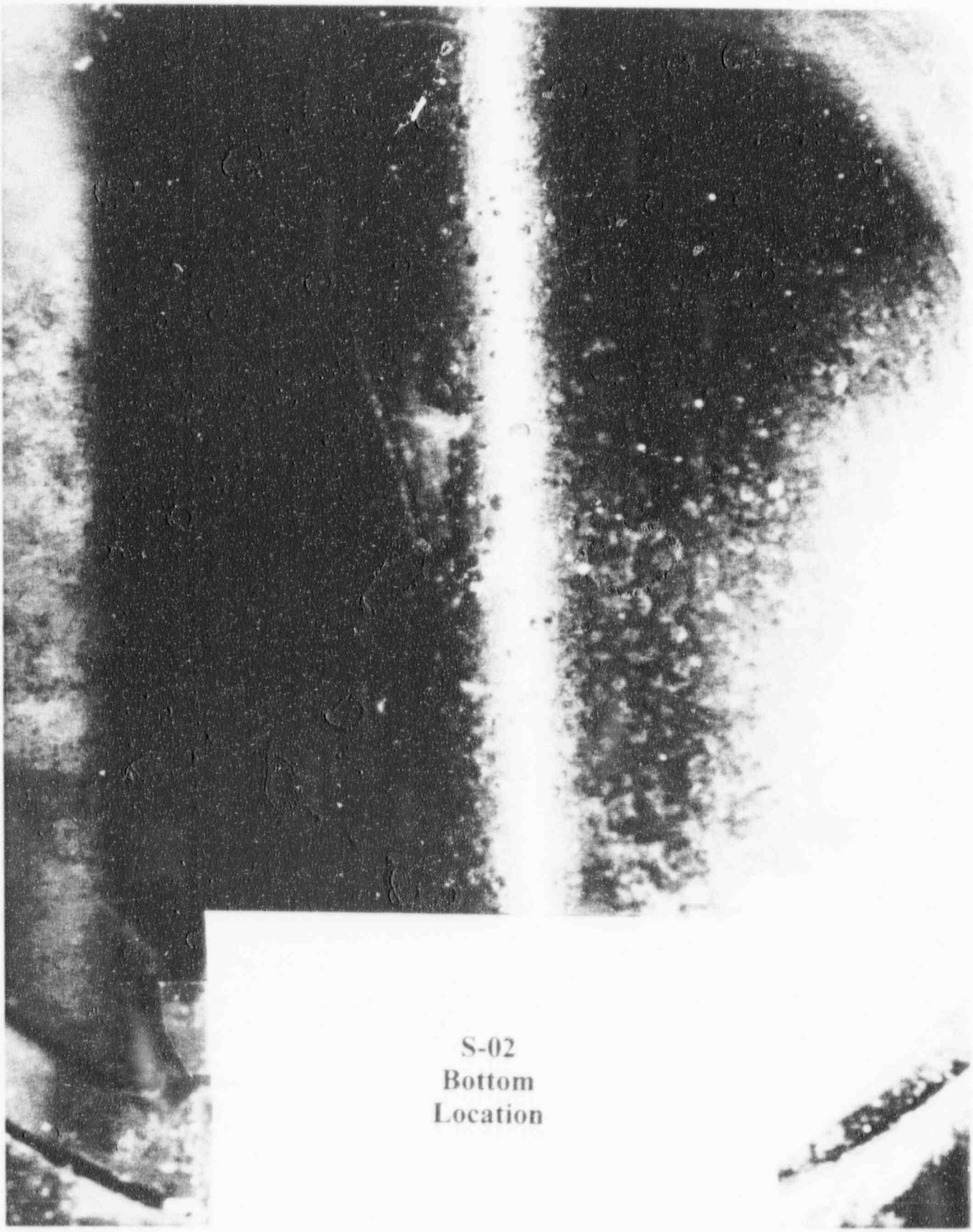

Figure 8-15 Photograph of Boiling at the Bottom of the Passive Residual Heat Removal Tubes for Test S02

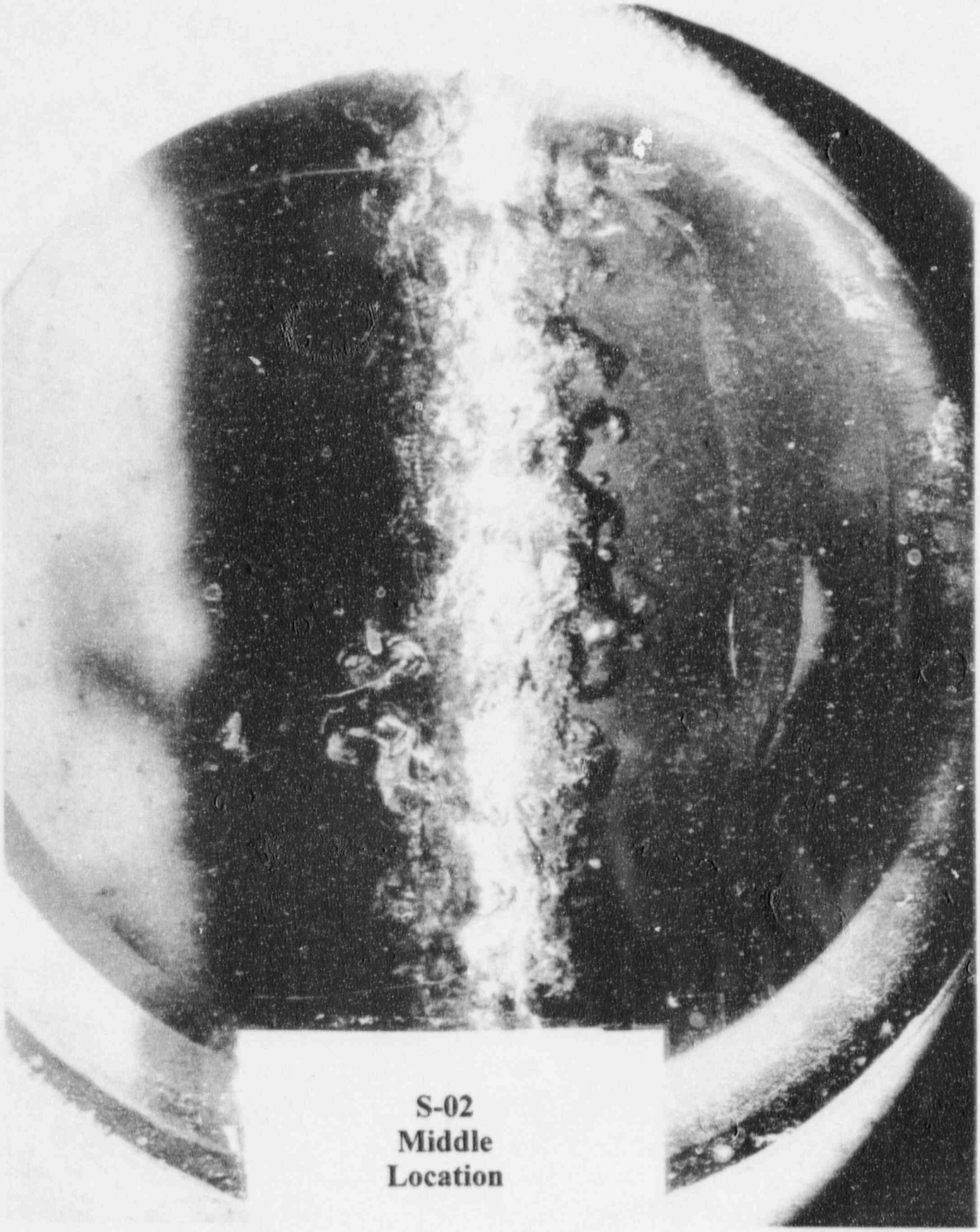

Figure 8-16 **Photograph of Boiling at the Mid-Plane of the Passive Residual Heat Removal Tubes for Test S02**

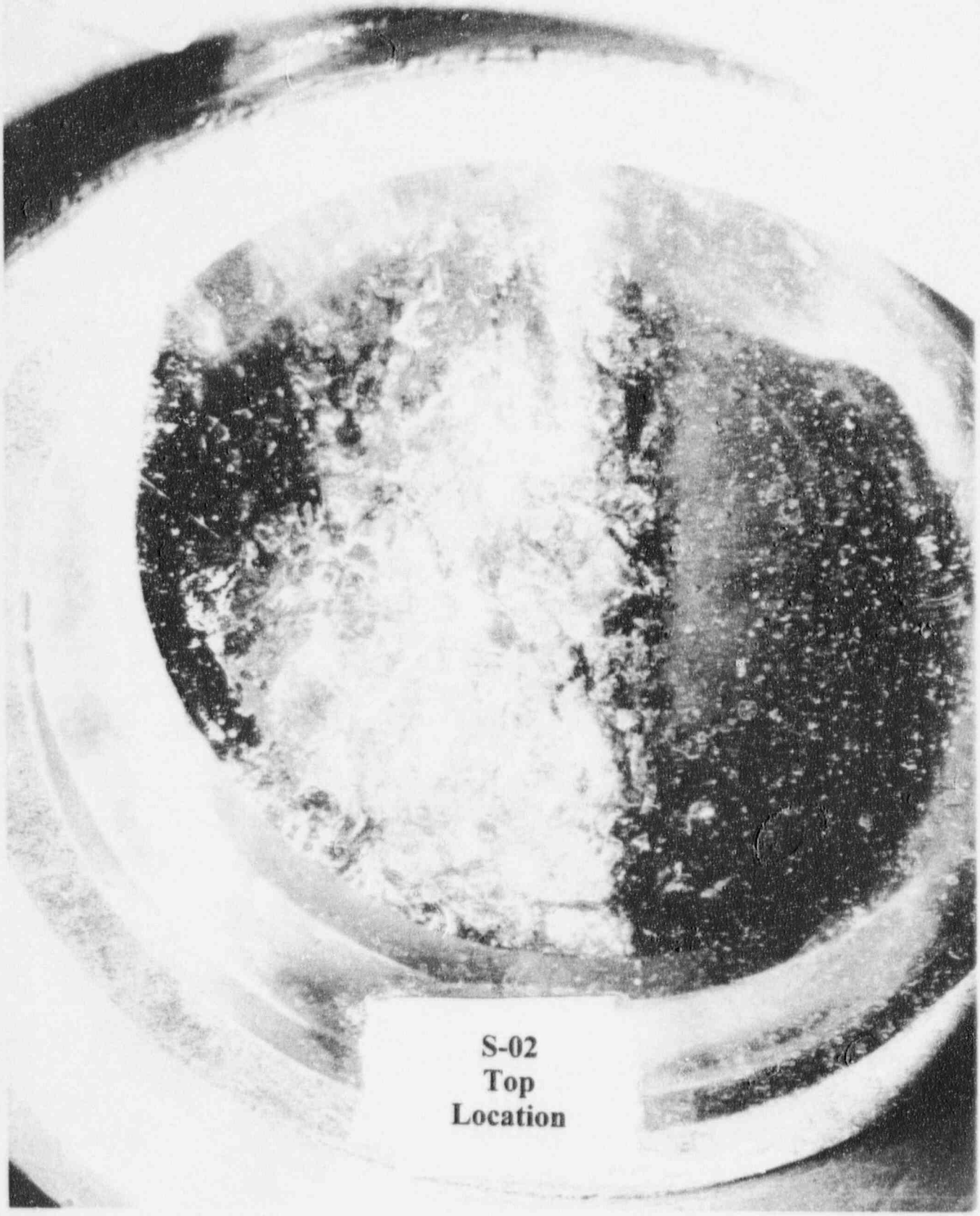

Figure 8-17 Photograph at the Top of the Passive Residual Heat Removal Tubes for Test S02

[ ] (a,b,c)

Figure 8-18 **Passive Residual Heat Removal Heat Flux, Boiling Curve Data for Steady-State Tests**

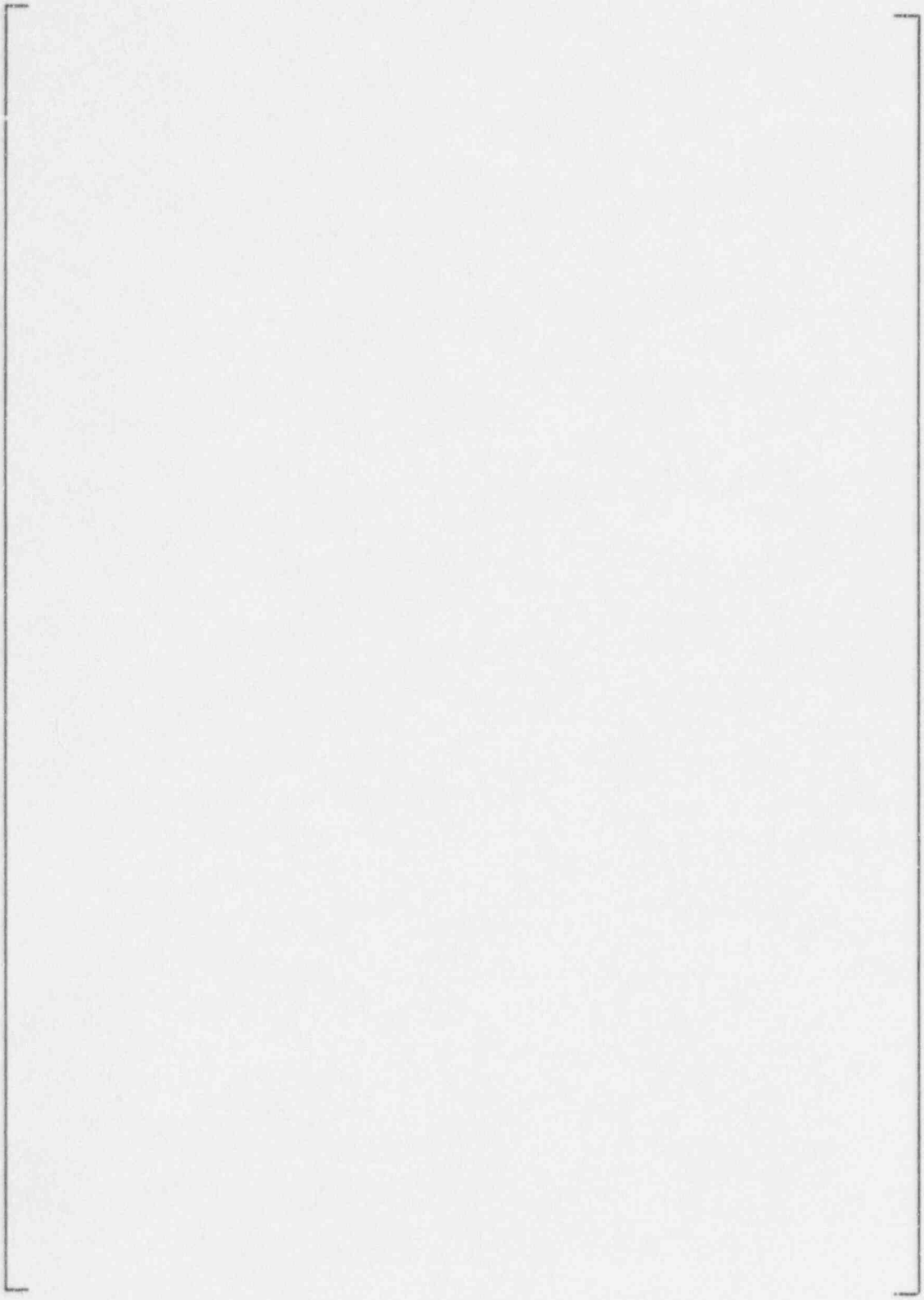

(a,b,c)

Figure 8-19 Local Wall Heat Flux for Steady-State Test S11 (Three Tubes at 1 gpm each)

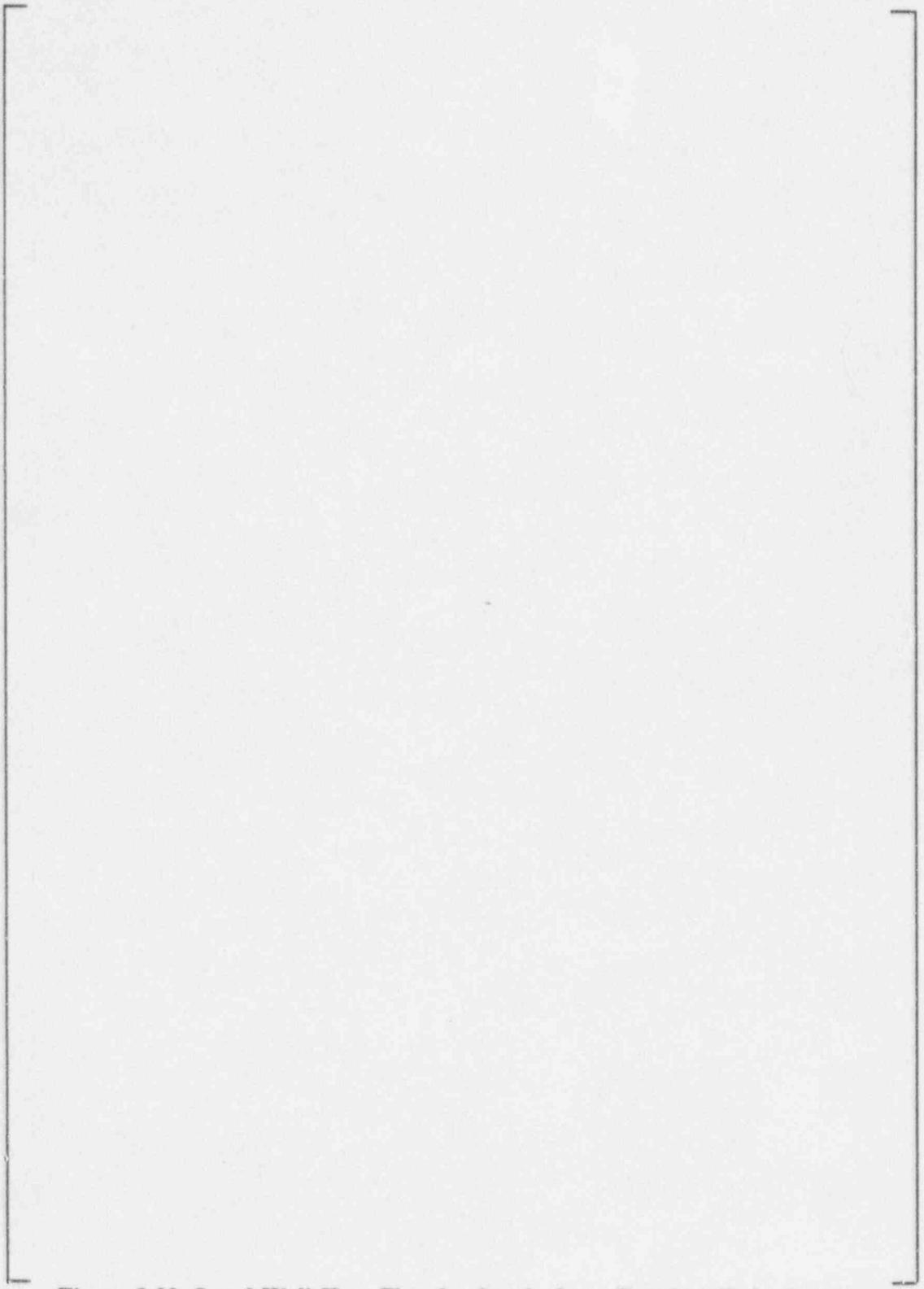

(a,b,c)

Figure 8-20 Local Wall Heat Flux for Steady-State Test S14 (Tube 2 at 1 gpm)

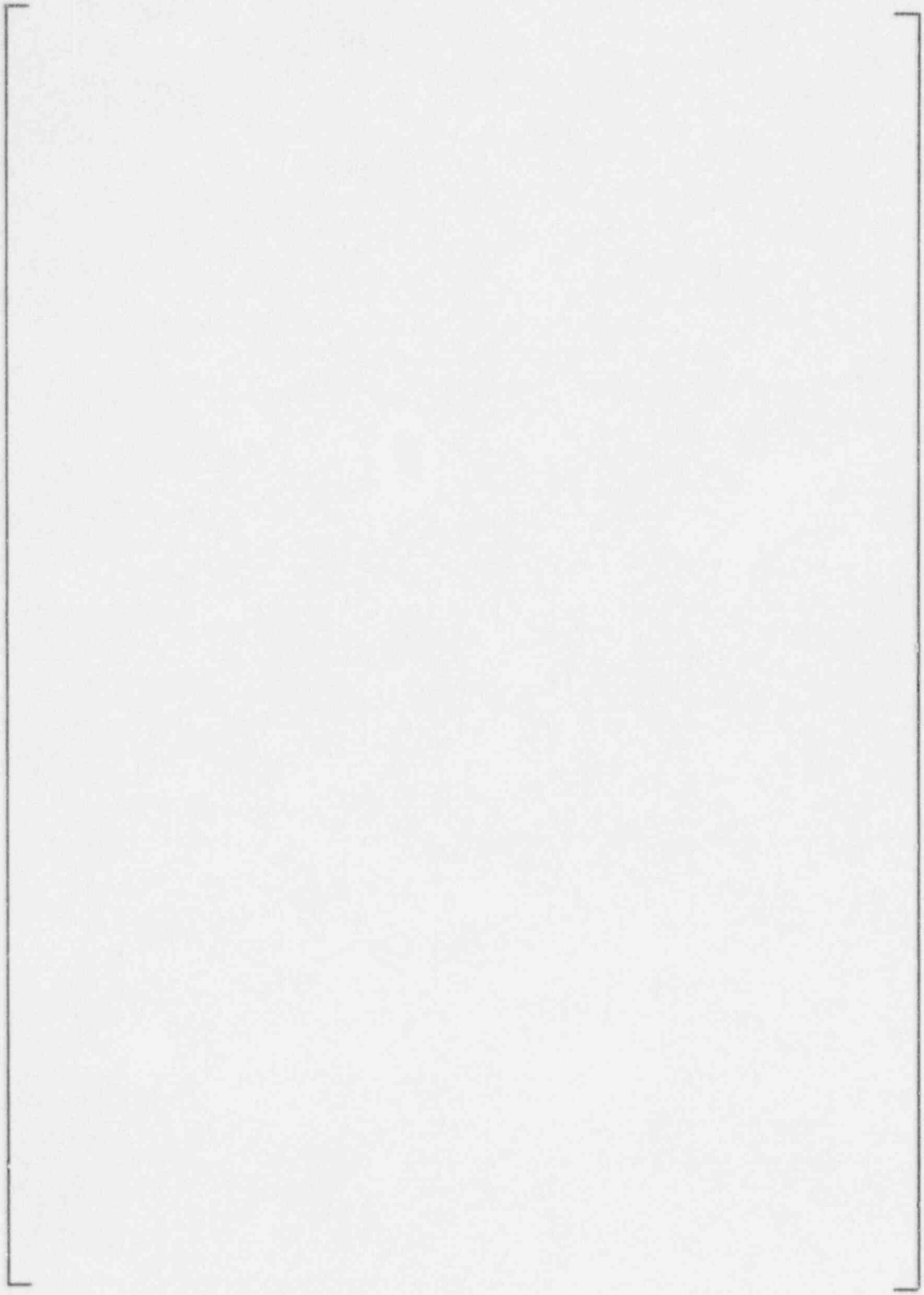

(a,b,c)

Figure 8-21 Local Wall Heat Flux for Steady-State Test S05 (Tubes 1 and 3 at 1 gpm each)

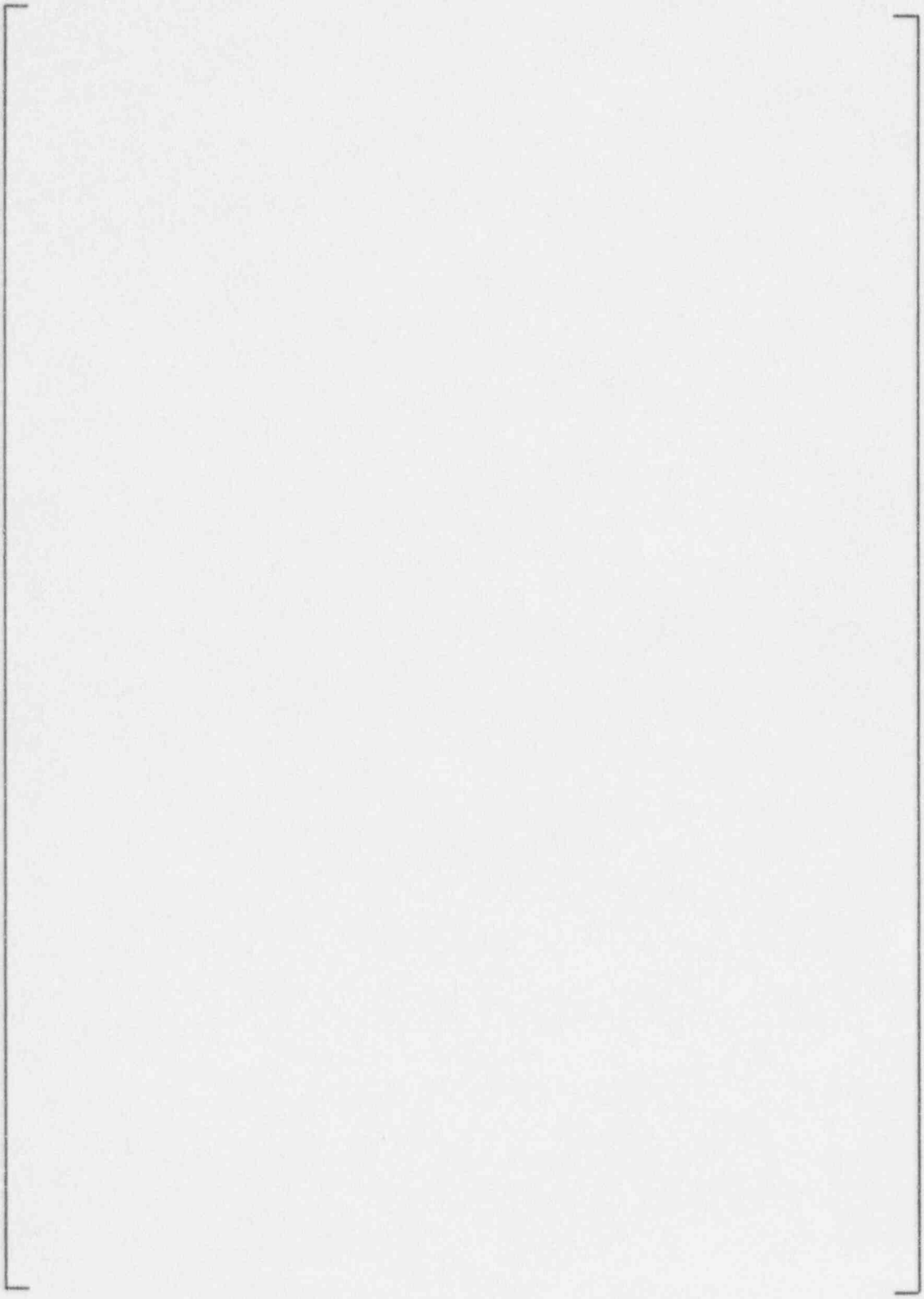

(a,b,c)

Figure 8-22 Comparison of Overall Tube Heat Transfer

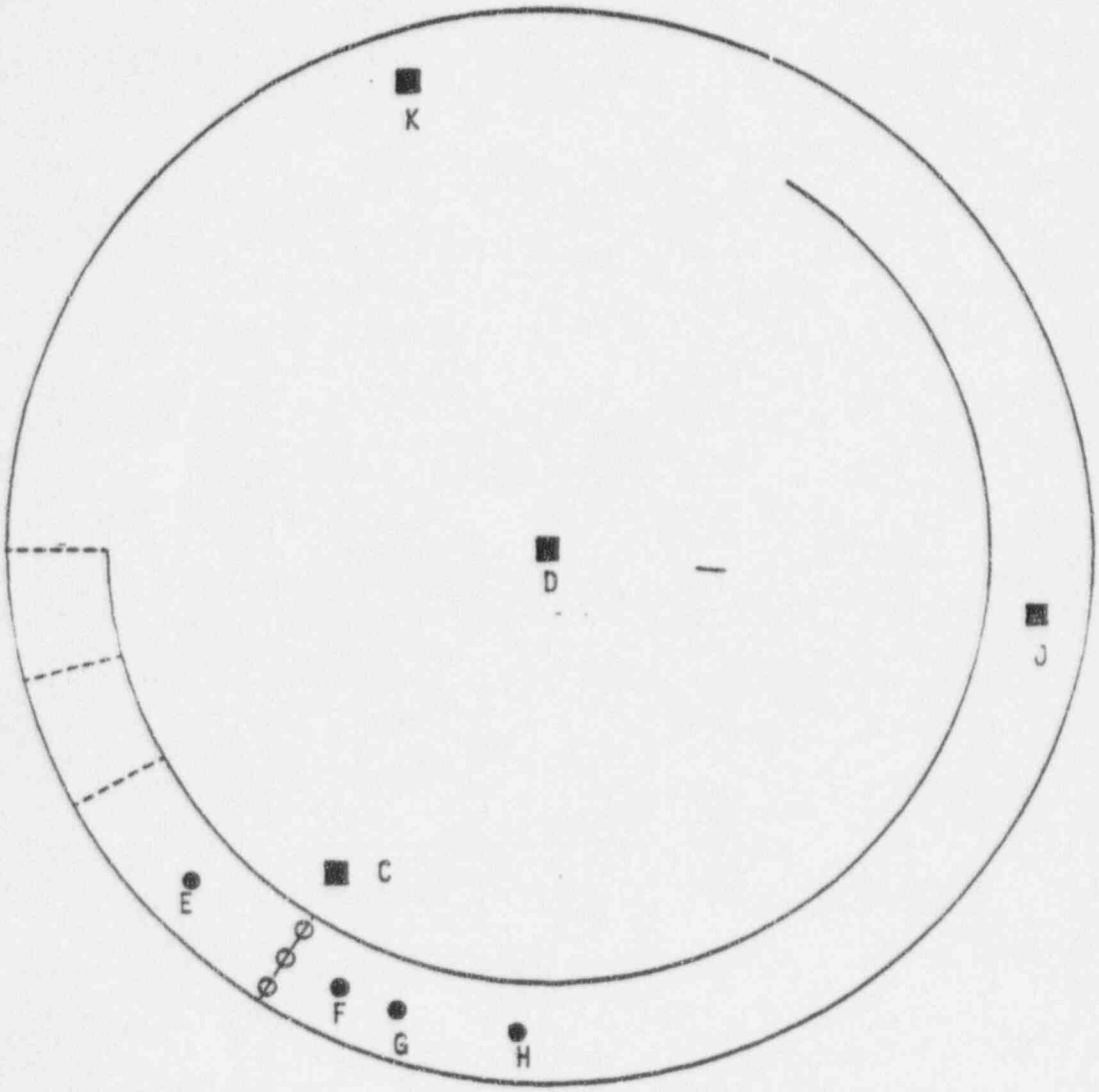

Figure 8-23 Passive Residual Heat Removal Tank Thermocouple Locations

(a,b,c)

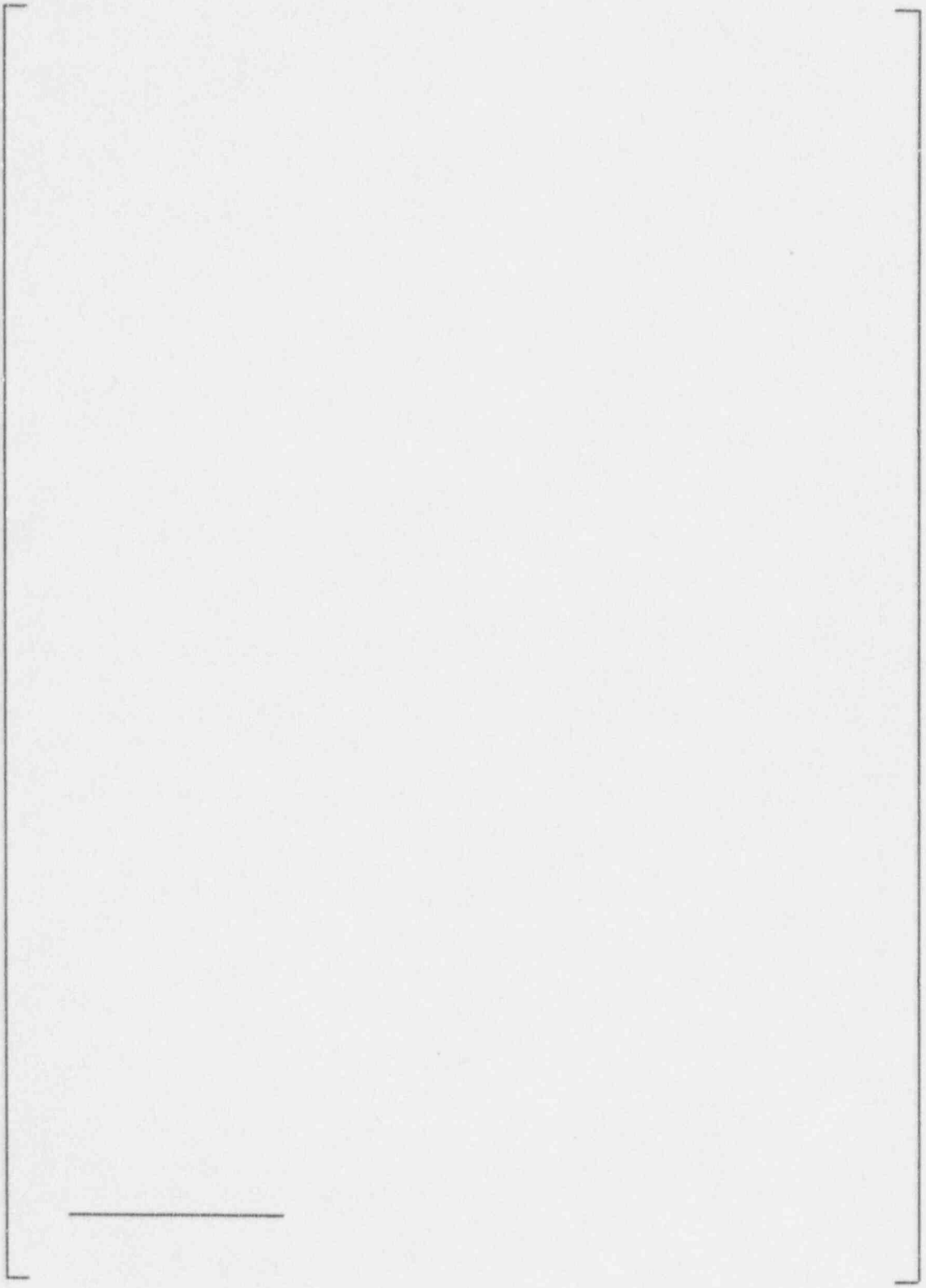

Figure 8-24 Transient Heating of the Center of the Passive Residual Heat Removal Tank for Test T02

(a,b,c)

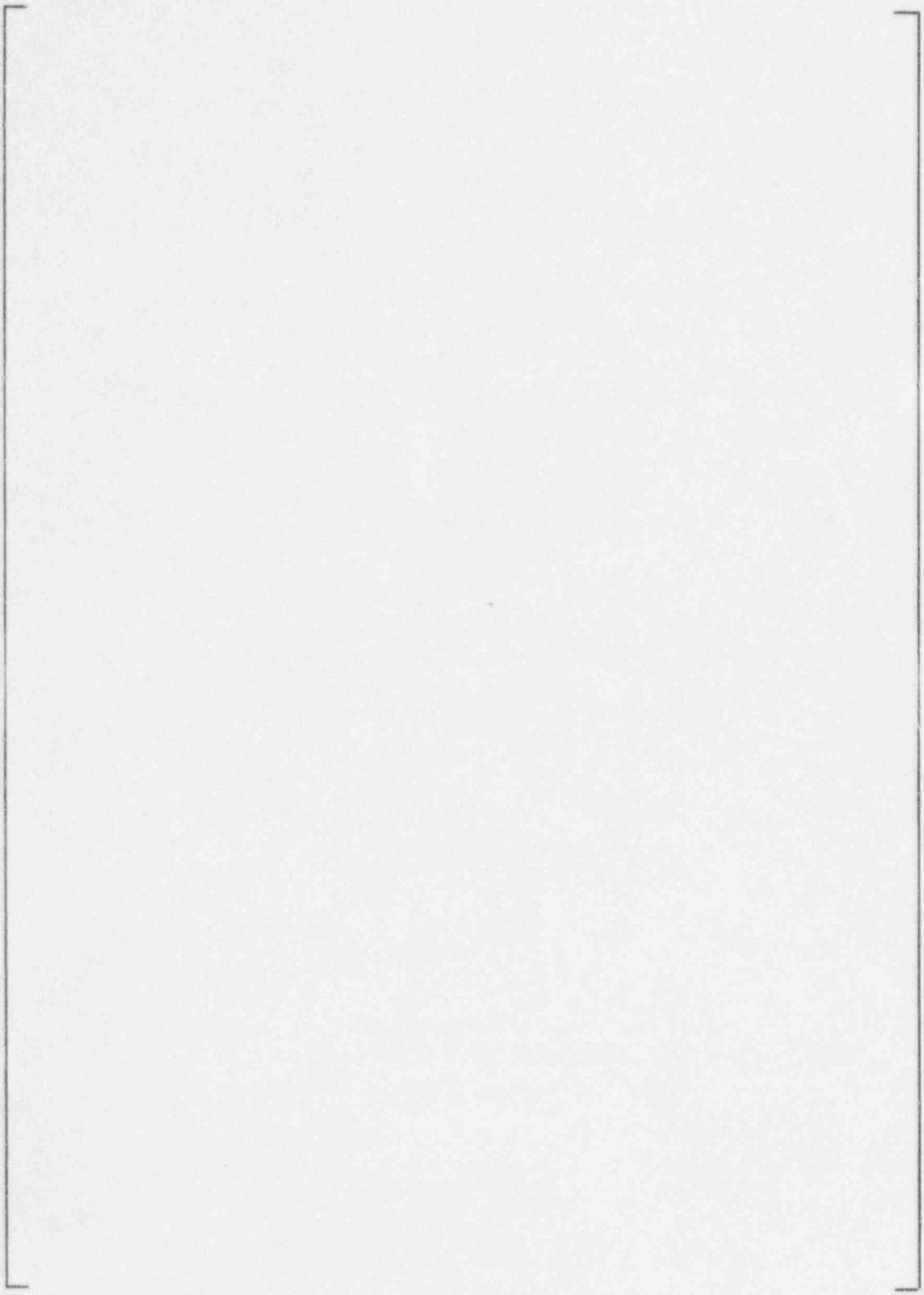

Figure 8-25 Transient Heating of Passive Residual Heat Removal Tank at Various Radial Locations at the 13.92 Foot Elevation for Test T02

(a,b,c)

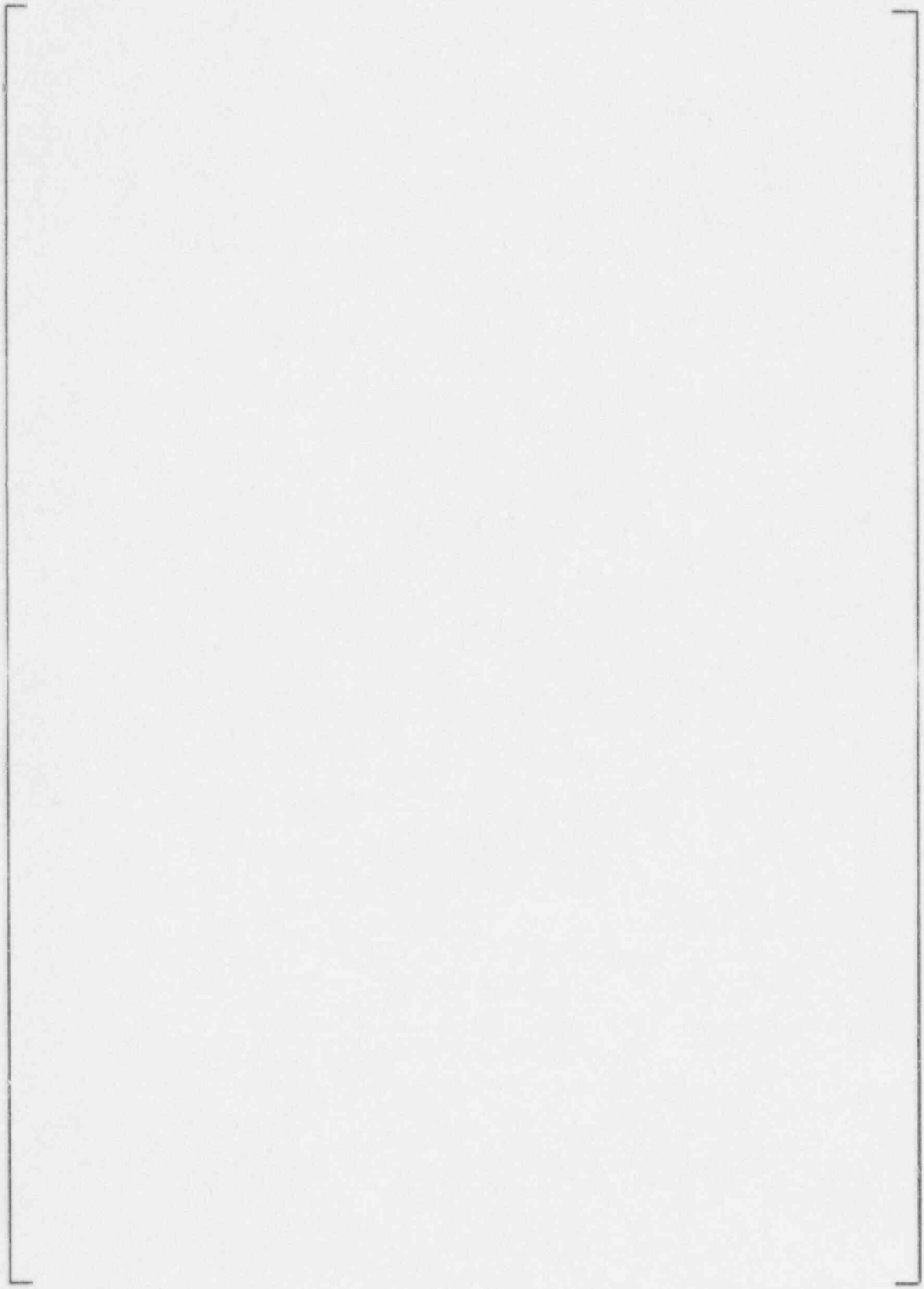

Figure 8-26 Passive Residual Heat Removal In-Containment Refueling Water Storage Tank Uncovery Temperature Data (25% Uncovery) for Tube 1

(a,b,c)

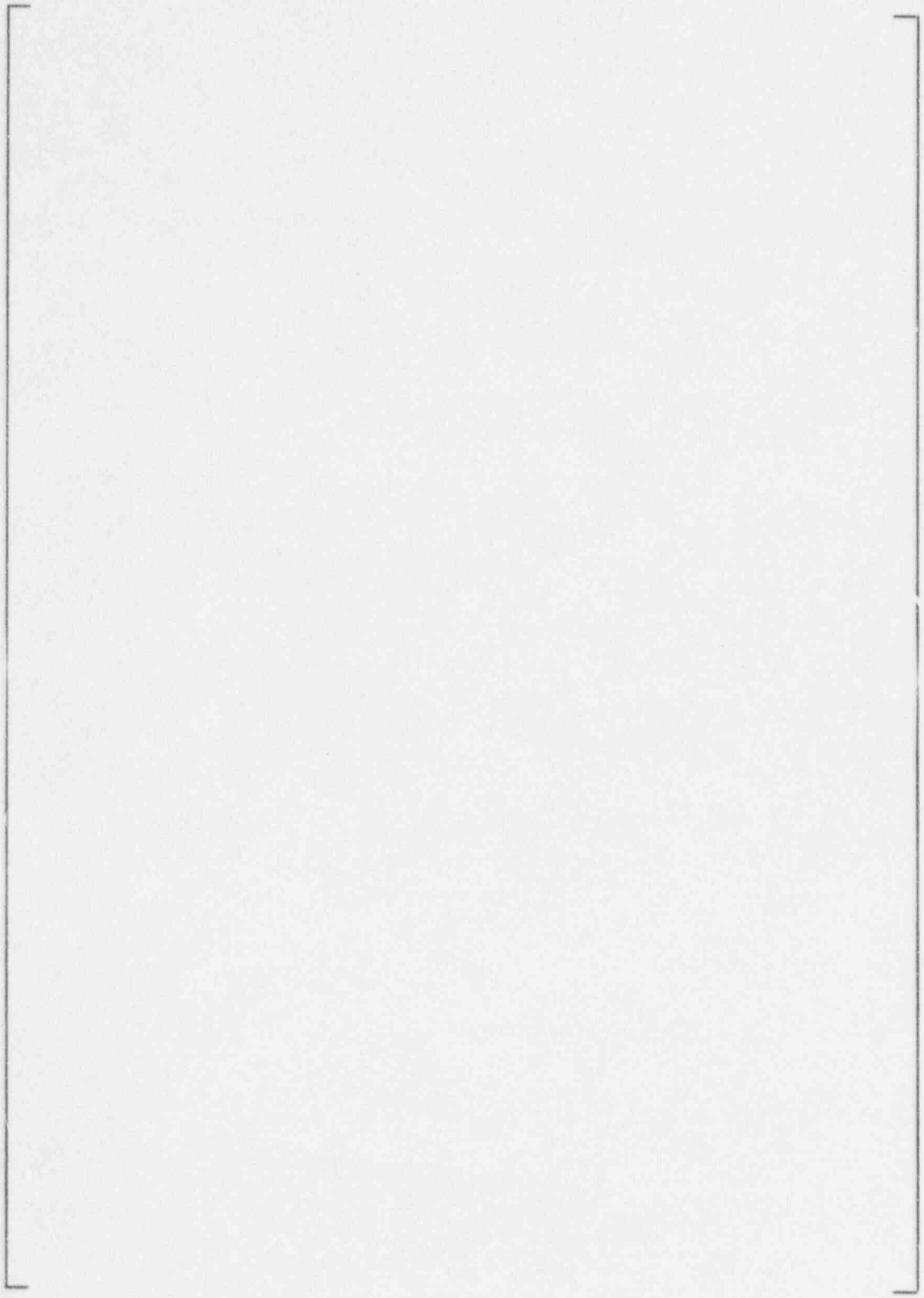

Figure 8-27 Passive Residual Heat Removal In-Containment Refueling Water Storage Tank Uncovery Temperature Data (25% Uncovery) for Tube 2

(a,b,c)

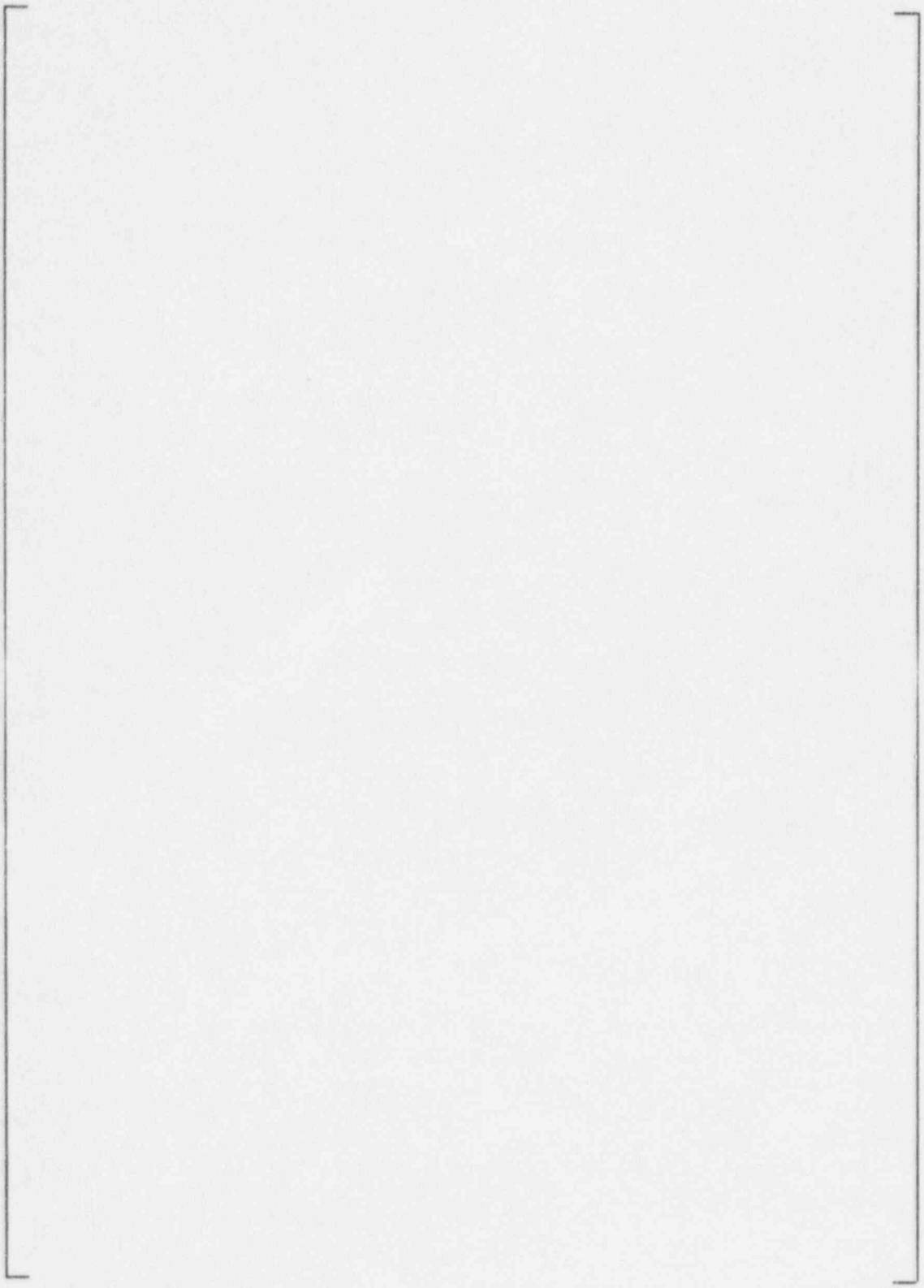

Figure 8-28 Passive Residual Heat Removal In-Containment Refueling Water Storage Tank Uncovery Temperature Data (75% Uncovery) for Tube 1

(a,b,c)

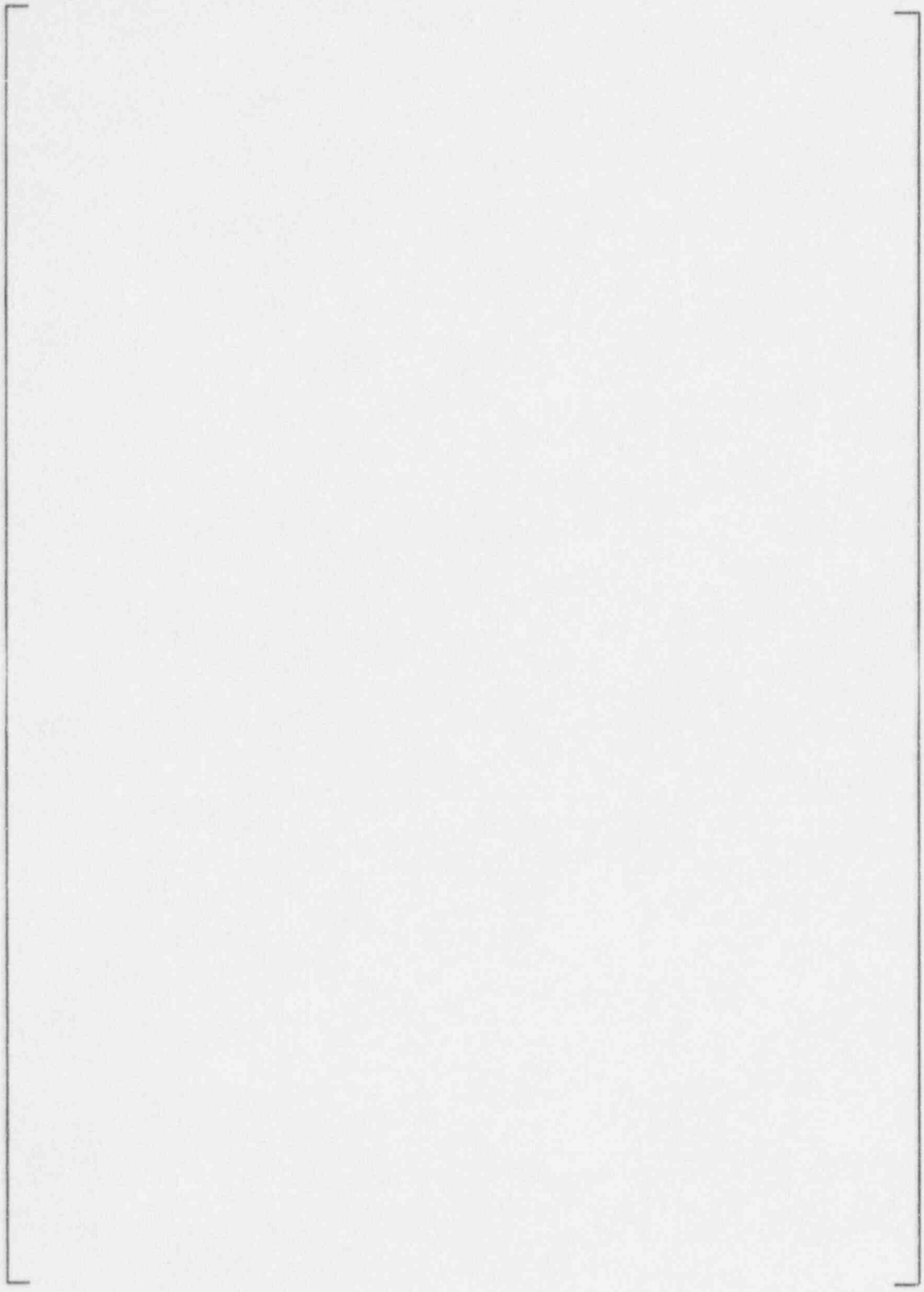

Figure 8-29 Passive Residual Heat Removal In-Containment Refueling Water Storage Tank Uncovery Temperature Data (75% Uncovery) for Tube 2

9.0 ANALYSIS OF THE PASSIVE RESIDUAL HEAT REMOVAL DATA

9.1 Introduction

The purpose of the passive residual heat removal (PRHR) tests was to provide a database to determine the heat transfer behavior on the outside of the PRHR tubes for a full-length heat exchanger (HX) and to examine the mixing behavior in the simulated PRHR tank. The single-phase heat transfer on the inside of the tubes was assumed to be known and confirmed by the tests. The mixing effects within the tank are discussed in Section 8.4 of this document. This section discusses the analysis of the heat transfer data and the comparisons to different correlations from the literature for both the outside tube heat transfer as well as the inside primary-side heat transfer.

9.2 Passive Residual Heat Removal Modes of Heat Transfer

The PRHR has several different modes of heat transfer, depending on the accident scenario during which it operates. For operational transients the primary side of the PRHR remains single-phase. The flow in the tubes is driven by either pumped flow from the reactor coolant pumps (RCPs) or by natural convection flow due to the buoyant head difference between the core and the in-containment refueling water storage tank (IRWST), which is the heat sink for the PRHR. The heat transfer on the primary side of the tubes is single-phase convection. The heat transfer on the secondary side of the HX (IRWST side) is a combination of natural convection and boiling, depending on the wall temperature as well as the temperature of the IRWST and the temperature of the PRHR primary-side water. The modes of heat transfer on the outside of the PRHR tubes that were investigated in the PRHR tests are shown in Figure 9-1.

For the small-break loss-of-coolant accident (LOCA), the above modes of heat transfer exist at the beginning of the transient. As the reactor system drains, a two-phase mixture enters the PRHR tubes and is condensed. The two-phase primary-side behavior is beyond the scope of the PRHR test program and is covered in the SPES-2 [Reference 13] and OSU [Reference 14] AP600 integral systems tests.

9.3 Primary Tube Side Heat Transfer

When the test data were reduced, existing conventional forced convection heat transfer correlations were used to estimate the inside wall temperatures, as shown in Section 7.0, where tube inside wall temperatures were estimated from Equation 7-6. The primary-side, single-phase heat transfer coefficients were calculated using the Dittus-Boelter [Reference 3] and Petukhov-Popov [Reference 2] single-phase forced convection correlations. The Dittus-Boelter correlation is given as:

$$Nu_{DB} = \frac{h_{DB} Di}{k_f} = 0.023(Re)^{0.8}(Pr)^{0.33} \qquad (9\text{-}1)$$

for cooling of the primary side tube flow.

where:

k_ℓ = thermal conductivity of liquid (Btu/hr-ft.-°F)
h_{DB} = Dittus-Boelter heat transfer coefficient (Btu/hr-ft.^{2}-°F)
Re = primary-side fluid Reynolds number
Pr = primary-side fluid Prandtl number
D_i = tube inside diameter (ft.)

The Petukhov-Popov correlation is given as:

$$Nu_{pp} = \frac{h_{pp} D_i}{k_\ell} = \left(\frac{(f/8)\ Re\ Pr}{K_1 + (K_2\ (f/8)^{0.5}\ ((Pr)^{2/3} - 1.))} \right) \tag{9-2}$$

where:

h_{pp} = Petukhov-Popov heat transfer coefficient (Btu/hr-ft.^{2}-°F)

$f = (1.82 \log_{10} Re_D - 1.64)^{-2.0}$ (9-3)

$K_1 = 1.0 + 3.4f$ (9-4)

$$K_2 = 11.7 + \frac{1.8}{Pr^{1/3}} \tag{9-5}$$

Figure 9-2 from Kreith-Bohm [Reference 2] shows the comparisons of the two correlations and the relative scatter of test data for single-phase convection. Both correlations share the same trend, but the Petukhov-Popov correlation lies within the scatter of their data. Dittus-Boelter is between 5 to 15 percent below the Petukhov-Popov values. Table 9-1 presents a comparison of the Dittus-Boelter and Petukhov-Popov heat transfer coefficients calculated from the two correlations for test S07.

The PRHR data have been analyzed to determine the applicability of the Dittus-Boelter and Petukhov-Popov correlations. A heat balance from the primary bulk temperature to the inside tube can be written as:

$$q = h_i\ \pi\ D_i L\ (T_b - T_{w_i}) \tag{9-6}$$

where:

D_i = tube inside diameter (ft.)
h_i = inside wall heat transfer coefficient (Btu/ft.^{2}-hr.-°F)
L = height of section (ft.)
T_b = primary-side bulk temperature (°F)
T_{w_i} = inside wall temperature of the PRHR tube (°F)

The tube wall conduction equation can be written in terms of heat flow through the tube as:

$$q = 2 \pi k_w L (T_{w_i} - T_{w_o}) / \ln \left(\frac{D_o}{D_i} \right) \quad (9\text{-}7)$$

where:

k_w = tube wall conductivity (Btu/hr-ft.-°F)
T_{w_o} = primary-side outside wall temperature (°F)

Heat flow is written as a function of the heat flux as:

$$q = q''_{w_i} \pi D_i L \quad (9\text{-}8)$$

Equations 9-6 and 9-7 are set equal to each other, and using Equation 9-8 for the heat flux, the inside heat transfer coefficient is calculated from the test data as:

$$\frac{1}{h_i} = \frac{T_b - T_{w_o}}{q''_{w_i}} - \frac{D_i \ln \left(\frac{D_o}{D_i} \right)}{2k_w} \quad (9\text{-}9)$$

Equation 9-9 represents a local averaged inside tube convective heat transfer coefficient for an 18-inch span along the PRHR tube. Equation 9-9 is used to calculate the inside convective heat transfer coefficient along the tube for different tests using the wall heat flux, as calculated from the primary fluid temperatures, as well as the measured extrapolated outside wall temperature. The test-calculated heat transfer coefficient is expressed in dimensionless form as a Nusselt number, which is divided by the Prandtl number to the 0.33 power as $Nu/Pr^{0.33}$ and plotted against the local tube Reynolds number to compare with the two convective correlations, as shown in Figure 9-3.

Figure 9-3 shows the comparison of the Dittus-Boelter correlation and the Petukhov-Popov correlation with the test-determined Nusselt/Prandtl number as a function of the primary system Reynolds number. The local Reynolds number is used to reflect the variation of the primary-side water properties as the flow progresses down the tube and is cooled. The comparison shows data scatter about the Dittus-Boelter correlation at high Reynolds numbers, and the data lie below this correlation at lower Reynolds numbers. The agreement with the Petukhov-Popov correlation is similar, as seen in Figure 9-3, and almost identical to the Dittus-Boelter equation for the current range of test conditions.

The generally more accepted single-phase convective heat transfer Dittus-Boelter correlation provides reasonable agreement with the PRHR data, particularly at higher tube Reynolds numbers. These

comparisons indicate that the Dittus-Boelter correlation is acceptable for calculating primary-side PRHR heat transfer. There is also a larger database, which suggests the Dittus-Boelter correlation is independent of the PRHR data shown here.

The primary-side heat transfer data were fitted to obtain a best fit to all the data. The resulting fitted correlation is given as:

$$\frac{Nu}{Pr^{0.33}} = [\quad]^{a,b,c} (Re)[\quad]^{a,b,c} \tag{9-10}$$

As Figure 9-3 indicates, the best fit to the data lies below the Dittus-Boelter correlation at lower Reynolds numbers, and is closer to the Dittus-Boelter correlation at high Reynolds numbers. The smaller difference observed between the Dittus-Boelter correlation and the Petukhov-Popov correlation in Figure 9-3 is the scale compression as compared to Figure 9-2 from Keith and Bohm.

9.4 Free Convection Heat Transfer on the Outside of the Passive Residual Heat Removal Tubes

Figure 9-1 indicates that a portion of the PRHR tube can be cooled by natural convection heat transfer when the wall heat fluxes are below what is needed to create significant bubble nucleation on the tube surfaces. The Eckert-Jackson [Reference 15] free convection heat transfer correlation can be applied to the outside of the PRHR tubes to model the natural convection heat transfer in the cases when boiling does not occur on the PRHR tubes. The Eckert-Jackson correlation is given as:

for Gr x Pr $\leq 10^9$ (laminar):

$$\bar{h}_{NC} = \frac{k_f}{L} 0.555 \, (Gr_L \, Pr_f)^{0.25} \tag{9-11}$$

for Gr x Pr $> 10^9$ (turbulent):

$$\bar{h}_{NC} = \frac{k_f}{L} 0.0210 \, (Gr_L \, Pr_f)^{0.40} \tag{9-12}$$

where:

- L = tube length (ft.), as measured from the bottom of the heated region
- Gr_L = dimensionless Grashof number
- Pr_f = liquid Prandtl number
- $\bar{h}_{NC}$ = average heat transfer coefficient over the surface (Btu/hr-ft^2-°F)

The Grashof number is based on the tube length (or height), L, from the bottom of the heated length as:

$$Gr_L = \frac{\rho_f^2 \, g \, L^3 \beta \, \Delta T}{\mu_f^2} \tag{9-13}$$

and the fluid Prandtl number is given as:

$$Pr_f = \frac{C_p \, \mu_f}{k_f} \tag{9-14}$$

where:

ρ_f = fluid density (lb/ft.^{3})
β = thermal expansion of liquid (1/°F)
ΔT = differential temperature (°F) (wall to bulk fluid)
g = acceleration of gravity (ft/sec^2)
C_p = liquid heat capacity (Btu/(lb$_m$-°F)
k_f = thermal conductivity of fluid (Btu/ft.-hr-°F)
μ_f = fluid viscosity (lb/ft.-hr)

The average heat transfer coefficient can be recast as a local coefficient based on the analysis of Burmeister [Reference 16] as:

$$h_{NC}(x) = \frac{6}{5} \bar{h}_{NC} \tag{9-15}$$

where:

$h_{NC}(x)$ = local heat transfer at position x along the vertical surface (Btu/hr-ft^2°F)

In addition to the Eckert and Jackson correlation, the McAdams [Reference 17] natural convection correlation, given as:

$$Nu = C \, (Gr_L \cdot Pr_f)^n \tag{9-16}$$

with

C = 0.13
n = 1/3

for vertical plates, has also been compared to the PRHR data.

Figures 9-4 and 9-5 show the comparison of the measured PRHR heat flux to the heat flux calculated using the Eckert-Jackson correlation and the McAdams correlation.

The region where the comparison is valid is at the low heat flux portion of the PRHR exchanger, which is at the bottom of the tubes. The heat flux is calculated from the difference of the primary fluid enthalpy using the fluid temperature measurements, where the temperature differences is the low heat flux region are small. Therefore, the uncertainty in the measured heat flux is larger for these conditions as compared to the heat fluxes at the top of the tube. Fitting the measured temperatures as an enthalpy profile reduces the uncertainty in the heat flux calculations.

As can be seen in the figures, the Eckert-Jackson correlation represents a best-estimate fit at the low heat flux values, while the McAdams correlation is more conservative.

9.5 Boiling Heat Transfer Correlations

A series of pool boiling correlations have been applied to the PRHR test data to evaluate their applicability. These correlations vary in complexity and are derived from a wide range of tests that are much smaller in scale than the PRHR HX test. The differing base assumptions are primarily the consideration of the microconvection effects caused by the bubble dynamics and the mechanisms of the generated bubbles, and how they leave the surface and mix with the thermal boundary layer. The microconvection process is believed to be responsible for the local enhanced heat transfer on boiling surfaces. Some models are simply correlations of data with little or no theoretical basis (for example, McAdams, et al., [Reference 18] and Jens-Lottes [Reference 19]), while other correlations attempt a theoretical basis and are then fit to the data (for example, Rohsenow [Reference 20], Forster-Zuber [Reference 21], and Forster-Greif [Reference 22]).

The pool boiling correlations are provided below.

Original Rohsenow correlation [Reference 20]:

$$q''_{w_{rh}} = \left(\frac{C_{p_\ell} \Delta T}{h_{fg} \left(C_{sf} \left(Pr_\ell \right)^{1.7} \right)} \right)^{3.0303} \frac{\mu_\ell \, h_{fg}}{\sqrt{\frac{\sigma \, g_c}{(\rho_\ell - \rho_g) g}}} \qquad (9\text{-}17)$$

where:

h_{fg} = latent heat of vaporization (Btu/lbm)
C_{sf} = correlating coefficient
σ = surface tension lbf/ft
ρ_g = density of gas phase ($lb/ft.^3$)
μ_ℓ = liquid viscosity (lbm/hr-ft.)

g_c = gravitational constant (lbm-ft/lbf-sec^2)
ΔT = temperature differential (T_{wall} - T_{sat})
C_{p_ℓ} = heat capacity of fluid (Btu/lbm-°F)
Pr_ℓ = liquid Prandtl number at saturated conditions

where the power on the Prandtl number is raised to the 1.7 power. More recently, Rohsenow [Reference 23] has recommended that the power on the Prandtl number be reduced to unity for water systems only.

Jens-Lottes correlation:

$$q''_{w_{jl}} = e^{0.01633} \left(\frac{\Delta T}{60}\right)^{4.0} (10^6) \qquad (9\text{-}18)$$

McAdams, et al. correlation:

$$q''_{w_{mc}} = 0.074\ (\Delta T)^{3.86} \qquad (9\text{-}19)$$

Collier's correlation [Reference 24]:

$$q''_{w_c} = 4.81\text{x}10^{-4}\ (\Delta T)^{3.33} (P_{cr})^{2.3} \left[1.8 \left(\frac{P}{P_{cr}}\right)^{0.17} + 4.0 \left(\frac{P}{P_{cr}}\right)^{1.2} + 10.0 \left(\frac{P}{P_{cr}}\right)^{10.0}\right]^{3.33} \qquad (9\text{-}20)$$

where:

P_{cr} = critical pressure (psia)
P = system pressure (psia) (°F)

Forster-Zuber correlation:

$$q''_{w_{fz}} = 0.0015\ (Re_b)^{0.62}\ (Pr_\ell)^{1/3} \left(\frac{k_\ell h_{fg} \rho_g}{C_{p_\ell} \rho_\ell \sqrt{\pi \alpha_\ell}}\right) (T_w - T_\ell) \left(\frac{2\sigma}{\Delta P}\right)^{-1/2} \left(\frac{\rho_\ell}{\Delta P}\right)^{-1/4} \qquad (9\text{-}21)$$

where:

σ = surface tension (lbf/ft)
T_ℓ = liquid temperature (°F)
α_ℓ = liquid thermal diffusivity (ft^2/hr)
Re_b = Bubble Reynolds number

The predictions of each correlation are presented in Figures 9-6 through 9-11, and are compared to the results of each test. The data and correlation are all plotted as wall heat flux versus the differential temperature measured by the extrapolated tube outside wall temperature minus the local tank saturation temperature. This differential temperature reflects the amount of superheat at the outer surface of the tube.

The heat fluxes from all the correlations consistently overpredict the test data. Collier, McAdams, et al., and Jens-Lottes overpredict the higher heat fluxes by almost an order of magnitude. The Forster-Greif and Forster-Zuber correlations also overpredict the data by up to a factor of 10. Given that the pool boiling critical heat flux is approximately 350,000 Btu/hr-ft.^{2} and the correlations are overpredicting the test heat flux, it is postulated that these correlations are not appropriate for direct application to the AP600 PRHR and a modification of the boiling heat transfer correlation is needed. It is also suspected that the onset of nucleate boiling may be suppressed due to the strong natural circulation flow up along the tube bundle as boiling occurs. The pool boiling correlations are parallel to the data, but displaced to a lower wall superheat than that observed in the tests.

9.6 Flow Analysis of the Passive Residual Heat Removal Data

The observations made from the videos taken during the tests at the different elevations along the PRHR tubes indicate that the heat transfer from the PRHR results in a local buoyant plume that rises along the tubes. If the heat flux values are large and the IRWST water temperature is near saturation, bulk boiling will occur along the tubes with net vapor generation, which enhances the buoyant driving head, increasing the velocity along the tubes. An analysis was performed to estimate the buoyant flow velocities, the flow quality, and the void fraction when boiling occurs within the buoyant plume. Conservation equations were written for a control volume that surrounds the tubes. The flow area for the control volume was chosen based on the temperature traversing measurements, which were discussed in Section 8.2 of this document. These measurements indicate the approximate "zone of influence," i.e., the local region that would be influenced by the heat transfer from the PRHR tubes.

The derivation of the conservation equations and the assumptions used to calculate the velocities, quality, and void fraction of the two-phase plume surrounding the tubes are given in Appendix A. The analysis equates the buoyant head along the tubes to the static pressure difference in the IRWST. The measured heat flux from the PRHR tubes to the IRWST fluid is used as the heat source in the calculation.

The key parameter is the cross-sectional area of the plume or the zone of influence that surrounds the tubes. The fluid in this zone is accelerated upward due to the heat transfer from the tubes. As noted above, the temperature traverse data taken on the outside of the PRHR tubes were used to estimate the cross-sectional area used in the calculations. The videos show that the plume becomes larger as the flow is accelerated vertically along the tubes and the buoyant plume entrains additional liquid. Using the temperature measurements, a "representative area" for the plume can be determined.

Using the estimated plume cross-sectional area, the conservation equations can be solved for the mixture flow and quality in the plume. The Yeh [Reference 25] void fraction correlation calculated the void fraction and the resulting mixture density that was used in the momentum equation to obtain the mixture velocity. Figure 9-12 shows the heat flux used in the analysis. Figure 9-13 shows the calculated quality for test S12 using the measured heat flux. As the figure indicates, given the choice of the cross-sectional area, the bulk plume is subcooled for most of the tube length. Towards the top of the tube the net positive quality is calculated and boiling occurs in the control volume. The calculated void fraction is shown in Figure 9-14 for the same case. The effect of boiling is clearly seen in Figure 9-15, which indicates that the mixture velocity increases toward the top of the tubes. This simple model will not calculate subcooled boiling such that the upward flowing liquid must reach saturation before bulk boiling occurs. When the control volume is calculated to saturate and boiling occurs, there is an increase in the buoyant driving head that accelerates the flow. This can be seen in Figure 9-15.

The calculations for the flow along the PRHR tubes for different tests could yield unconverged solutions. This would occur when the calculated void fractions and mixture velocities became unrealistically high. The most likely reason for this behavior is that the wall heat flux is a fixed input into the calculation and is uncoupled from the fluid solution. Reasonable results were obtained for lower heat flux cases when the flow is weakly two-phase.

Therefore, the model given in Appendix A does give qualitative results that are consistent with the observations made on the flow behavior for the PRHR tubes. There is a single-phase convection region at the bottom of the PRHR tubes that changes to a two-phase buoyant plume that accelerates vertically upward along the tubes as boiling occurs at the tube surface. The observations confirmed the analysis results in a qualitative manner.

9.7 Correlation of the Passive Residual Heat Removal Boiling Data

The PRHR data clearly indicate two different heat transfer regimes: a natural convection regime and a developed boiling regime as seen in Figure 9-1. As seen previously in Section 9.4, the natural convection heat transfer can be represented by the Eckert-Jackson correlation or the McAdams natural convection heat transfer correlation. As the wall superheat increases and local boiling occurs, the heat transfer transitions into fully developed nucleate boiling at the surface of the PRHR tubes. The videos taken of the PRHR tubes confirm the natural convection to boiling heat transfer regimes, as evidenced in the test data.

One of the objectives of the PRHR data analysis was to either verify the application of an existing boiling correlation for use in calculating the PRHR heat transfer, or develop a new correlation that would represent the PRHR data. As indicated previously, existing body correlations over-estimated the PRHR heat flux for a given wall superheat.

The approach used was to modify the Rohsenow [Reference 20] boiling correlation for the PRHR application. The Rohsenow correlation has been shown to be applicable for developed boiling situations even when a convective flow exists. Figures 9-16 and 9-17 from Rohsenow's paper, show that as the wall superheat increases, the convection curves for a wide range of flow velocities merge with the boiling correlation developed by Rohsenow.

The PRHR data, which was in the fully developed boiling regime, was separated from the total data set, and the Rohsenow parameters were calculated. PRHR data that had wall superheats greater than 20°F were used. Rohsenow's model is intended to be valid for regions of vigorous boiling where the bulk fluid or pipe velocity does not influence the heat transfer rate, as seen in Figures 9-16 and 9-17, where the heat transfer is due to the local microconvection created by the boiling at the heated surface. Using a dimensionless analysis forced convection analogy, he found that the proper grouping was:

$$N_{Nu,b} = f(N_{Re,b}, N_{pr}) \tag{9-22}$$

where:

$N_{Nu,b}$ = bubble Nusselt number
$N_{Re,b}$ = bubble Reynolds number
N_{Pr} = liquid Prandtl number

Rohsenow regroups the dimensionless variables as:

$$\frac{N_{Re,b}N_{Pr}}{N_{Nu,b}} = \frac{C_{p_l}\Delta T}{h_{fg}} \tag{9-23}$$

where:

C_{p_l} = liquid heat capacity
ΔT = wall superheat
h_{fg} = latent heat of evaporation

Substituting in the values for the dimensionless groups from Rohsenow's paper [Reference 20], the parameters that were used to correlate the boiling data are given as:

$$\left[\frac{C_f \Delta T}{h_{fg}}\right] \quad \frac{1}{Pr_f}$$

and (9-24)

$$\left[\frac{q/A}{\mu_f h_{fg}} \sqrt{\frac{g_c \sigma}{g(\rho_f - \rho_v)}}\right]^n$$

where:

q/A	=	wall heat flux (Btu/hr-ft^2)
μ_f	=	liquid viscosity (lbm/ft-hr)
σ	=	surface tension (lbf/ft)
g_c	=	gravitational constant $\frac{\text{lbm-ft}}{\text{lbf-sec}^2}$
g	=	local gravity acceleration (ft/sec^2)
ρ_f, ρ_v	=	saturated liquid and vapor densities lbm/ft^3
Pr_f	=	liquid Prandtl number

where:

n	=	0.33 was used by Rohsenow

Rohsenow plotted boiling data from different sources to validate the dimensionless groups. He found that the data would correlate using these groups with a coefficient, C_{sf}, which was dependent on the wall and fluid properties. The correlating constant C_{sf} accounts for the nucleation characteristics of the surface-fluid combination. Table 9-2 from Vachon, et al. [Reference 26], shows the range of values for C_{sf} different liquid-metal surfaces. In the original Rohsenow paper [Reference 20], the liquid Prandtl number in Equation 9-24 was originally raised to the 1.7 power. However, recently Rohsenow has recommended that the power on the liquid Prandtl number be set at unity [Reference 23]. The Rohsenow nucleate boiling correlation, becomes:

$$\left(\frac{1}{Pr_f}\right)\left(\frac{C_f \Delta T}{h_{fg}}\right) = C_{sf}\left(\frac{q/A}{\mu_f h_{fg}}\sqrt{\frac{g_c \sigma}{g(\rho_f - \rho_v)}}\right)^{0.33} \quad (9\text{-}25)$$

where the coefficient C_{sf} characterizes the nucleation behavior of the surface.

The fully developed boiling portion of the PRHR data ($T_{woe} - T_{sat} > 20°F$) was used to calculate the parameters in Equation 9-24 to determine the best fit for the coefficient, C_{sf}, and the power n, for the

PRHR data. The PRHR data were fit using a least squares regression technique, where the power on the heat flux term in Equation 9-26 was allowed to vary to find the best fit. The PRHR boiling data was originally fit using n = 0.333 as in the original Rohsenow paper. It was found that using this exponent would not give the best fit to the data. Therefore, both the coefficient, C_{sf}, and the power parameter, n, were determined by the least squares regression analysis. The variation of the PRHR data was reflected in the resulting value of C_{sf}.

Fitting the PRHR developed boiling data to the Rohsenow form of the equation gives:

$$\left(\frac{1}{Pr_\ell}\right)\frac{C_\ell \Delta T}{h_{fg}} = C_{sf_{PRHR}}\left(\frac{q/A}{\mu_\ell h_{fg}}\sqrt{\frac{g_c \sigma}{g(\rho_\ell - \rho_v)}}\right)^{[\quad]^{a,b,c}} \qquad (9\text{-}26)$$

where:

$$C_{sf_{PRHR}} = [\quad]^{a,b,c}$$

Figure 9-18 shows the PRHR data and the resulting best fit coefficient. The coefficient is [ ]^{a,b,c} than the traditional value of 0.013 for water-steel boiling combinations, and the exponent on the heat flux is [ ]^{a,b,c}, reflecting the lower values of the measured wall heat flux as compared to the original Rohsenow correlation presented in Equation 9-25.

It should be noted that larger values of C_{sf} will result in lower values of q/A, wall heat flux, for the same wall superheat, ΔT. This is consistent with the earlier comparison of the PRHR data to a wide range of boiling correlations, all of which overpredicted the PRHR data.

While the best fit coefficient and exponent are [ ]^{a,b,c} than the standard value, the figure does show that the Rohsenow parameters given in Equation 9-26 do correlate the data. Figure 9-19 shows the original correlation by Rohsenow for pool boiling of platinum wires in water.

It was expected that the value of C_{sf} would be different for the PRHR data relative to the Rohsenow value of 0.013. However, the best fitted power for the PRHR data was not 0.333, as given by Rohsenow, but a [ ]^{a,b,c} power. The PRHR data only extends a decade on a log-log plot as seen in Figure 9-18, whereas the Rohsenow data extends over 3 decades for the heat flux parameter on the y-axis as seen in Figure 9-19.

The original Rohsenow fit given in Figure 9-19 used a liquid Prandtl number based to the 1.7 power [Reference 20]. Rohsenow later recommended a change in the power of the Prandtl number to 1.0 for water systems only. The original data used by Rohsenow, given in Figure 9-19 was digitized and refit using the same approach as that for the PRHR data. The x-axis parameter for the data in Figure 9-19

was recalculated for a Prandtl number raised to the power of one. The resulting "new" Rohsenow data was refitted by least squares to give:

$$\left[\frac{C_{pf}\,\Delta T}{h_{fg}}\right]\frac{1}{Pr_f} = 0.0128\left[\frac{q/A}{\mu_f\, h_{fg}}\sqrt{\frac{g_c\,\sigma}{g\,(\rho_f - \rho_v)}}\right]^{0.3658} \qquad (9\text{-}27)$$

which is close to the original correlation. While refitting the original data used by Rohsenow did raise the power on the heat flux term, it was [ ]^{a,b,c} than the value determined from the PRHR data. The recalculated Rohsenow data points and the PRHR data are shown in Figure 9-20 with the best fit equations.

The data used by Rohsenow is from Addomis [Reference 27], which was for boiling on a horizontal platinum wire in water. As stated in Rohsenow's paper, and as seen in Figures 9-16 and 9-17, the data is intended to capture the vigorous boiling conditions that are independent of the convective flow velocity. Examining the data sets in Figure 9-20 clearly indicates that if the Rohsenow data is characterizing vigorous boiling, the PRHR is clearly in a weak boiling heat transfer regime in which convection is also present.

Using the PRHR data, the fitted value for C_{sf} is [ ]^{a,b,c} than the range of values given in Table 9-2 from Vachon et al. Fitting the data in this manner places all the uncertainty in the coefficient C_{sf}. The recommendation from the *Heat Exchanger Design Handbook*, Section 2.7, pg 2-4, is that C_{sf} is unique to a surface-fluid situation, and initial tests are recommended to determine C_{sf} for the surface-fluid combination. The C_{sf} variation in Table 9-2 is a factor of 2 (0.0074 to 0.015), so that the larger values calculated from the fit to the PRHR data are not unexpected.

The PRHR data were also analyzed so that the coefficient, $C_{sf_{.95}}$, for the upper-bound 95th-percentile value was determined and the lower-bound 95th-percentile, $C_{sf_{-95}}$, was calculated. The definition used for the 95th percentile upper bound is that the Rohsenow correlation with the upper bound coefficient, $C_{sf_{.95}}$, encompasses 95 percent of the data. A similar approach is used for the, $C_{sf_{-95}}$, coefficient for the lower bound of the data. In determining the upper and lower 95th percentile bounds of the data, only the coefficient C_{sf} was varied. The exponent of the heat flux expressions given in Equation 9-26 remains at [ ]^{a,b,c}. Therefore, the upper and lower bound curves are "parallel" to the best fit to the data on a log-log plot.

Therefore, for those transients for which it is conservative to have higher PRHR heat transfer, the $C_{sf_{.95}}$ value should be used when calculating the PRHR heat flux for a given wall superheat. Conversely, for those transients for which lower PRHR heat transfer is conservative, the $C_{sf_{-95}}$ value

should be used. The exponent of the heat flux term given in Equation 9-26 remains the same. The different values of C_{sf} become:

$$C_{sf_{-95}} = \left[\begin{array}{l} \\ \\ \end{array}\right]^{a,b,c} \begin{array}{l} \text{95th percentile upper bound} \\ \text{best fit, mean value} \\ \text{95th percentile lower bound} \end{array}$$

$$C_{sf_{PRHR}} =$$

$$C_{sf_{-95}} =$$

The plots of the upper and lower bound limits and the best fit, as compared to the PRHR data, are shown in Figure 9-20.

The PRHR boiling data has been successfully correlated by modifying the surface-to-fluid parameter C_{sf} and the exponent of the heat flux term. The Rohsenow correlation was specifically chosen because it was for fully developed boiling that should be independent of the convective nature of the flow. Comparing the reanalyzed data which was used in the Rohsenow correlation to the PRHR data as seen in Figure 9-20 indicates that the boiling may be fully developed for the PRHR tests.

The majority of the data that were used to develop the literature values of C_{sf} were obtained from small test sections or wires, most of which were horizontal [References 20 and 26]. In most cases, there was not a long heated length over which a strong convective flow could develop. The PRHR tubes are 18 feet in vertical height so that significant convective flows can be present. Additional analysis of the PRHR data indicated that if the pool boiling correlations were shifted to higher wall superheats, the agreement would be significantly improved. This is true of all the correlations given previously in Section 9.5. Shifting of the boiling curve is consistent with the analysis by Hsu [Reference 28], which showed that convection can suppress boiling since the liquid superheated layer is too thin to support bubble growth and the effective wall superheat is reduced. As a result, the wall superheat must increase to promote bubble nucleation and growth. Since the pool boiling correlations have been developed and verified in either a low flow or no flow situation, the wall superheat is fully effective. Therefore, one method that can be used to account for the convective effects in suppressing boiling is to increase the effective value of the wall superheat in the pool boiling correlations.

In Figures 9-21 and 9-22, the wall superheat value was increased by a factor of 1.75 in the pool boiling correlations. The scaling factor was determined by modifying the Twall-Tsat value and replotting the Forster-Zuber correlation until the results agreed with the test series 7 data (straight line). Increasing the wall superheat shifts the pool boiling curve to the right but maintains the same slope as seen in Figures 9-21 to 9-22.

Shifting the wall superheat translates into an increase of 5°F to approximately 40°F at the upper limit of the data. This same modification, if made to the Jens-Lottes, Collier, and McAdams, et al., correlations will also result in good agreement with the PRHR data. The modification brought the results of the correlations into much better agreement with the test data. The results presented by Hsu

indicated that superheats on the order of 5°F to 15°F would be expected for water at atmospheric conditions. The use of the 1.75 multiplier results in superheats that do exceed Hsu's upper bound.

9.8 Conclusions

The PRHR test program provides heat transfer data that can be used to verify specific heat transfer correlations for both tube side and pool side heat transfer, on representative PRHR geometries over the range of applications. The tube side heat transfer correlations were found to be in agreement with the primary-side PRHR calculated heat transfer coefficients.

The pool-side natural convection heat transfer coefficients agreed reasonably well with the low heat flux PRHR data.

The boiling portion of the PRHR was correlated by modifying the Rohsenow pool boiling correlation and determining a revised value for the liquid-to-surface coefficient, C_{sf} and the exponent for the heat flux term. In addition, values of C_{sf} were also determined that can be used to bound the data at a 95th percentile level for either high or low PRHR heat transfer.

a,b,c

TABLE 9-1
PRHR REDUCED DATA FROM TEST S07
Tube No. 2
Reduced Data

TABLE 9-2

VALUES OF THE COEFFICIENT C_{sf} FOR THE ROHSENOW EQUATION FOR VARIOUS LIQUID SURFACE COMBINATIONS (r= 0.33) [REFERENCE 23]

Liquid-Surface Combination		C_{sf}	s**
Water	on polished copper	0.0128	1.0
	on lapped copper	0.0147	1.0
	on scored copper	0.0068	1.0
	on ground and polished stainless steel	0.0080	1.0
	on Teflon-pitted stainless steel	0.0058	1.0
	on chemically etched stainless steel	0.0133	1.0
	on mechanical polished stainless steel	0.0132	1.0
	on nickel	0.006	1.0
	on platinum	0.013	1.0
	on brass	0.006	1.0
n-Pentane	on polished copper	0.0154	1.7
	on polished nickel	0.0127	1.7
	on lapped copper	0.0049	1.7
	on emery-rubbed copper	0.0074	1.7
	on chromium	0.015	1.7
Carbon Tetrachloride on polished copper		0.0070	1.7
Benzene on chromium		0.101	1.7
Ethyl alcohol on chromium		0.0027	1.7
Isopropyl alcohol on copper		0.0025	1.7
n-Butyl alcohol on copper		0.0030	1.7
35% K_2CO_3 on copper		0.0054	1.7
50% K_2CO_3 on copper		0.0027	1.7

Note:

(1)Whenever possible, it is recommended that a pool boiling test be carried out to determine the value of C_{SF} applicable to the particular conditions of interest. In the absence of such information, a value of C_{SF} of 0.013 may be used as a first approximation.

** s is the exponent on the liquid Prandtl number.

a,b,c

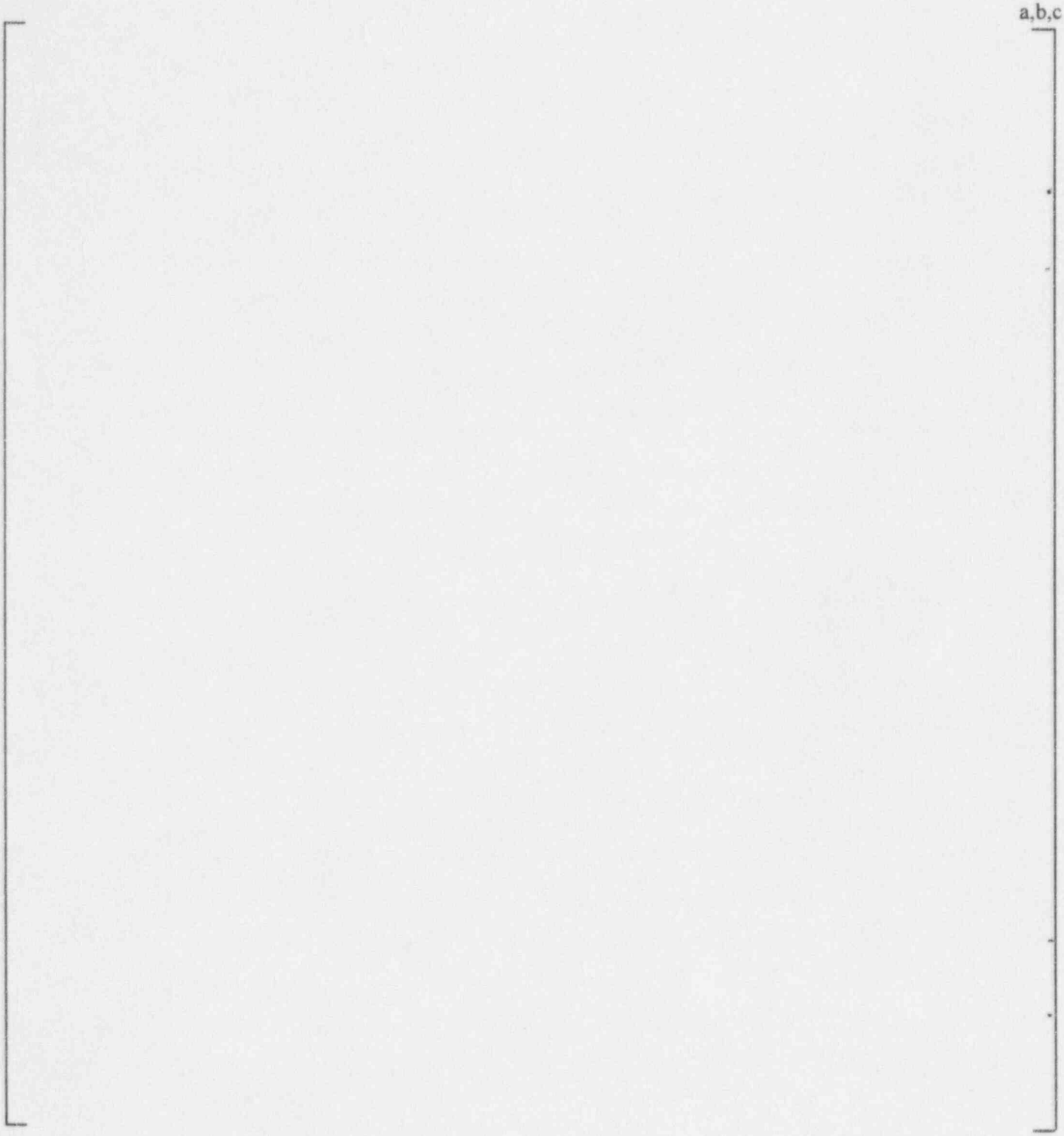

Figure 9-1 AP600 PRHR Transfer Modes on Outside of Tubes

a,b,c

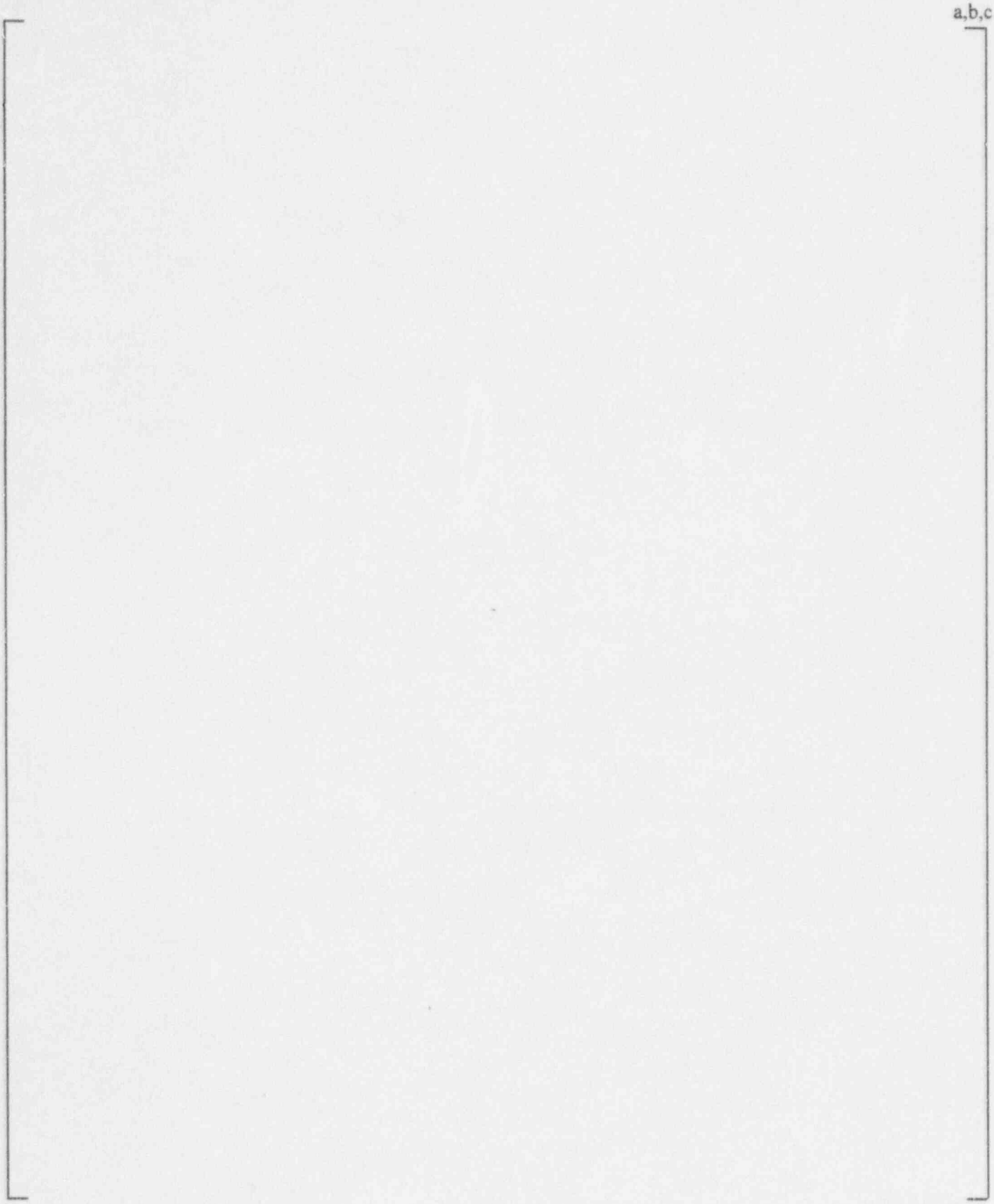

Figure 9-2 Comparison of Predicted and Measured Nusselt Number for Turbulent Flow of Water in a Tube (26.7°C; Pr = 6.0). [From Kreith-Bohm, Reference 2]

a,b,c

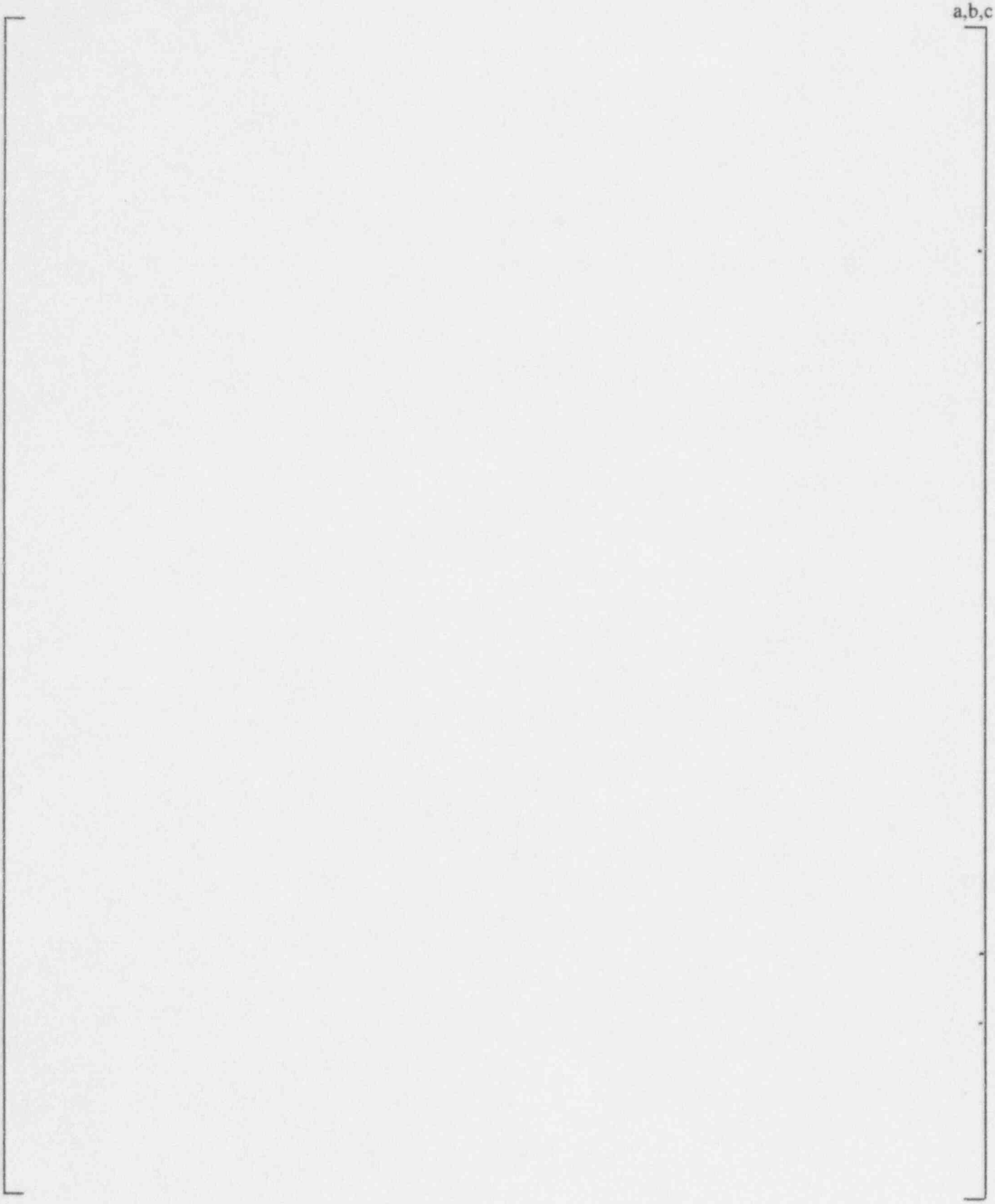

Figure 9-3 Comparison of Passive Residual Heat Removal Primary-Side Heat Transfer with Single-Phase Correlations

a,b,c

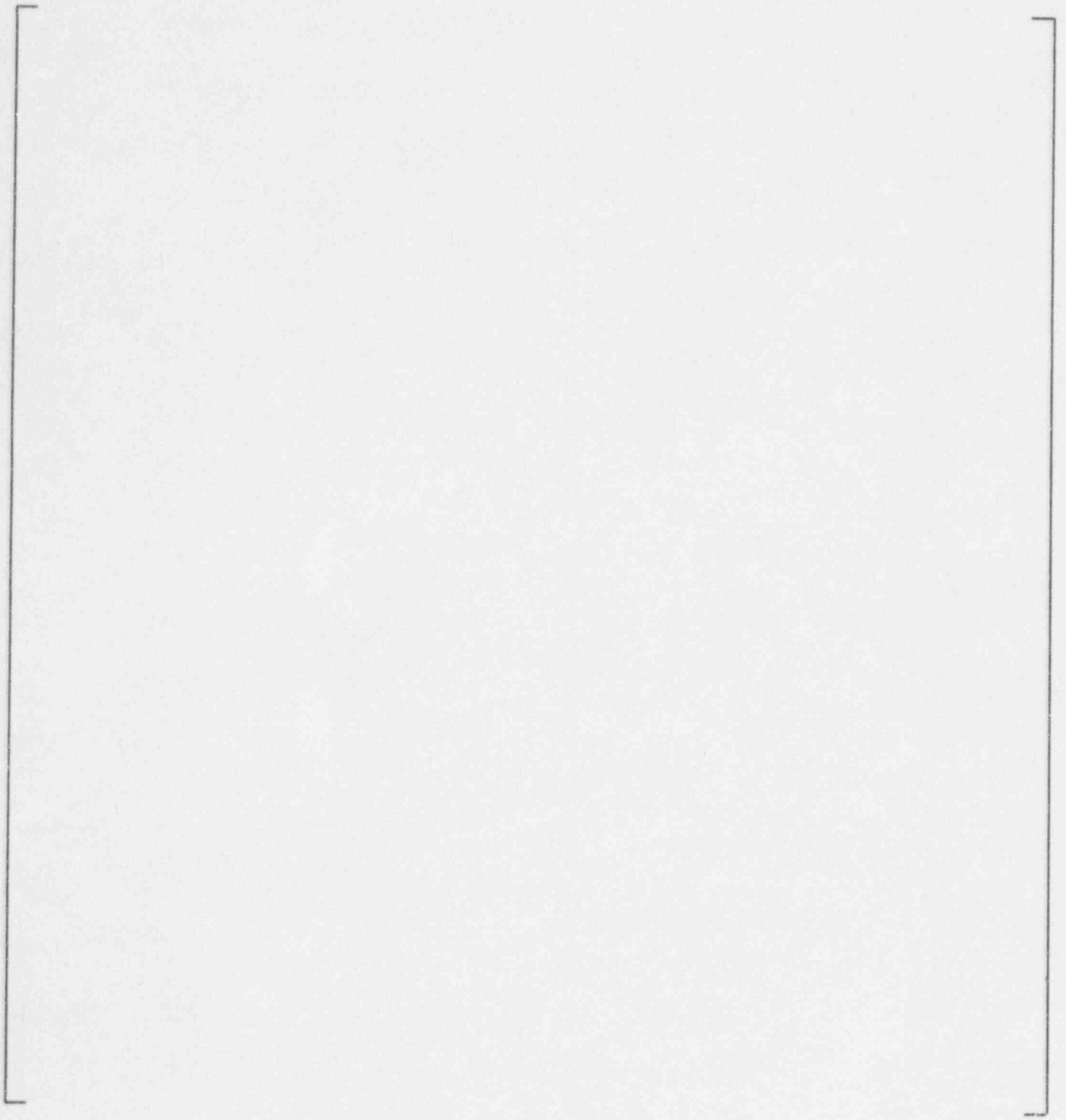

Figure 9-4 Low Heat Flux Test Data From Test S07 Comparisons to Eckert-Jackson and McAdams Correlations

a,b,c

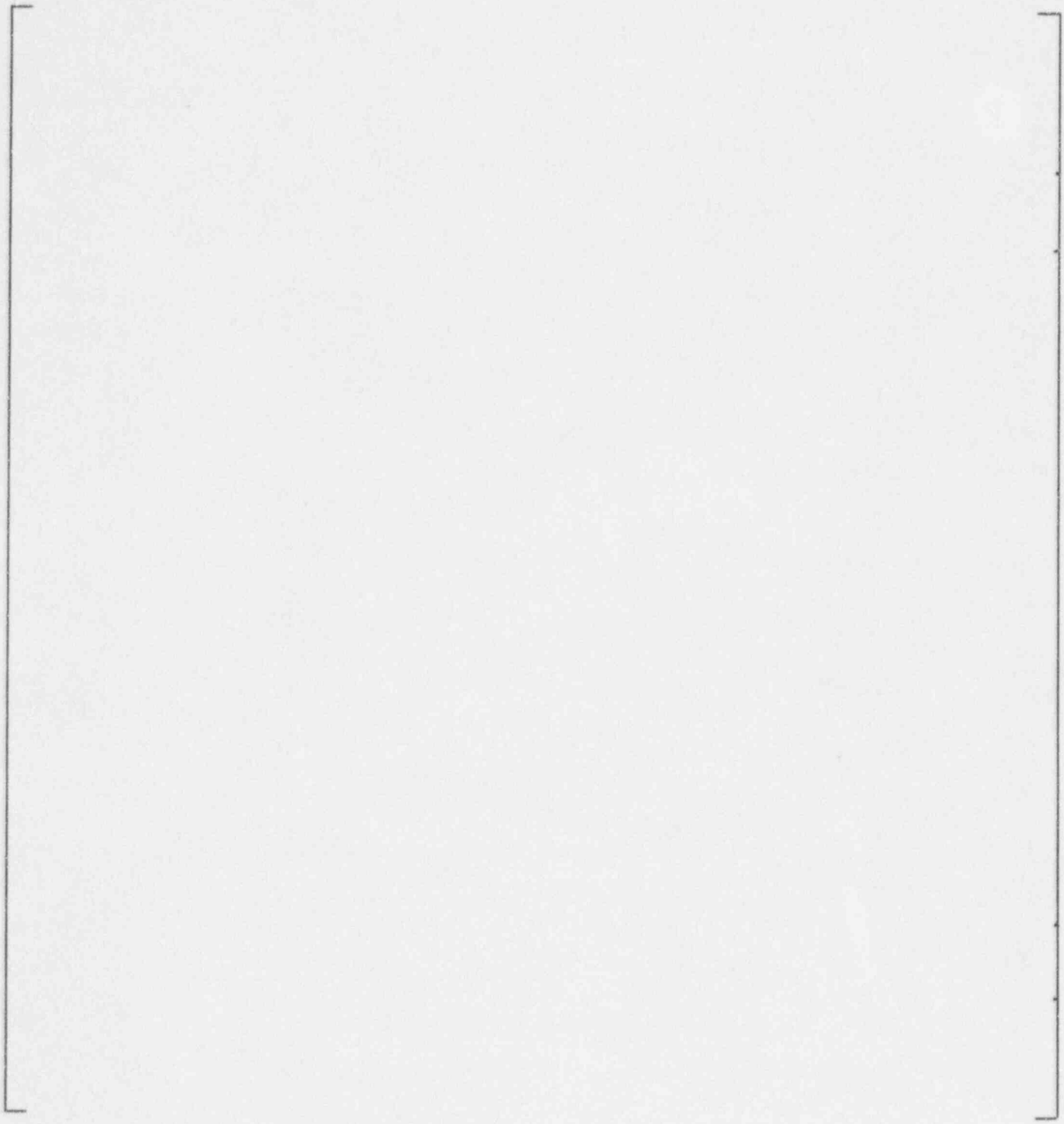

Figure 9-5 Low Heat Flux Test Data From Test S08 Comparisons to Eckert-Jackson and McAdams Correlations

a,b,c

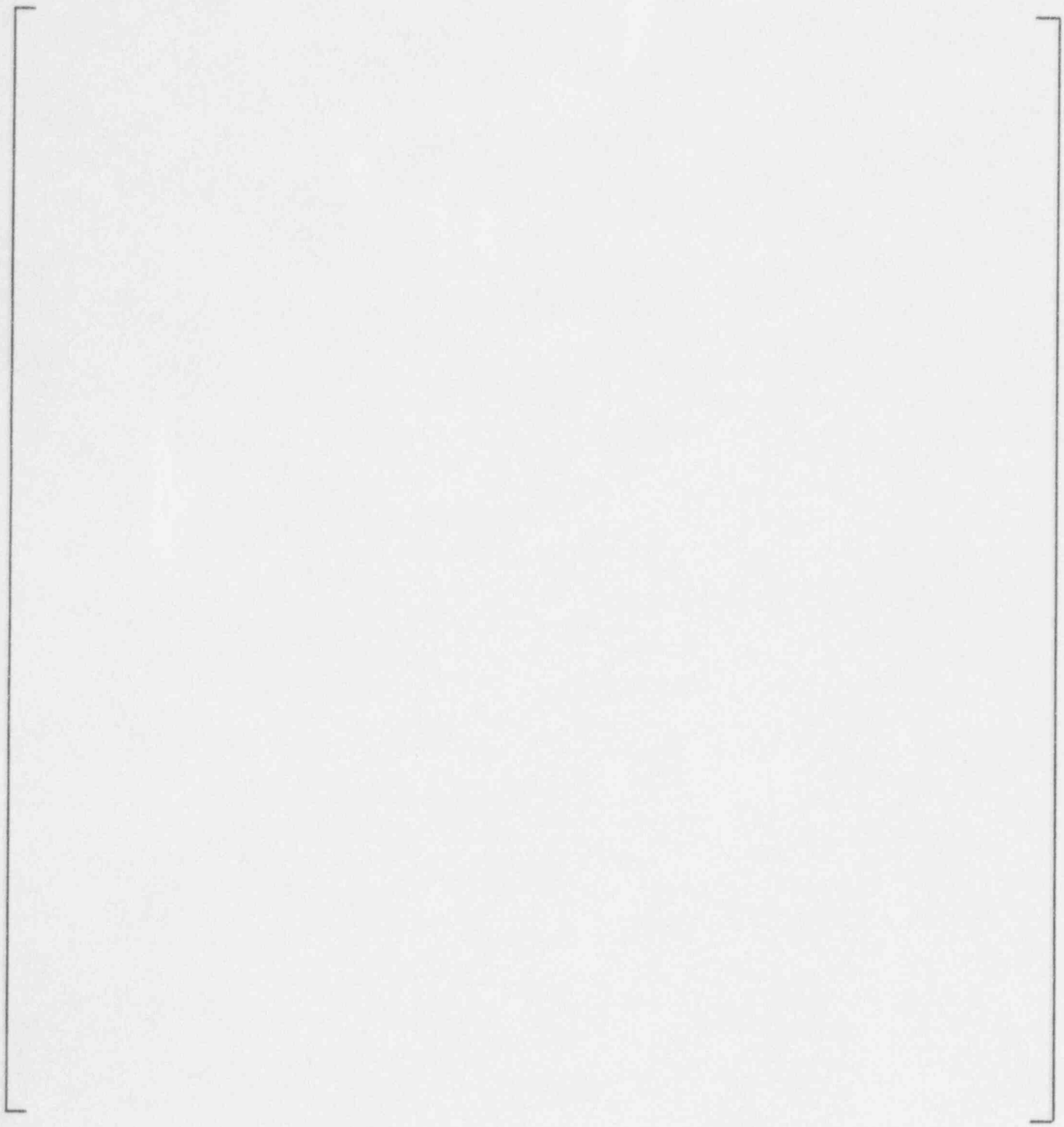

Figure 9-6 Test Series S07 versus Rohsenow, Original Correlation with $Pr_\ell^{1.7}$

a,b,c

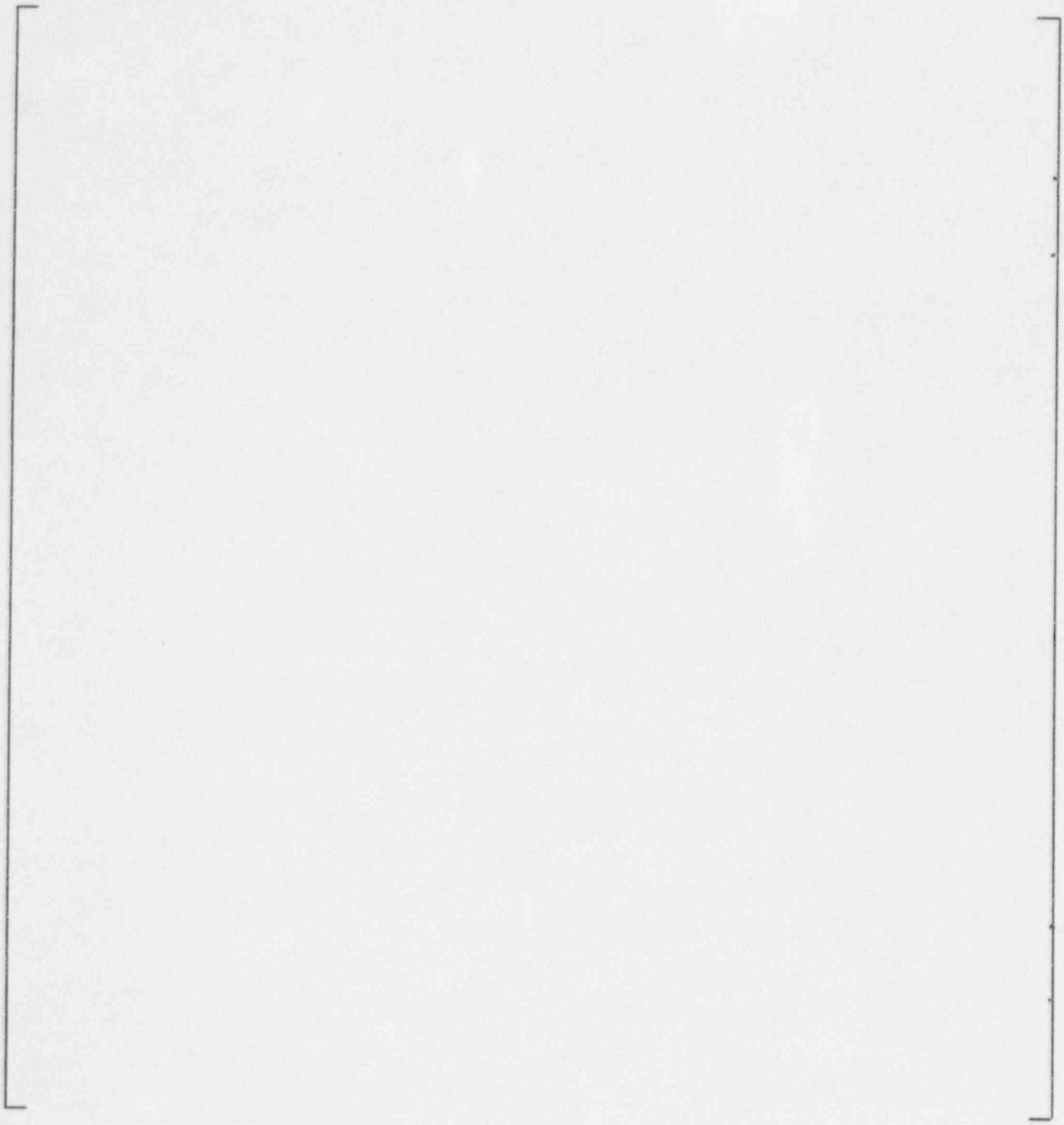

Figure 9-7 Test Series S07 versus Jens-Lottes

a,b,c

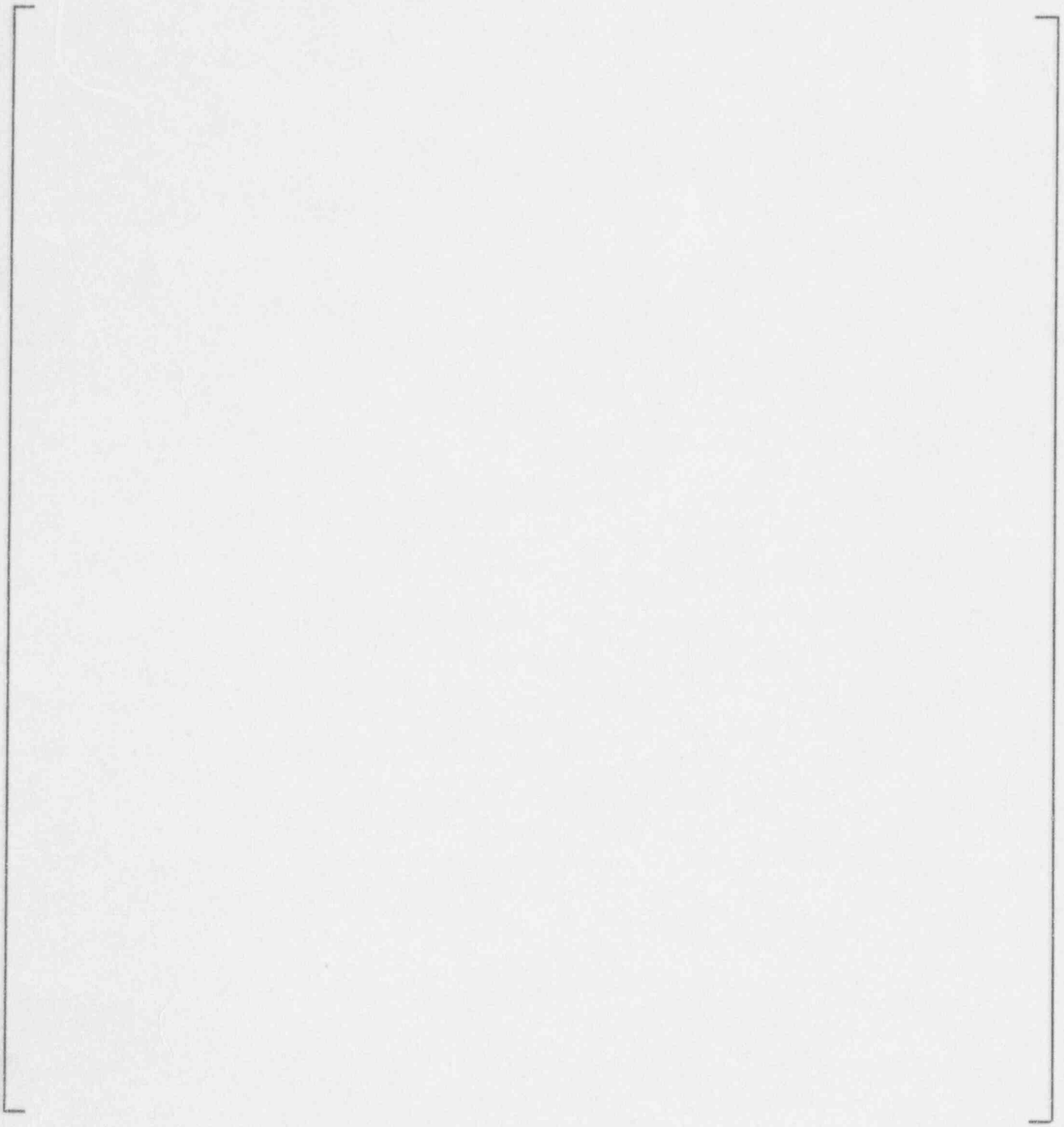

Figure 9-8 Test Series S07 versus McAdams, et al.

a,b,c

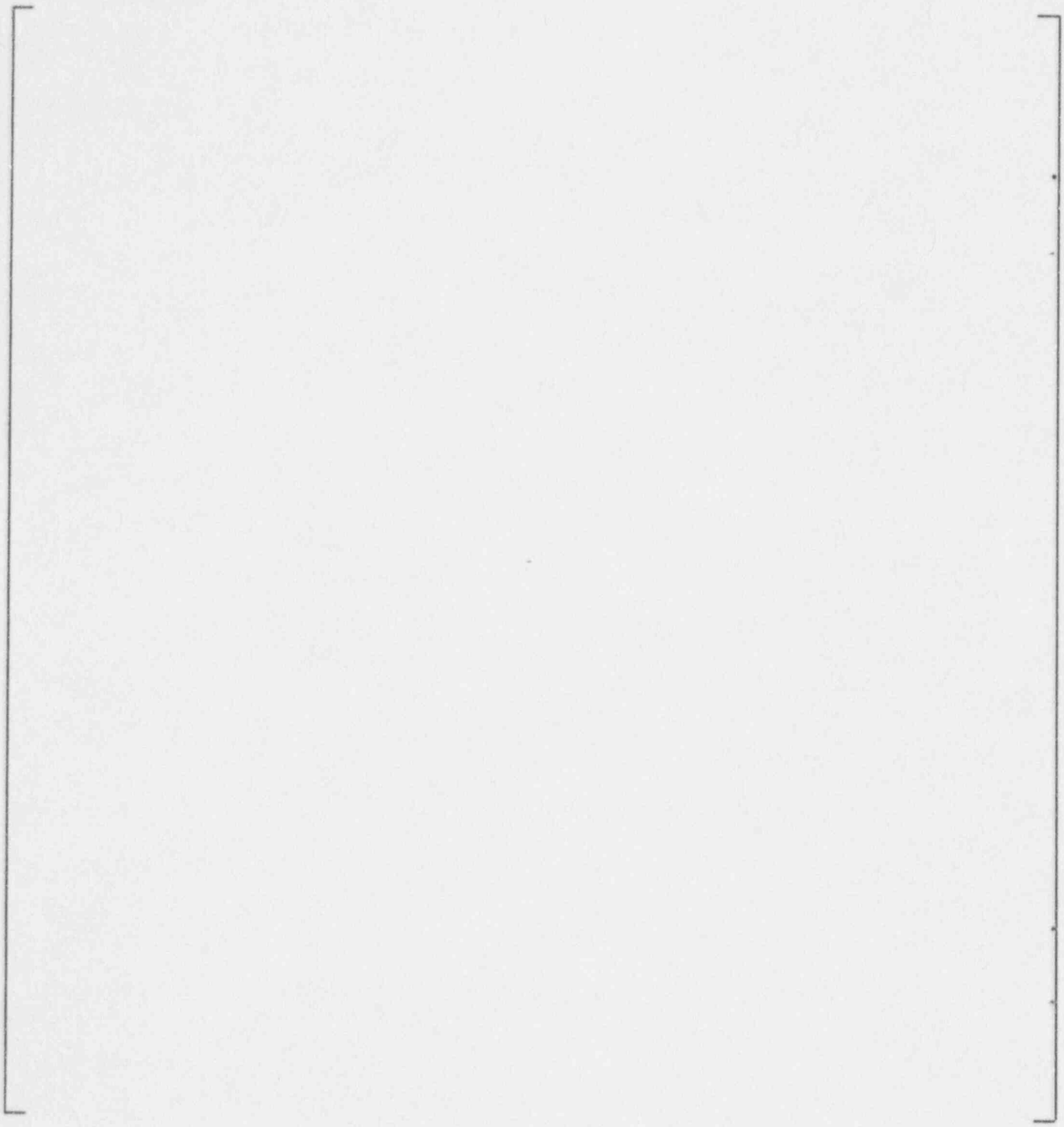

Figure 9-9 Test Series S07 versus Collier

a,b,c

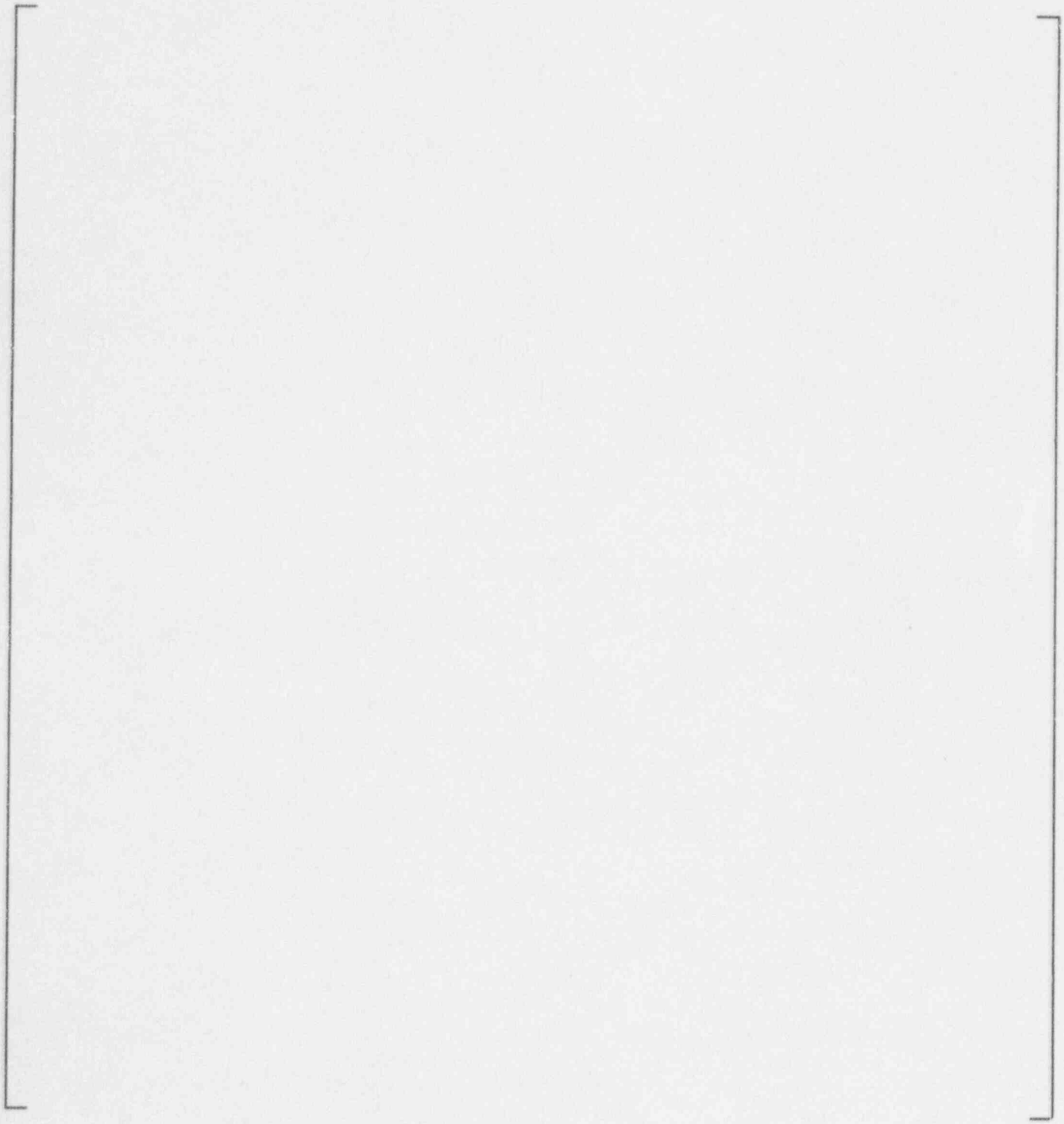

Figure 9-10 Test Series S07 versus Forster-Zuber

a,b,c

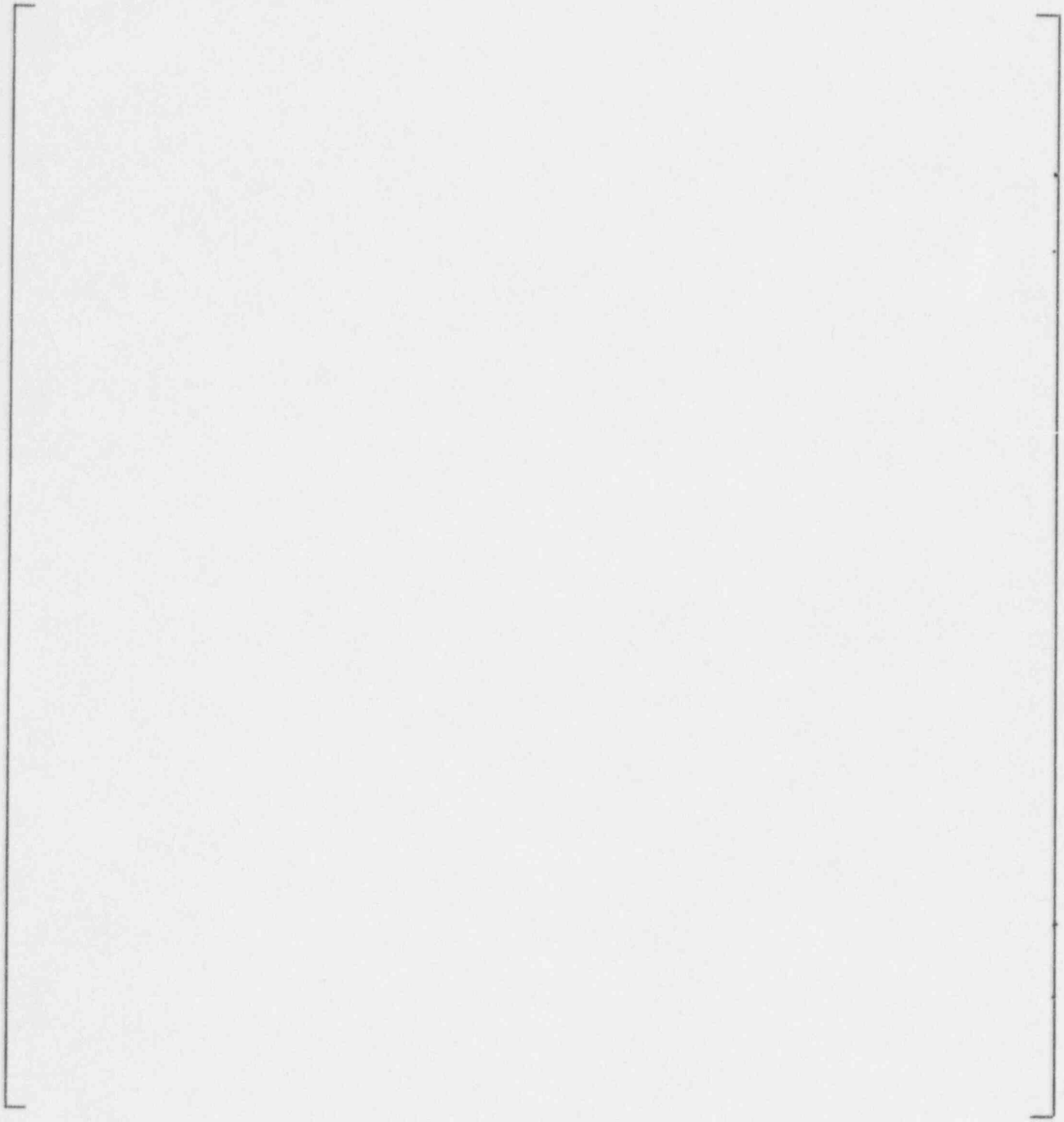

Figure 9-11 Test Series S07 versus Forster-Greif

a,b,c

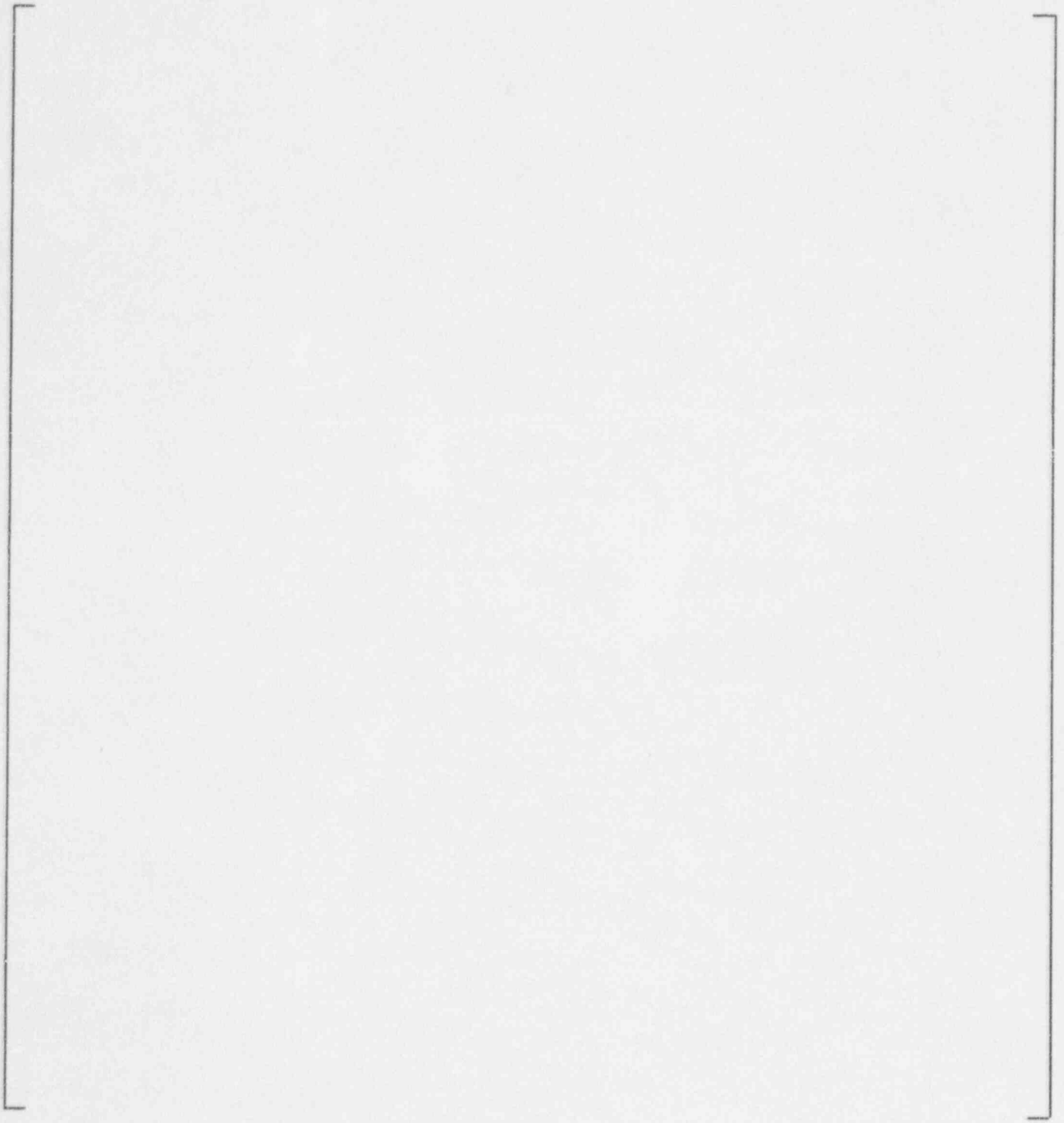

Figure 9-12 PRHR Heat Flux Used in Flow Calculation from Test S12

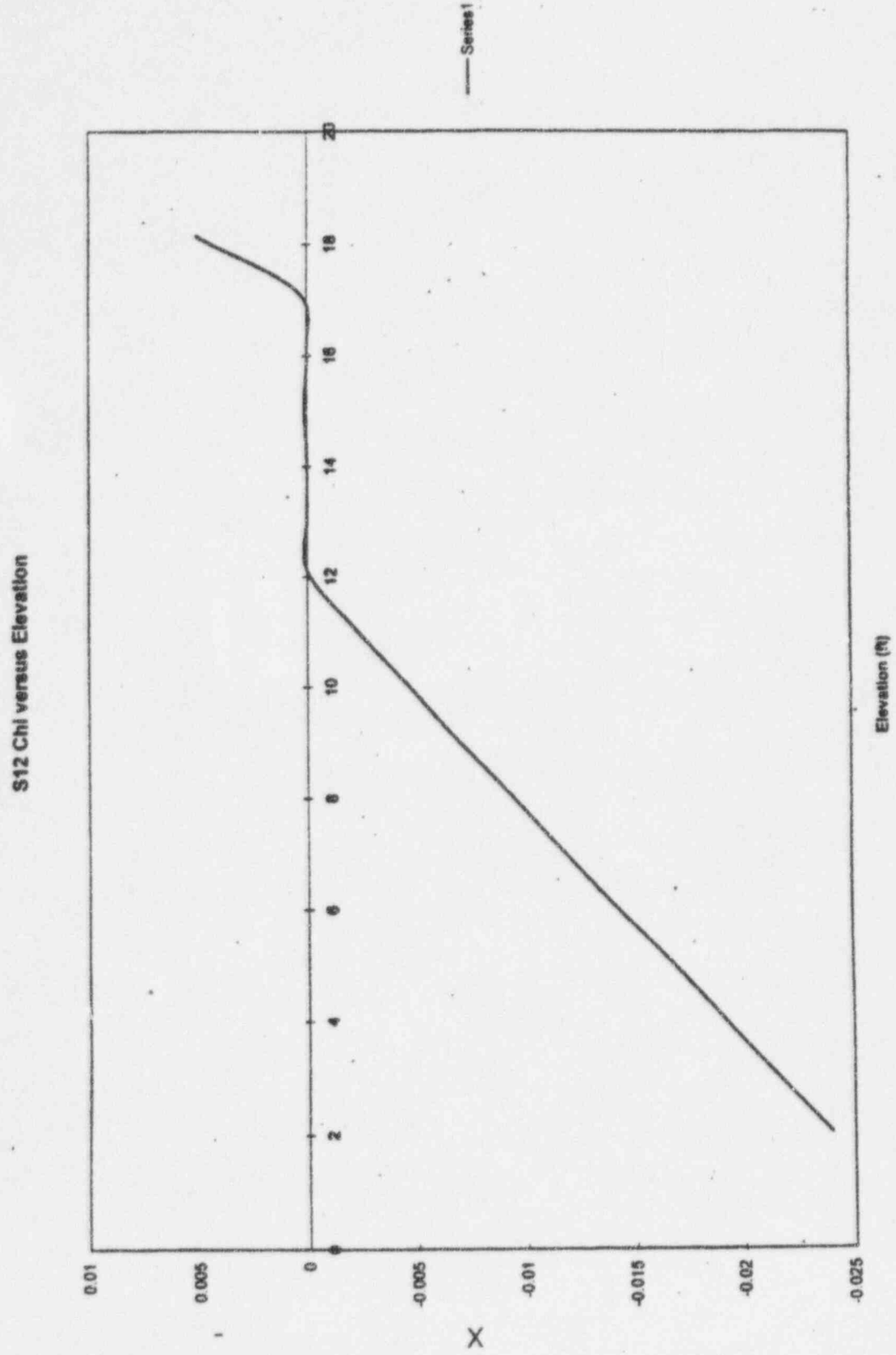

Figure 9-13 Calculated Quality along the PRHR Tubes for Test S12

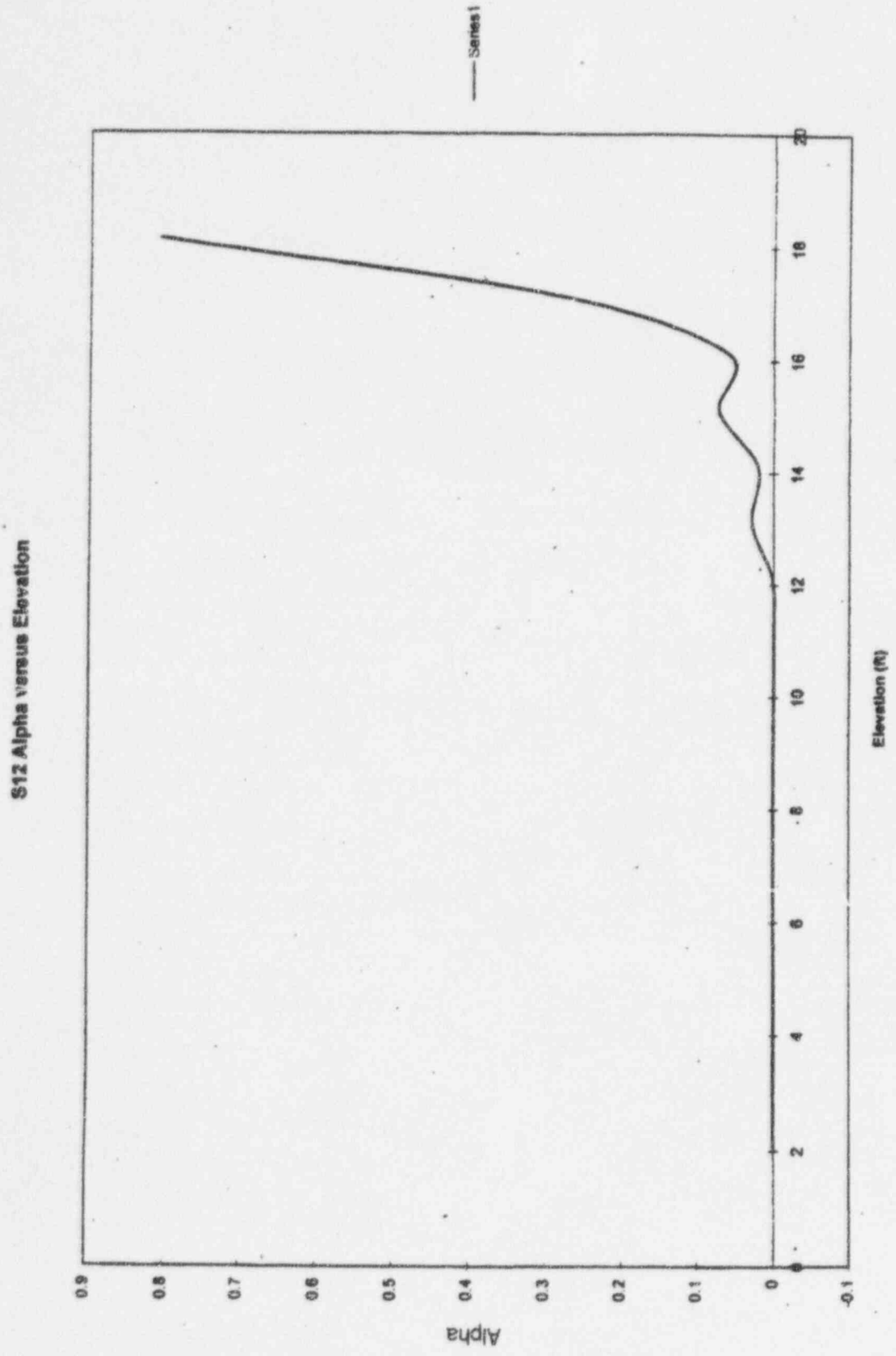

Figure 9-14 Calculated Void Fraction along the PRHR Tubes for Test S12

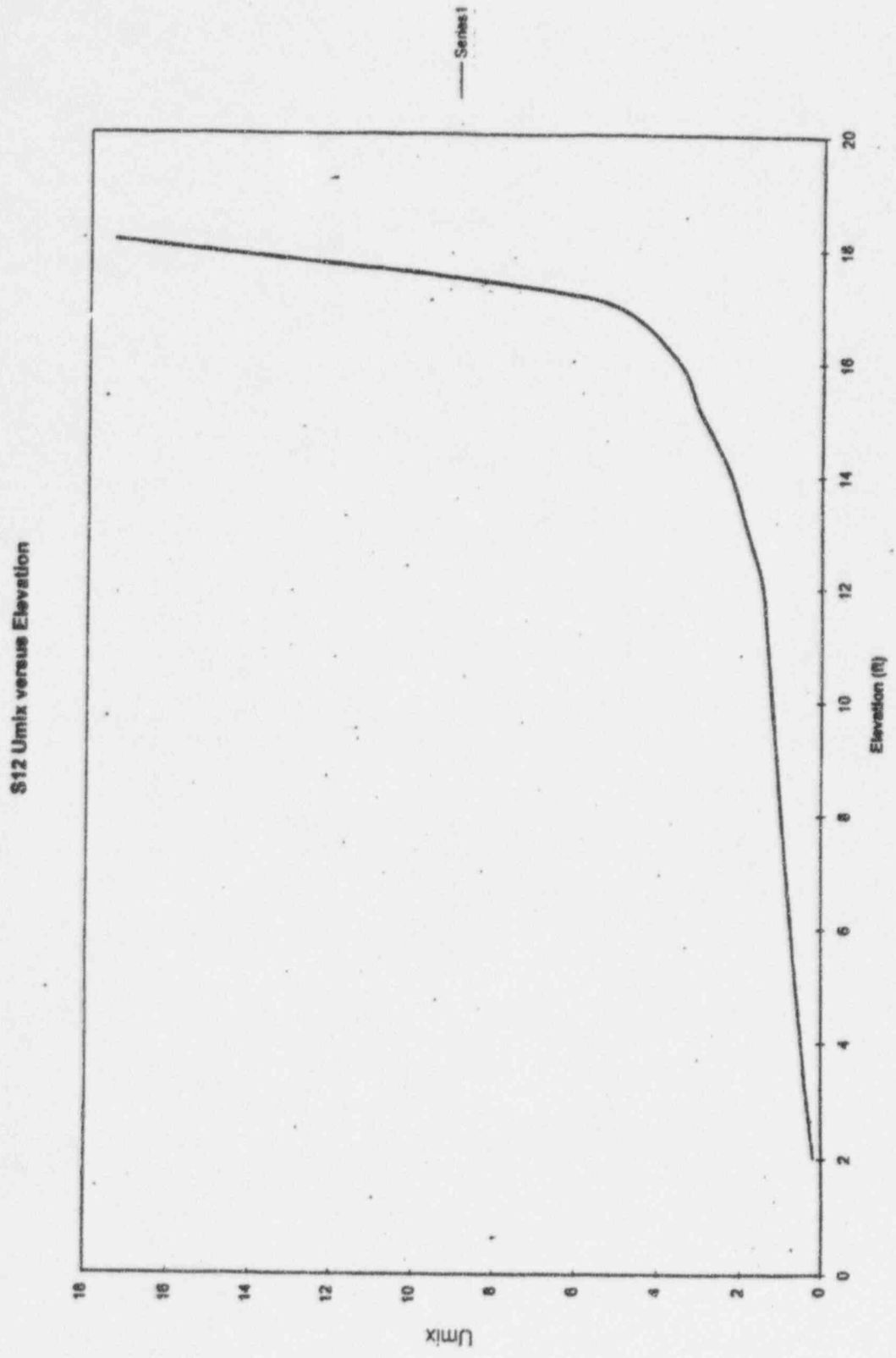

Figure 9-15 Calculated Mixture Velocity along PRHR Tubes for Test S12

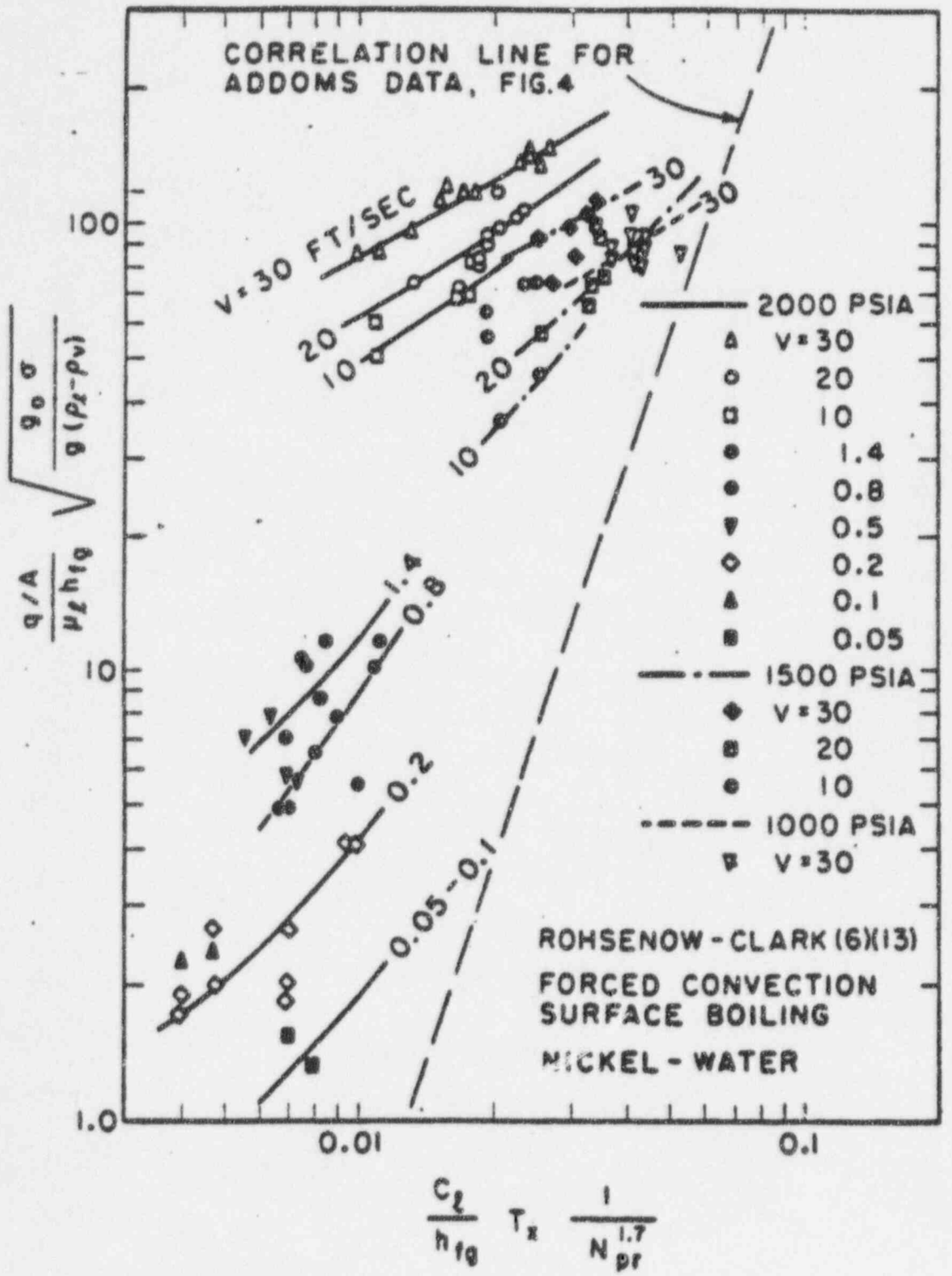

Figure 9-16 Data of Rohsenow-Clark for Nickel-Water Interface for Forced-Convection Surface Boiling [Reference 5]

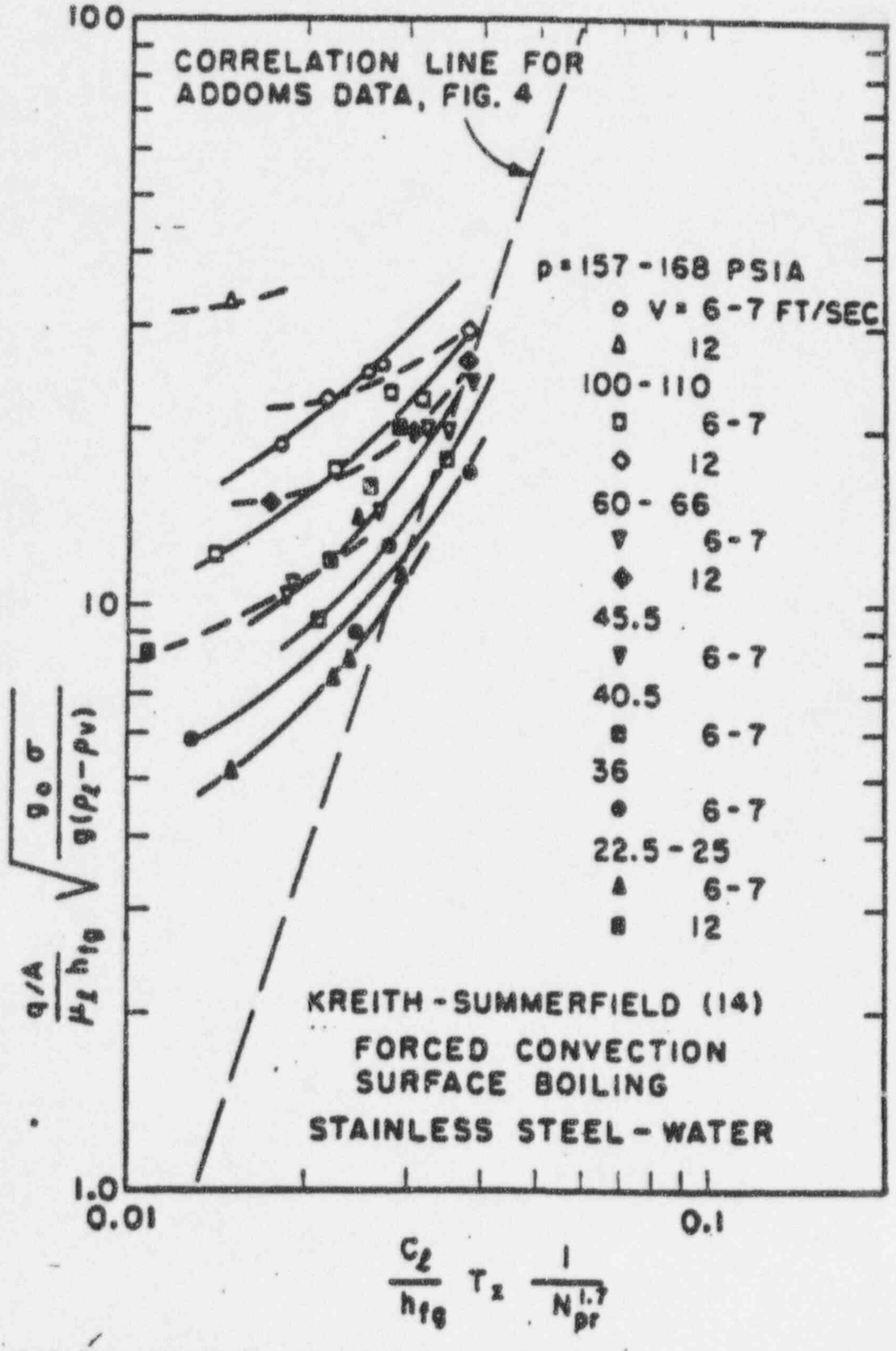

Figure 9-17 Data of Kreith-Summerfield for Stainless Steel Water Interface for Forced-Convection Surface Boiling [Reference 5]

a,b,c

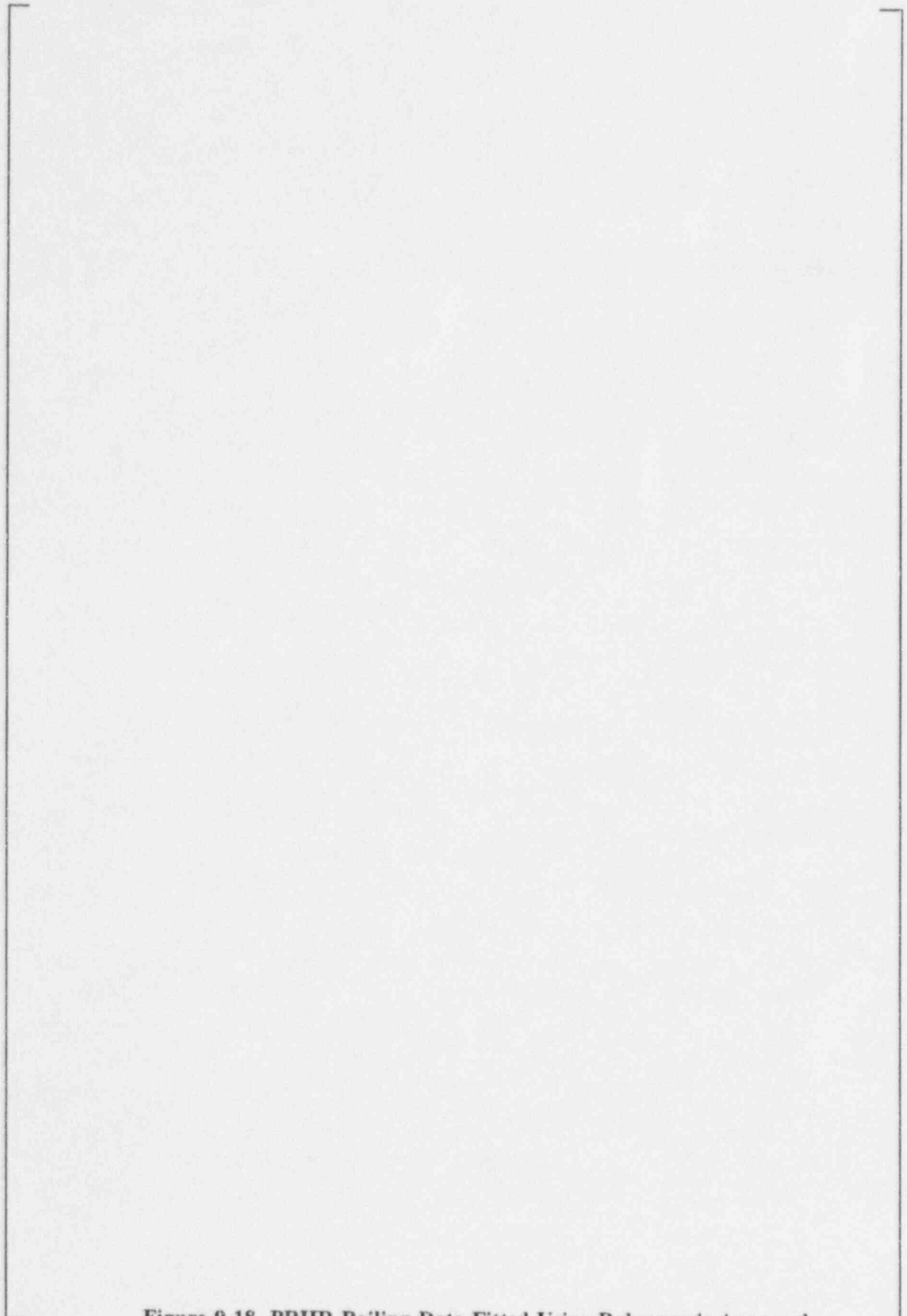

Figure 9-18 PRHR Boiling Data Fitted Using Rohsenow's Approach

a,b,c

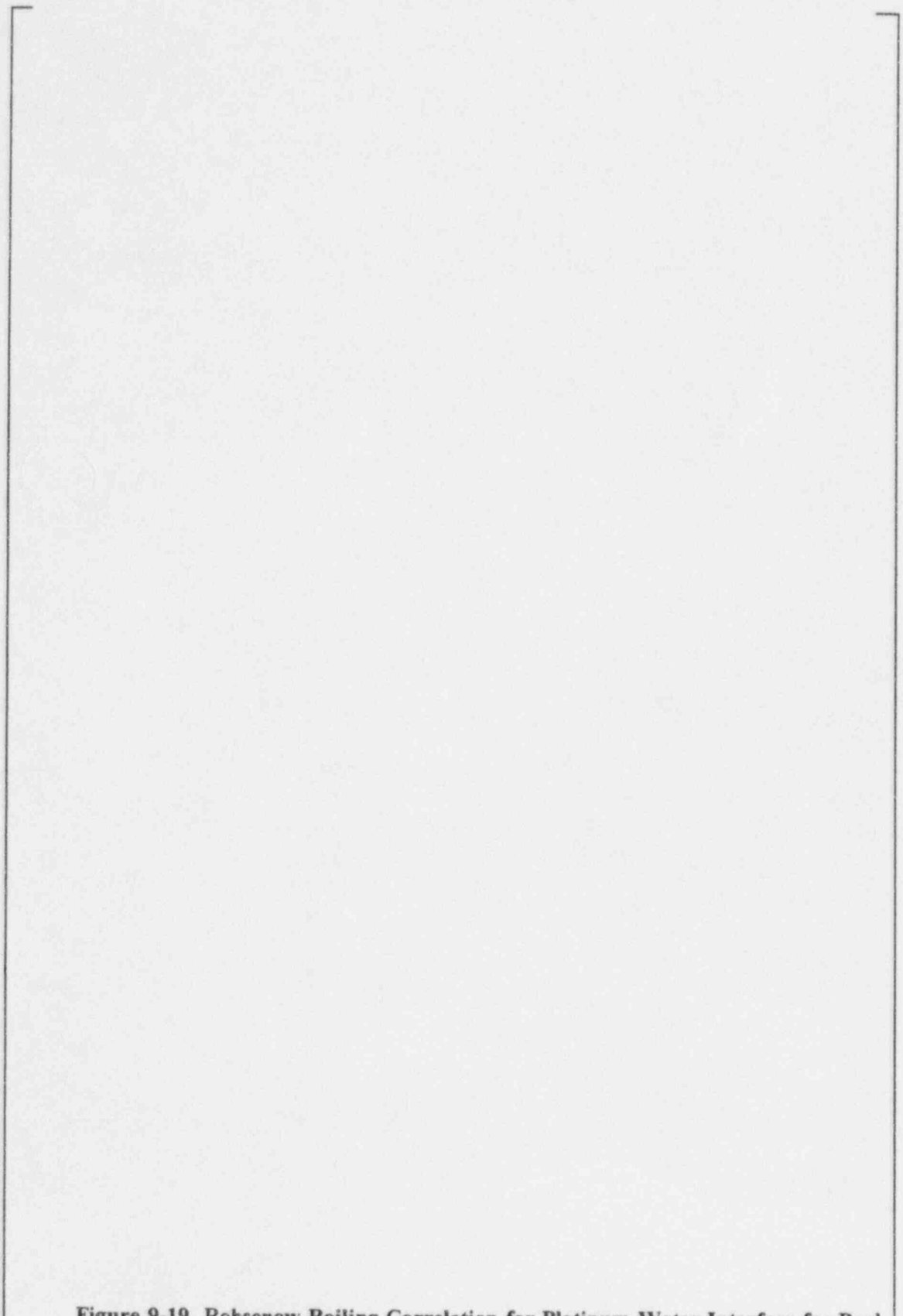

Figure 9-19 Rohsenow Boiling Correlation for Platinum-Water Interface for Pool Boiling [Reference 5]

a,b,c

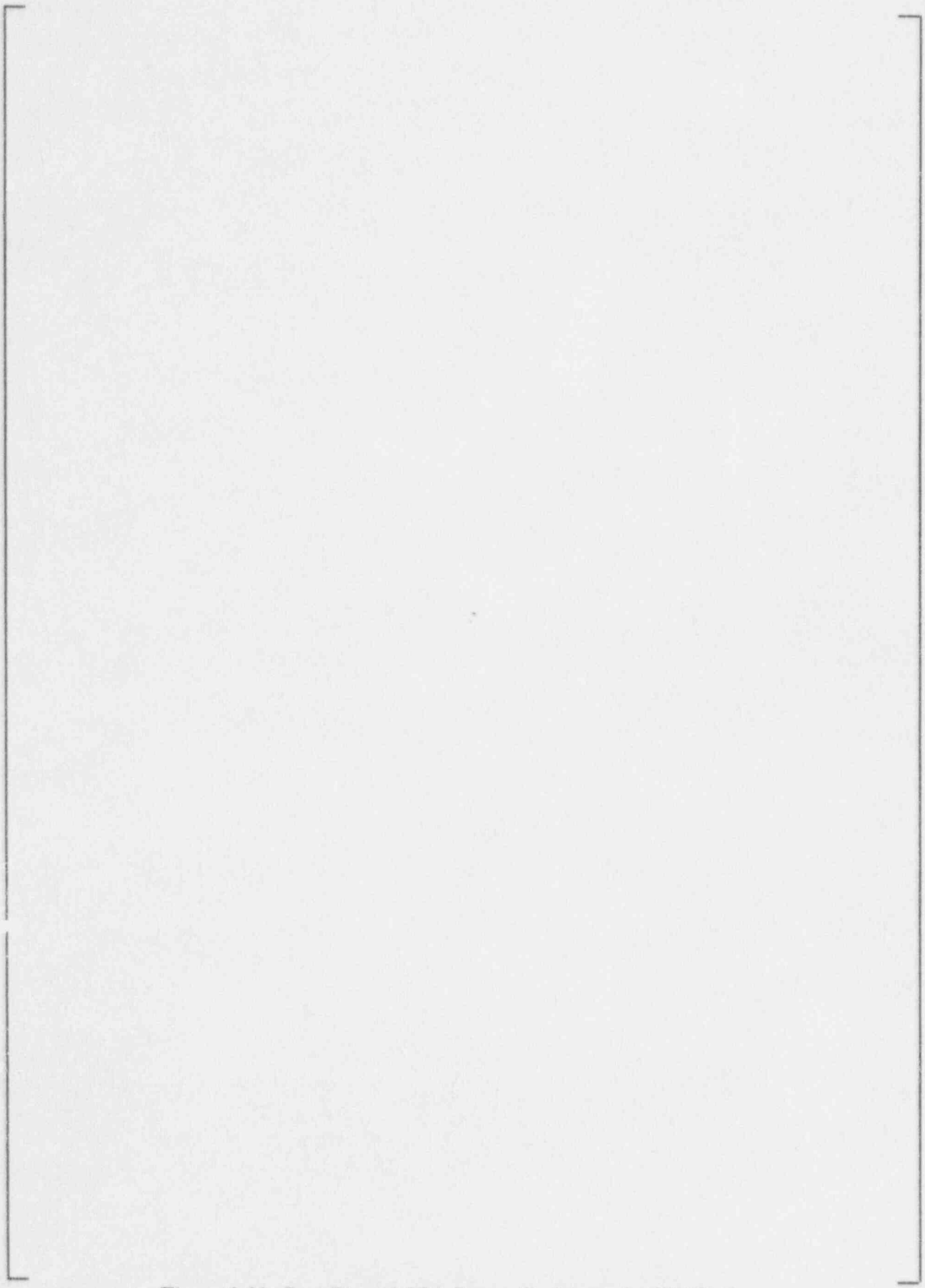

Figure 9-20 Best Fit and 95th Percentile Limits for PRHR Data

a,b,c

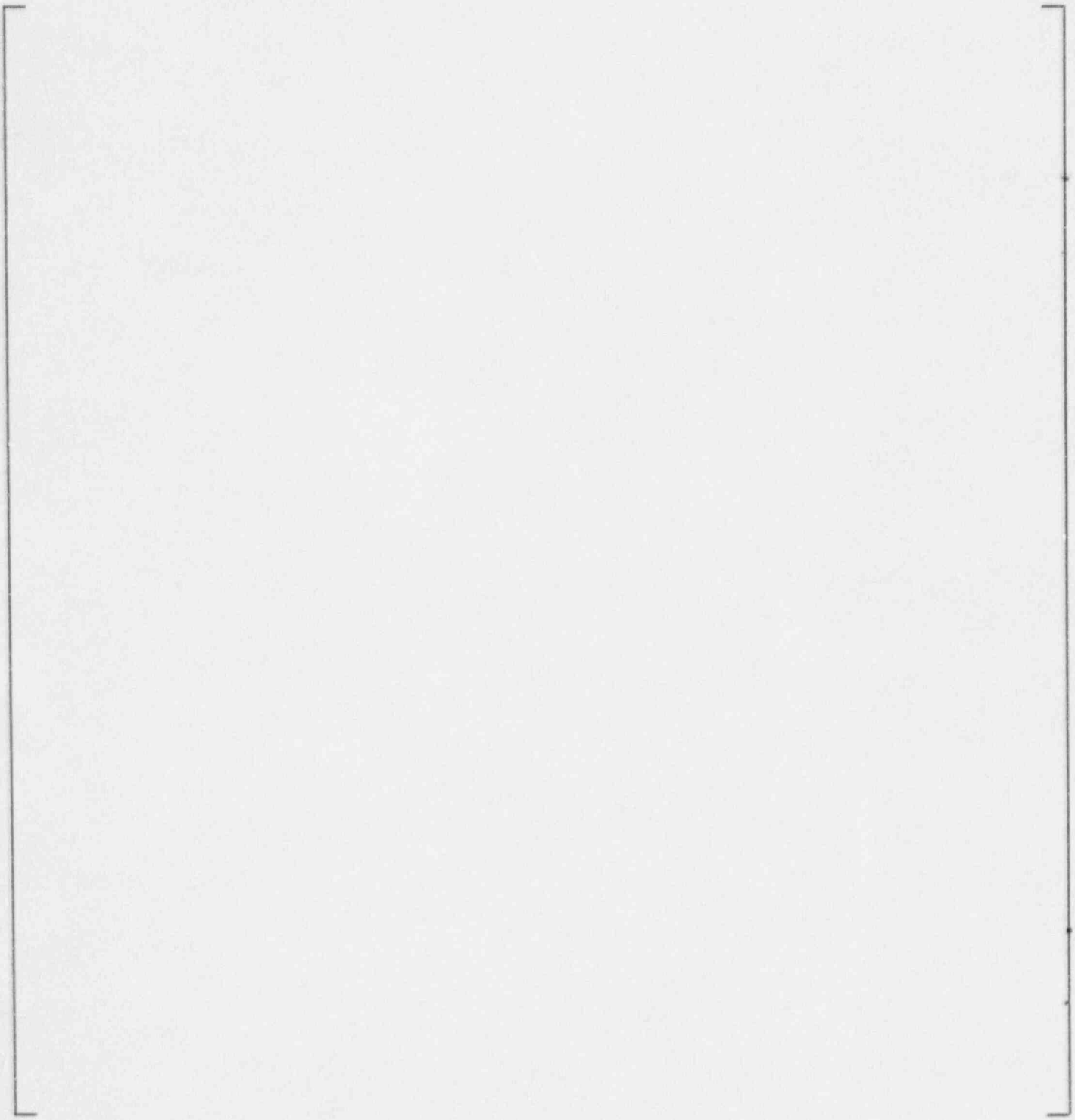

Figure 9-21. Test Series S07 Data versus Rohsenow, Original Correlation with $Pr_f^{1.7}$

a,b,c

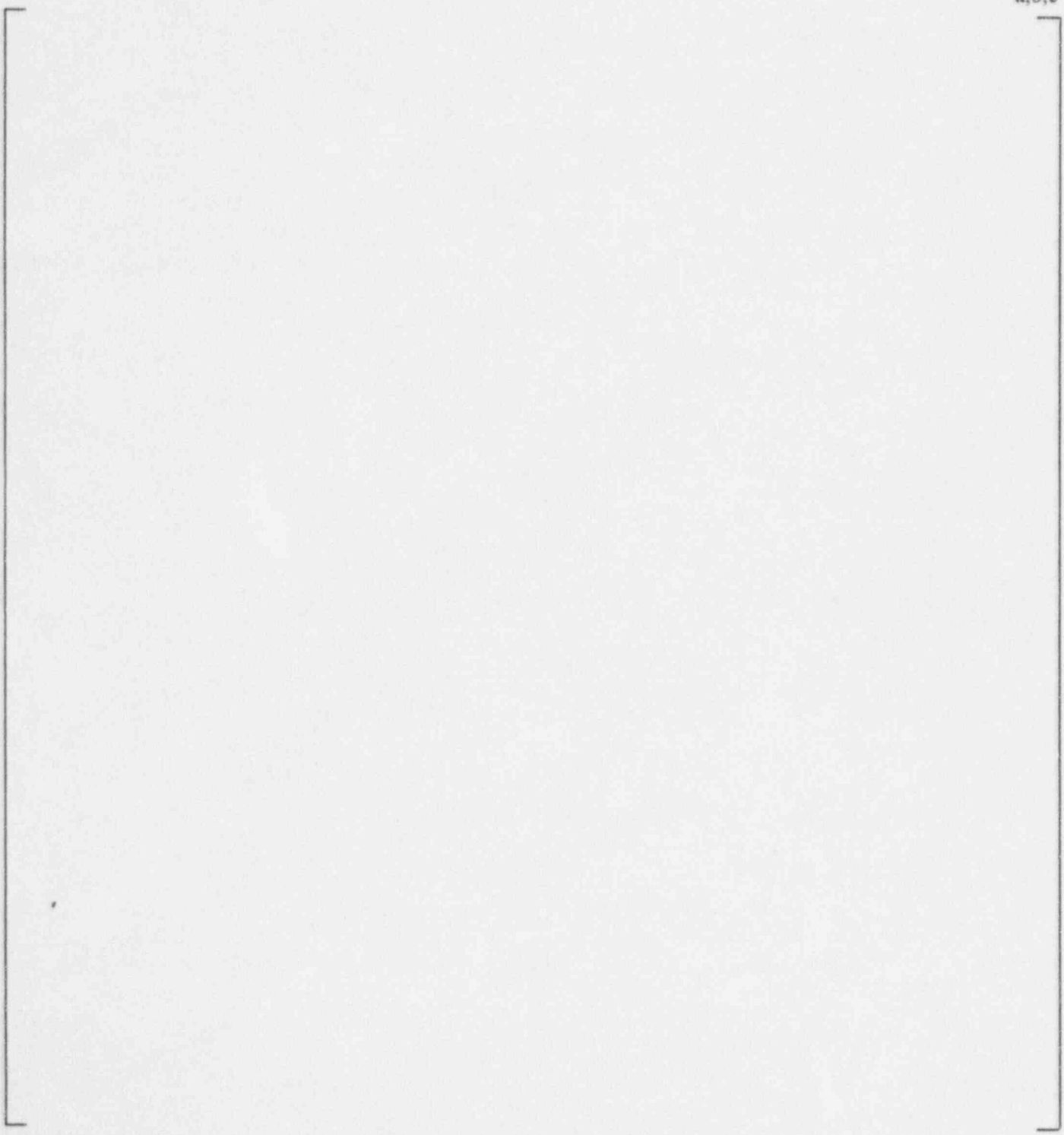

Figure 9-22 Test Series S07 Data versus Forster-Zuber with Modified Wall Superheat

10.0 CONCLUSIONS

The following conclusions can be drawn from the test results.

- The heat removal capability of the passive residual heat removal heat exchanger (PRHR HX) has been characterized. A heat transfer correlation based on the test data has been developed for the nuclear safety computer codes to assess PRHR performance.

- The mixing capability of the water in the PRHR test tank was good; therefore, sufficient mixing of the water in the IRWST can be expected, and localized boiling or "hot spots" will not be a problem. The temperature in the PRHR test tank was nearly uniform throughout the tank at a given elevation, thus proving that most of the tank volume will be used as a heat sink. The interface of the pronounced vertical temperature gradient in the tank is moving continuously downward when the tank water is boiling, and after several hours of heat removal most of the tank water may reach a uniform boiling temperature of 212°F. The desired objective of demonstrating good mixing of the IRWST is therefore achieved.

- The data from different possible PRHR configurations showed no real impact on the heat transfer performance, indicating that the existing data equally apply to the revised PRHR design with multi-tube banks.

- The PRHR performance was characterized with partial draindowns of the IRWST, which can be used to support the safety analysis models of the PRHR.

11.0 REFERENCES

1. Jensen, M. K., "Advances in Shellside Boiling and Two-Phase Flow," 1989 National Heat Transfer Conference, HTD - Vol. 108, Heat Transfer Equipment Fundamentals, Design, Application, and Operating Problems; (1989).

2. Westinghouse Electric Corporation, *AP600 Passive Residual Heat Removal Heat Exchanger Test: Test Report*, NSE-90-0073, February 1990.

3. Corletti, M. M., Hochreiter, L. E. and W. A. Stewart, *AP600 Passive Residual Heat Removal Heat Exchanger Test, Final Report*, WCAP-12980-Rev. 0, December 1991.

4. Westinghouse Responses to NRC Requests for Additional Information on the PRHR Heat Exchanger, NSD-NRC-96-4660, March 1996.

5. Miller, Richard W., *Flow Measurement Engineering Handbook*, Second Edition, pp. 9-10 to 9-17.

6. Petukhov, B. S., "Heat Transfer and Friction in Turbulent Pipe Flow with Variable Properties," *Advances in Heat Transfer*, Volume 6, pp. 503-564, Academic Press New York, 1970.

7. Dittus, F. W. and L. M. K. Boelter, University of California Berkeley Publ. Eng. Vol. 2, pg. 433, 1930.

8. Kreith, F. and M. S. Bohm, *Principles of Heat Transfer*, Fourth Edition, pp. 324-325, Harper and Row Publishers, New York, 1986.

9. Kays, W. M. and M. E. Crawford, *Convective Heat and Mass Transfer*, McGraw-Hill Book Company, 1980.

10. Schlichting, H., *Boundary Layer Theory*, McGraw-Hill Book Company, 1960.

11. Knudsen, J.G., and D. L. Katz, *Convective Heat and Mass Transfer*, McGraw-Hill Book Company, 1979.

12. Private Communication, Bill Lucas, Lucas Milhaupt, Inc.

13. Cunningham, J. P., Friend, M. T., Hochreiter, L. E., Hundel, R., Merrett, V., Orinsh, M. and R. F. Wright, *AP600 SPES-2 Test Analysis Report*, WCAP-14254, May 1995.

14. Dumsday, C. L., et al., *AP600 Low Pressure Integral Systems Test at Oregon State University Final Data Report*, WCAP-1425, Proprietary, May 1995.

15. Eckert, E. R. G. and T. W. Jackson, *Analysis of Turbulent Free Convection Boundary Layer on Flat Plate*, NACA Report 1015 July 1950.

16. Burmeister, L.C., *Convective Heat Transfer*, John Wiley and Sons Publishers, pg. 543, 1983.

17. McAdams, W. H., *Heat Transmission*, McGraw-Hill Publishers, pg. 172, 1954.

18. McAdams, W. M., C. S. Kennel, R. Carl, P. M. Picarnell, and J. E. Drew, "Heat Transfer at High Rates to Water with Boiling," Ind. Eng. Chem., Vol. 41, 1945.

19. Jens, W. H. and P. A. Lottes, *Analysis of Heat Transfer, Burnout, Pressure Drops and Density Data for High Pressure Water*, ANL-4627 1951.

20. Rohsenow, W. M., "A Method of Correlating Heat Transfer Data for Surface Boiling Liquids," Trans ASME Vol. 74, pp. 969-975 1952.

21. Forster, H. K. and N. Zuber, "Dynamics of Vapor Bubbles and Boiling Heat Transfer," American Institute Chemical Engineering Journal, Vol.1, No.4, December 1955.

22. Forster, H. K. and R. Greif, "Heat Transfer to a Boiling Liquid - Mechanism and Correlations," Transactions of the American Society of Mechanical Engineers, 1959.

23. *Heat Exchanger Design Handbook*, "Fluid Mechanism and Heat Transfer," Hemisphere Publishing Corporation, 1983.

24. Collier, J. G., *Convective Boiling and Condensation*, McGraw Hill Book Company, 1972.

25. Cunningham, J. P. and H. C. Yeh, "Experiments and Void Correlation for PWR Small Break LOCA Conditions," Tranactions of the American Nuclear Society, Vol. 17, pg 363, 1973.

26. Vachon, R. I., Nix, G. H. and G. E. Tanger, "Evaluation of Constants for the Rohsenow Pool-Boiling Correlation," ASME, Journal of Heat Transfer, Vol. 90C, No. 2, pp. 239-247, May 1968.

27. Addoms, J. N., *Heat Transfer at High Rates to Water Boiling Outside Cylinders*, DSc Thesis, Chemical Engineering Department, Massachusetts Institute of Technology, June 1948.

28. Hsu, Y.Y., "On the Size Range of Active Nucleation Cavities on a Heating Surface," Transactions of the American Society of Mechanical Engineers Journal of Heat Transfer, Vol. 84, 1962.

APPENDIX A
PRHR CHANNEL ANALYSIS METHOD

Appendix A presents a method used to compute the fluid velocity and the flow quality along the vertical PRHR tube bundle assuming a buoyant-driven natural circulation flow. The fluid velocity and flow quality are used for predicting the type of flow patterns that are present around the PRHR tubes for different conditions.

The momentum equation for the vertical tube bundle is given as:

$$A\ dP + \frac{d(\rho_{mix}\ A\ u_{mix}^2)}{2\ g_c} + \rho_{mix}\ \frac{g}{g_c}\ A\ dz + A\ \frac{f\ dz}{D_o}\ \frac{u_{mix}^2}{2\ g_c}\ \rho_{mix} = 0 \qquad \text{(A-1)}$$

where the mixture velocity u_{mix} is defined as follows:

$$u_{mix} = \frac{\dot{m}}{A\ \rho_{mix}} \qquad \text{(A-2)}$$

$$u_{mix} = \frac{\alpha\ \rho_g\ u_{g,a} + (1-\alpha)\ \rho_f u_{f,a}}{\rho_{mix}} \qquad \text{(A-3)}$$

or

$$u_{mix} = \frac{\rho_g u_g + \rho_f u_f}{\rho_{mix}} \qquad \text{(A-4)}$$

where:

dP	=	axial change in pressure over suction (lbf/ft^2)
g	=	acceleration of gravity ($ft./sec^2$)
g_c	=	gravitational constant ($lbm \cdot ft./ (lbf \cdot sec.^2)$)
dz	=	height along tube bundle (ft.)
f	=	friction factor
α	=	void fraction
D_o	=	effective diameter (ft.)
A	=	Area $(ft.)^2$
u_{mix}	=	mixture velocity (ft./sec)
ρ_{mix}	=	mixture density (lbm/ft^3)
$u_{g,a}$	=	actual gas velocity (ft./sec)
$u_{f,a}$	=	actual fluid velocity (ft./sec)

u_g = superficial gas velocity (ft./sec)
u_f = superficial fluid velocity (ft./sec)

$$\rho_{mix} = \alpha\ \rho_g + (1-\alpha)\ \rho_f \tag{A-5}$$

The cross-sectional area, A, in Equation (A-1) is cancelled. Therefore:

$$dP + \frac{d(\rho_{mix}\ u_{mix}^2)}{2\ g_c} + \rho_{mix}\ \frac{g}{g_c}\ dz + \frac{fdz}{D_o}\ \frac{\rho_{mix}\ u_{mix}^2}{2\ g_c} = 0 \tag{A-6}$$

The pressure in the bundle is the same as the pressure away from the bundle at the same elevation in the IRWST pool. That is:

$$dP = -\rho_{\ell,\infty}\ \frac{g}{g_c}\ dz \tag{A-7}$$

where:

$\rho_{\ell,\infty}$ = fluid density at elevation ℓ (lbm/ft^3) away from the tube

Thus, Equation A-6 becomes:

$$-(\rho_{\ell,\infty} - \rho_{mix})_{avg}\ \frac{g}{g_c}\ dz + \frac{1}{2\ g_c}\ d(\rho_{mix}\ u_{mix}^2) + \frac{f}{D_o}\ \frac{\rho_{mix}\ u_{mix}^2}{2\ g_c}\ dz = 0 \tag{A-8}$$

In finite difference form, Equation (A-8) is written as:

$$-(\rho_{\ell,\infty} - \rho_{mix})_{avg}\ \frac{g}{g_c}\ (z_j - z_{j-1}) + \frac{1}{2\ g_c}\ (\rho_{mix,j}\ u_{mix,j}^2 - \rho_{mix,j-1}\ u_{mix,j-1}^2) + \frac{f}{2\ g_c\ D}\ (\rho_{mix}\ u_{mix}^2)_{avg}\ (z_j - z_{j-1}) = 0 \tag{A-9}$$

where the subscript j indicates the respective properties at elevation j, and "avg" means the average within the interval between z_j and z_{j-1}. These average quantities are written as:

$$-(\rho_{\ell,\infty} - \rho_{mix})_{avg} = -(\rho_{\ell,\infty} - \rho_{mix,\ avg}) = -\left[\rho_{\ell,\infty} - \frac{1}{2}\ (\rho_{mix,\ j} + \rho_{mix,\ j-1})\right] \tag{A-10}$$

and

$$(\rho_{mix}\ u^2_{mix})_{avg} = \frac{1}{2}\ (\rho_{mix,\ j}\ u^2_{mix,\ j} + \rho_{mix,\ j-1}\ u^2_{mix,\ j-1}) \tag{A-11}$$

Substituting Equations (A-10) and (A-11) in (A-9) gives:

$$-[\rho_{\ell,\infty} - \frac{1}{2}\ (\rho_{mix,\ j} + \rho_{mix,\ j-1})]\ \frac{g}{g_c}\ (z_j - z_{j-1}) + \frac{1}{2\ g_c}\ (\rho_{mix,\ j}\ u^2_{mix,\ j} - \rho_{mix,\ j-1}\ u^2_{mix,\ j-1})$$
$$+ \frac{1}{2}\ (\rho_{mix,\ j}\ u^2_{mix,\ j} + \rho_{mix,\ j-1}\ u^2_{mix,\ j-1})\ \frac{f}{2\ g_c\ D_o}\ (z_j - z_{j-1}) = 0 \tag{A-12}$$

From this equation, u_j is calculated as:

$$u_{mix,\ j} = \sqrt{\frac{[\rho_{\ell,\infty} - \frac{1}{2}\ (\rho_{mix,\ j} + \rho_{mix,\ j-1})]g(z_j - z_{j-1}) + \frac{1}{2}\ \rho_{mix,\ j-1} u^2_{mix,\ j-1}[1 - \frac{f}{2D}(z_j - z_{j-1})]}{\frac{1}{2}\rho_{mix,\ j}\left[1 + \frac{f}{2D_o}(z_j - z_{j-1})\right]}} \tag{A-13}$$

The mixture density is evaluated from the void fraction:

$$\rho_{mix,\ j} = \alpha_j \rho_{g,\ j} + (1 - \alpha_j)\rho_{f,\ j} \tag{A-14}$$

The void fraction at elevation j (α_j) is computed from the Yeh correlation [Reference 21] as:

$$\alpha_j = 0.925 \left(\frac{\rho_{g,\ j}}{\rho_{f,\ j}}\right)^{0.239} \left(\frac{u_{g,\ j}}{u_{bcr,\ j}}\right)^{a} \left(\frac{u_{g,\ j}}{u_{g,\ j} + u_{f,\ j}}\right)^{0.6} \tag{A-15}$$

where: $\alpha_j = 1$ when calculated $\alpha_j > 1$, and

$$a = 0.67 \text{ if } u_{g,\ j}/u_{bcr,\ j} \leq 1$$
$$a = 0.47 \text{ if } u_{g,\ j}/\ u_{bcr,\ j} > 1 \tag{A-16}$$

and

$$u_{bcr,\ j} = \frac{2}{3}\sqrt{g\ R_{bcr,\ j}} \tag{A-17}$$

where: $R_{bcr,\ j}$ is the critical bubble radius, given as:

$$R_{bcr,\,j} = \left(\frac{1.53}{2/3}\right)^2 \sqrt{\frac{\sigma_j}{g\,\rho_{f,\,j}}} \qquad \text{(A-18)}$$

where:

σ_j = surface tension

Since $u_{f,\,j}$ is generally much smaller than $u_{g,\,j}$, the last factor in Equation (A-15) approaches 1 and is neglected.

The superficial steam velocity, $u_{g,\,j}$, and the flow quality, x_j, is derived from the energy equation:

$$\dot{m}_{in}\,(h_{out,\,j} - h_{in}) = Q_j \qquad \text{(A-19)}$$

and

$$h_{out,\,j} = x_j\,h_{fg,\,j} + (1 - x_j)\,h_{f,\,j} \qquad \text{(A-20)}$$

where:

h_{fg} = heat evaporation (Btu/lbm)
h_{out} = exit enthalpy (Btu/lbm)
h_{in} = inlet enthalpy (Btu/lbm)

Eliminating $h_{out,\,j}$ for Equations (A-19) and (A-20) and solving for quality, gives:

$$x_j = \frac{1}{h_{fg,\,j}}\left[\frac{Q}{\dot{m}_{in}} - (h_{f,\,j} - h_{in})\right] \qquad \text{(A-21)}$$

The steam mass flow rate and superficial steam velocity is expressed as:

$$\dot{m}_{g,\,j} = x_j\,\dot{m}_{in} = \frac{1}{h_{fg,\,j}}\left[Q - \dot{m}_{in}\,(h_{f,\,j} - h_{in})\right] \qquad \text{(A-22)}$$

where:

$$V_{g,\,j} = \frac{\dot{m}_{g,\,j}}{A\,\rho_{g,\,j}} \qquad \text{(A-23)}$$

where:

V_{gj} = the superficial vapor velocity (ft./sec)

Note that Q_j is the integrated heat flux from the bottom of the tube bundle, z = 0, to the location z_j. That is:

$$Q_j = \int_0^{z_j} q' \, dz \qquad \text{(A-24)}$$

Also note that the height of the PRHR bundle is 18 feet, which is large. Therefore, the changes of the pressure and, hence, the saturation temperature and fluid properties, are significant. Consequently, all fluid properties in the above equations carry the subscript "j" to denote the variation with the elevation z_j. The pressure is evaluated by the following formula:

$$p_j = 14.7 + \rho_{\ell,\infty} \frac{g}{g_c} (z_{water} - z_j) \qquad \text{(A-25)}$$

where z_{water} is the height from the bottom of the bundle to the water level in the IRWST. The $\rho_{\ell,\infty}$ and h_{in} are the water density and enthalpy away from the bundle, which are considered constant and are independent of the elevation. In fact, in the PRHR test, the water temperature away from the bundle is practically independent of the elevation.

These equations were programmed to predict the natural circulation flow, flow quality, and void fraction inside the PRHR bundle so that the local fluid conditions could be determined. As indicated in Section 9.0, the calculation could become unstable for high heat fluxes since the void fraction would be calculated to be unrealistically large, resulting in unrealistic velocities, which would be inconsistent with the video observations. The calculations yielded more realistic behavior at lower wall heat fluxes.

APPENDIX B

This Appendix contains the electronic data from all the PRHR tests in engineering units. The files names XXXXY.all indicate the test matrix number (XXXXX) followed by a run letter (Y) a,b,etc., if appropriate, with the file extension ".all" indicating all the test data. The data is stored in tab delimited text files. The engineering units are indicated at the top of each file according to the following code:

- F = °F
- PS = psia
- lb = lb/sec
- MV = millivolt
- IN = inch
- FT = feet
- KW = Kilowatts
- KH = Kilowatt-hour